Agenzia Nazionale per le Nuove Tecnologie,
l'Energia e lo Sviluppo Economico Sostenibile

Ministero dello Sviluppo Economico

RICERCA DI SISTEMA ELETTRICO

Comportamento del combustibile nucleare durante rampe di potenza: analisi di esperimenti con codici di calcolo di comportamento del combustibile, in particolare in condizioni di alto burn-up

Federico Cantini, Martina Adorni, Francesco D'Auria

Report RdS/2011/360

COMPORTAMENTO DEL COMBUSTIBILE NUCLEARE DURANTE RAMPE DI POTENZA: ANALISI DI ESPERIMENTI CON CODICI DI CALCOLO DI COMPORTAMENTO DEL COMBUSTIBILE, IN PARTICOLARE IN CONDIZIONIDI ALTRO BURN-UP

Federico Cantini, Martina Adorni, Francesco D'Auria (Università di Pisa)

Novembre 2011

Report Ricerca di Sistema Elettrico
Accordo di Programma Ministero dello Sviluppo Economico – ENEA
Area: Governo, gestione e sviluppo del sistema elettrico nazionale
Progetto: Fissione nucleare: metodi di analisi e verifica di progetti nucleari di generazione evolutiva ad acqua pressurizzata

Responsabile Progetto: Massimo Sepielli, ENEA

ENEA Ricerca Sistema Elettrico	Sigla di identificazione	Distrib.	Pag.	di
	PAR2010-CIRTEN-LB1-013	L	1	

Titolo

"Comportamento del combustibile nucleare durante rampe di potenza: Analisi di esperimenti con codici di calcolo di comportamento del combustibile, in particolare in condizioni di alto burn-up".

Ente emittente CIRTEN

PAGINA DI GUARDIA

Descrittori

Tipologia del documento: **Rapporto tecnico**

Collocazione contrattuale: ACCORDO DI PROGRAMMA Ministero dello Sviluppo Economico – ENEA sulla Ricerca di Sistema Elettrico PIANO ANNUALE DI REALIZZAZIONE 2010 Progetto 1.3.2.a: Fissione nucleare: Metodi di analisi e verifica di progetti nucleari di generazione evolutiva ad acqua pressurizzata.

Argomenti trattati: Combustibile nucleare

Sommario

Per investigare in condizioni di alto burn-up il fenomeno indicato con PCI-SCC (Pellet Cladding Interaction-Stress Corrosion Cracking) o anche solo con PCI, dati sperimentali del il progetto PWR Super-Ramp (reattore di ricerca R2, Studsvik) sono stati analizzati con il codice TRANSURANUS. E' stato constatato che tale codice predice la rottura delle barrette in modo conservativo.

Note

Lavoro eseguito da CIRTEN, Università di Pisa, Gruppo Ricerche Nucleari San Pietro a Grado.
Obiettivo 3.1 Contratto ENEA-CIRTEN

Copia n. **In carico a:**

2			NOME			
			FIRMA			
1			NOME			
			FIRMA			
0	EMISSIONE		NOME			
			FIRMA	M. Ciotti	M.Sepielli	M. Sepielli
REV.	DESCRIZIONE	DATA		CONVALIDA	VISTO	APPROVAZIONE

CIRTEN

Consorzio **I**nteruniversitario per la **R**icerca **TE**cnologica **N**ucleare

UNIVERSITY OF PISA

San Piero a Grado Nuclear Research Group

MODELLAZIONE DEL COMBUSTIBILE NUCLEARE DURANTE RAMPE DI POTENZA: Analisi di esperimenti con codici di calcolo di comportamento del combustibile, in particolare in condizioni di alto burn-up

Autori

Federico Cantini
Martina Adorni
Francesco D'Auria

CERSE-UNIPI RL 1501/2011

PISA, Novembre 2011

Lavoro svolto in esecuzione dell'Obiettivo 3.1 Attività B1
AdP MSE−ENEA sulla Ricerca di Sistema Elettrico- Piano Annuale di Realizzazione 2010
Progetto 1.3.2.a "Fissione nucleare: Metodi di analisi e verifica di progetti nucleari di generazione evolutiva alimentati ad acqua pressurizzata"

(This page has been intentionally left blank)

Sommario

Dopo anni di residenza del combustibile in un reattore, lo spazio tra la camicia e la pasticca di combustibile può chiudersi, come risultato di diversi fenomeni che avvengono all'interno del combustibile stesso, per effetto non solo della temperatura ma anche dell'irraggiamento. In caso di aumento localizzato di potenza si possono generare tensioni circonferenziali nella camicia dovute alla differente espansione di pasticca e camicia. In presenza di proditti di fissione corrosivi (e.g. Iodio) e oltre specifici limiti di tensione, si può innescare il meccanisco della crescita della cricca dalla superficie interna della camicia. La cricca può progredire verso l'esterno, ed in certi casi può causare la rottura del combustibile stesso. Questo fenomeno è noto come "*pellet cladding interaction-stress corrosion cracking*" PCI-SCC o anche solo PCI, ed è stato identificato come problema dagli anni '70.

Per investigare questo problema, in particolare in condizioni di alto burnup, è stato selezionato il progetto sperimentale "*PWR Super-Ramp*", effettuato nel reattore di ricerca R2 di Studsvik in Svezia, per essere analizato con il codice di calcolo TRANSURANUS. I dati disponibili per simulare gli esperimenti fanno parte del database IFPE dell'OECD. Le attività hanno riguardato l'analisi dei dati sperimentali disponibili, la preparazione degli input necessari, idonei per essere utilizzati con il codice di calcolo TRANSURANUS e le analisi di sensibilità. L'obiettivo è valutare la possibilità di utilizzare il codice TRANSURANUS per combustibili ad alto burn-up.

I risultati ottenuti si sono focalizzati sui principali fenomeni che caratterizzano i test durante le rampe di potenza ed hanno mostrano che il codice TRANSURANUS predice la rottura delle barrette in modo conservativo.

Abstract

After years of normal operation in a LWR, the fuel–cladding gap may close, as a result of the several phenomena and processes due to temperature and irradiation. The Increase of local power induces circumferential stresses in the cladding because of the differential expansion of the pellet and the cladding. In presence of corrosive fission products (i.e. Iodine) and beyond specific stress threshold and level of burnup, cracks typical of stress corrosion may grow-up. The crack of the cladding may spread out from the internal surface, causing the fuel failure. This is the phenomenon called pellet cladding interaction-stress corrosion cracking PCI/SCC, or PCI. It has been idenfied as problem since the 70's.

To address this issue, the "PWR Super-Ramp" project is investigated by means of TRANSURANUS code. It comprises the data of twenty-eight (PWR Super-Ramp) fuel rods, which have been modeled and simulated through suitable input decks. The burn-up values range between 30 and 45 MWd/kgU. The database is part of the OECD/NEA "International Fuel Performance Experiments (IFPE) database". Focus is given to the main phenomena which are involved or may influence the cladding failure behavior. The selected experiment is suitable to perform the assessment of the predictive capabilities of the code models in simulating the behavior of the fuel rod of the main PWR designs up to a burnup of 45 MWd/kgU.

The results, achieved in the framework of the present agreement with CIRTEN, are analyzed giving emphasis to the main phenomena that characterize power ramp tests at high burnup. Systematic comparisons of the code results with the experimental data are performed for the parameters relevant for the PCI phenomenon. Sensitivity calculations on fission gas release models are also performed in order to address the impact of selected parameters and/or code options on the results. The analysis of the results brings to the conclusion that the code predicts the failures due to PCI conservatively in the case of PWR fuel and Zircaloy-4 cladding (for burn-up values consistent with the database). It shall be underlined that larger number of tests would be helpful to provide a more complete analysis.

The work is subdivided in six sections. The first one introduces the framework of the activity and points out the objectives. The second section provides, briefly, the main features of the considered experiment. An overview of the main model options, which have been chosen in the models preparations, is presented in section three. In section four, the attention is focused on the TU models retained relevant in PCI assessment. The results of the analysis are presented in section five for PWR Super-Ramp. In section six, the conclusions are presented. An appendix reports the boundary conditions implemented for the current analysis.

CONTENTS

Abbreviations

AR	After Ramp
BOCA	BOiling Capsules
BI	Base Irradiation phase
BIRP	BOiling CApsules (BOCA) Inter-Ramp Project
BOL	Beginning Of Life
BWR	Boiling Water Reactor
CL	Conditioning Level
CNEA	Comisiòn Nacional de Energìa Atòmica
CRP	Coordinate Research Program
C/T	Correct previsions versus total rods considered
DIMNP	Dipartimento di Ingegneria Meccanica Nucleare e della Produzione
EOL	End Of Life
F	Failed
FGR	Fission Gas Release
FRAPCON-3	“Steady state fuel rod performance code”
FP	Fission Product
Gd	Gadolinium
GRNSPG	Gruppo di Ricerca Nucleare San Piero a Grado
HBS	High burnup structure.
He3	Helium isotope 3
HPG	High Power Group
IAEA	International Atomic Energy Agency
ITU	Institute for Transuranium Elements
IFPE	International Fuel Performance
JRC	Joint Research Centre
KWU	Kraft-Wert Union
LHR	Linear Heat Rate
LPG	Low Power Group
LWR	Light Water Reactor
MIL	Mean Intercept Length
MOX	Mixed Oxide (fuel)
MTR	Material Testing Reactor
NCE	Not Conservative Error
Nd	Neodymium
NEA	Nuclear Energy Agency
NF	Non Failed
NFF	Neutron Fast Flux
NI	Not Implemented
NPP	Nuclear Power Plant
NSC	Nucelar Science Committee
OECD	Organization for Economic Co-operation and Development
PCI	Pellet-Clad l Interaction
PHWR	Pressurized Heavy Water Reactor
PIE	Post Irradiation Examination
POLIMI	Politecnico di Milano
PTI	Prior To Irradiation
PTR	Prior To Ramp
Pu	Plutonium

PWR	Pressurized Water Reactor
R2	Studsvik Research Reactor
Rx	Re-crystallized anneal
RTL	Ramp Terminal Level
RR	Ramp Rate
SCC	Stress Corrosion Cracking
SR	Cold work plus stress relief anneal
TU	TRANSURANUS
U	Uranium
UNIPI	Università di Pisa
UO2	Uranium Oxide
Zr-2	Zircaloy-2
Zr-4	Zircaloy-4
W	Westinghouse

List of figures

List of tables

1 Introductory remarks

TRANSURANUS is a computer program for the thermal and mechanical analysis of fuel rods in nuclear reactors [1][2][3]. The TRANSURANUS code consists of a clearly defined mechanical–mathematical framework into which physical models can easily be incorporated. The mechanical–mathematical concept consists of a superposition of a one-dimensional radial and axial description (the so called quasi two-dimensional or 1½-D model). The code was specifically designed for the analysis of a whole rod.

TRANSURANUS code incorporates physical models for simulating the thermal and radiation densification of the fuel, the fuel swelling, the fuel cracking and relocation, the generation of fission gases, the redistribution of oxygen and plutonium, etc. Mainly research institutions, industries and license bodies exploit the code. Besides its flexibility for fuel rod design, the TRANSURANUS code can deal with a wide range of different situations, as given in experiments, under normal, off-normal and accident conditions. The time scale of the problems to be treated may range from milliseconds to years. The code has a comprehensive material data bank for oxide, mixed oxide, carbide and nitride fuels, Zircaloy and steel claddings and several different coolants. It can be employed in two different versions: as a deterministic and as a statistical code [3].

The present report is focused on the behavior of the fuel component, with the aim to study of the PCI phenomenon during power ramp in water nuclear reactor. The relevance of PCI in nuclear technology is connected with the prevention of fuel failures due to stress corrosion cracking (SCC), involving the loss of integrity of the first and second barriers (defence in depth concepts), during normal, off normal and accident conditions.

The Studsvik Super-Ramp Project [4] investigates the failure propensity of typical LWR when subjected to power ramps, after the base irradiation. The experimental database includes 28 PWR rods and 16 BWR rods (only PWR is considered in the present analysis). The PWR rods were all tested using high ramp rates. The rods were base irradiated in a power reactor environment KK Obrigheim or BR-3. The time averaged heat ratings are mainly in the range 14-26 kW/m. The final burn-ups range from 33 to 45 MWd/kgU. The ramp tests are carried out in the research reactor R2 at Studsvik, Sweden. Pre-, during-, and post- irradiation, non destructive and destructive examinations are executed, in order to determine and understand the behavior of the fuel rods, but also to provide suitable data, useful for code validation.

1.1 Objective of the activity

The objective of this activity is the validation of TRANSURANUS code in predicting fuel and cladding behavior under pellet cladding interaction conditions using the experimental database based on PWR rods at burnup ranging from 30 to 45MWd/kgU. The main objective is pursued assessing the capabilities of the code models in simulating several phenomena and parameters such as the cladding creep down, fuel swelling, cladding outer corrosion, grain growth, etc. This analysis allows to have a cohomprensive understanding applicability and limitations of the code in verifying the fuel design as well as the analysis of the fuel behavior. Moreover, the code is also used in order to improve the understanding of the phenomena involved in the experiments as well as to check or complete the data provided with the databases. The validation is performed against PWR Super-Ramp [4]. The datasets of the Super-Ramp Project, described in sections 2.3, are part of the International Fuel Performance Experiments (IFPE) [6][7].

The experimental data are used to assess the TU capabilities in predicting phenomena related to PCI and fuel failure. The objective of the activity has been fulfilled developing twenty-eight input decks suitable for the assessment of TU code versions "v1m1j11".

1.2 Structure of the report

The work is subdivided in six sections. This first section introduces the framework of the activity and points out the objectives. The second section provides, briefly, the main features of the considered experiment. An overview of the main model options, which have been chosen in the models preparations, is presented in section three. In section four, the attention is focused on the TU models retained relevant in PCI assessment. The results of the analysis are presented in section five for PWR Super-Ramp. Section six reports the conclusions. Boundary conditions are included in appendix A.

1.3 Validation domain

The validation is performed against PWR-Studsvik Super-Ramp Project [4]. The datasets of the Project, described in section 2.3, are part of the International Fuel Performance Experiments (IFPE) [6] [7].

The validation domain of the activity is reported in Tab. 1. It includes:

- the version code used for the independent assessment;
- the main objective of the independent assessment;
- the range of parameters for which the assessment is performed;
- the parameters, part of the experimental database, which are suitable for the comparisons;
- the parameters adopted for the comparison between the experimental data and the code results.

VALIDATION DOMAIN

Main phenomenon	Experiment	No. rods	Thermal modules	Mechanical modules	FGR modules	Burn-up modules	Validation documentation
PCI/SCC	*PWR Super-Ramp*	*28*	*X*	*X*	*X*	*X*	*CERSE-UNIPI RL 1501/2011*

Range (parameters) of validity

Parameter	Unit	Values/ Descript.
Pellet material	--	**UO_2**
Cladding material	--	**Zr-2**
Enrichment	%	**3.19-8.26**
Gd content	%wt	**0-4**
Pellet outer diameter	mm	**8.19-9.14**
Diametral gap size	µm	**142-200**
Clad outer diameter	mm	**9.50-10.76**
Active length	mm	**311-977**
Initial grain size	µm	**5.5-22.0**
He filling pressure	MPa	**1.38-2.25**
Average burnup	MW_d/kg_U	**28-45**
Operative pressure	MPa	**14-14.5**
Average LHR3 (BI)	kW/m	**14-23**
Average NFF4 (BI)	10^{13} n/cm^{2}s	**3.12-8.30**
Ramp rate	kW/mh	**360-660**
Ramp Terminal Level	kW/m	**35-50.5**
LHR change	kW/m	**10-25.5**
Holding time at RTL5	hrs	**0.02-12**

Parameters for validation

#	PWR SR EXP	TU simulation
Burnup	●	X
Cladding max creep down in BI[1]	●	X
Cladding expansion in ramp (two types of measures)	●	X
Cladding corrosion after ramp	●	X
Grain size after ramp (pellet centre/pheriphery)	●	X
FGR after ramp	●	X
Elongation after ramp	○	X
Ridges height (avg. and max) in BI	●	--$
Ridges height (avg. and max) after ramp	●	--$
Clad ovality after ramp	●	--$
Inner cladding oxidation after ramp	●	--
Failure / Not Failure	●	X

● suitable for code assessment
○ limited suitability
— not suitable

1 BI: Base Irradiation
2 AR: After Ramp
3 LHR: Linear Heat Rate
4 NFF: Neutron Fast Flux (>1 MeV)
5 RTL: Ramp Terminal Level
$ Not predictable by 1½D code (outside TU code capabilities)

Tab. 1 – Validation domain of TU “v1m1j11”.

2 Description of the experiments

2.1 Introduction

The datasets, used to perform the activity, are part of the IPFE [6][7][8] database. It is the result of an OECD/NEA Project with the objective to provide a comprehensive and well-qualified database on Zircaloy clad and UO_2 fuel for models development and code validation. The data encompasses both normal and off-normal operation and include prototypic commercial irradiations as well as experiments performed in Material Testing Reactors (MTR).

The Studsvik Super-Ramp Project [4] investigated the failure propensity of typical LWR when subjected to power ramps, after the base irradiation. The experimental database includes 28 PWR rods and 16 BWR rods (only PWR is considered in the present analysis). The PWR rods were all tested using high ramp rates. On the contrary, the BWR sub-programme comprises two sets of BWR rods: one is tested at high ramp rate, and the other at slow ramp rate. In detail, the PWR Sub-programme consists of 6 groups of rods with variations in design and material parameters. The rods were base irradiated in a power reactor environment KK Obrigheim or BR-3. The time averaged heat ratings are mainly in the range 14-26 kW/m. The final burn-ups range from 33 to 45 MWd/kgU. The ramp tests are carried out in the research reactor R2 at Studsvik, Sweden.

Non-destructive and selectively detailed destructive examinations were also carried out in order to determine the fuel rod changes of typical PWR fuel when subjected to power ramps, after base irradiation to medium burn-up (28-44 MWd/kgU).

2.2 The Studsvik R2 research reactor general description

The R2 was a 50 MWth tank type Material Testing Reactor (MTR) located in Studsvik (Sweden) in operation since 1960 [9] (now decommissioned). The reactor was cooled and moderated by light water and reflected by beryllium, heavy and light water. The R2 reactor has a high neutron flux (Fig. 1) and special equipment for performing sophisticated in-pile experiments. An important feature of the R2 test reactor is that it is possible to run fuel experiments up to and beyond failure of the cladding. This is obviously not possible in a commercial power reactor. The reactor core is contained within an aluminium vessel. The vessel is 4.5 m high, 1.6 m in diameter and situated at one end of a large open pool, which also serves as storage for spent fuel elements and irradiated samples. Light water is used as reactor coolant and moderator and the design pressure is 3.3 bars. The coolant water is circulated through the reactor vessel and flows through pipes and a large decay tank below the reactor hall to an adjoining building containing pumps and heat exchangers cooled with seawater.

The components are arranged in an 8 × 10 lattice. The peripheral positions are occupied on two sides by beryllium reflector elements. In order to achieve a high thermal neutron flux; the core is surrounded on three sides by D_20. The core typically comprises 46 fuel elements of the materials test reactor (MTR) type with 18 curved plates. The assemblies are 7.9 ×8.2 cm^2 in cross-section and the fuel length is 60cm. The control rods consist of an upper neutron-absorbing section containing cadmium and a lower fuel section. They are moved vertically by drive mechanisms placed below the reactor vessel. The composition of the core can be altered to suit the experimental programme.

There are two high-pressure loops in the core (loop 1 and loop 2). These loops can be operated under either BWR or PWR pressure and temperature conditions (see Tab. 3). They are used for all irradiations under power changes, some of the base irradiations, some materials testing experiments and the in-pile corrosion experiments. Most base irradiations of test fuel, i.e. irradiations at constant

power, where fuel burn-up is accumulated under well-defined conditions, are performed in boiling capsules (BOCA rigs).

Structural materials, such as samples of Zircaloy cladding and steels for pressure vessels and vessel internals, can all be irradiated in special NaK-filled irradiation rigs with a well-controlled irradiation temperature. The position of instrumented test rigs penetrating the top lid can easily be altered. A choice of 10 positions with different neutron flux levels is available. The R2 core has an active length of 60 cm. Most fuel rods irradiated are segments of power reactor fuel rods, so-called rod lets, with lengths in the range 30-100 cm.

2.2.1 **Pool side examination**

Non-destructive examination of fuel rods can be performed in the R2 pool during short pauses in the irradiation programme or between various phases of an experiment [9]. All the handling and examinations are performed with the fuel rods in a vertical position. The general appearance of the irradiated fuel rods can be studied by visual inspection in the R2 pool. Dimensional changes, ridge formation, rod bow and creep-down can be investigated with equipment for profilometry and length measurements. The existence and location of fuel rod defects can be established by means of eddy current testing. The axial distribution of certain nuclides is determined by axial γ scanning of fuel rods or cladding samples. Data obtained before ramp tests are used as a check on the burn-up profile during the base irradiation. Data obtained after the test are used to check the power profile during the R2 irradiation and for studies of the fission product redistribution.

Neutron radiography gives as a primary result a visual picture of the interior of a fuel rod. It can be used to study the general appearance and dimensions of the fuel, the extent of filling out of pellet dishing, of centre porosities and of centre melting. This type of examination also reveals the presence of special fuel cracks, inter-pellet gaps, etc. Indications of cladding failure and of structural changes in the fuel can also be observed. In cases where there is no leakage of fission products from failed fuel rods, neutron radiography is an important tool. This is because cladding leaks are indicated by the existence of hydrides in the cladding or by the presence of water.

2.2.2 **In piles loops**

There are two pressurized in-pile light water loops simulating realistic BWR and PWR temperature and pressure conditions [9]. The loops can be used for irradiation at constant power of up to four or five test fuel rods simultaneously, and for power ramp tests of single rods. The in-pile parts of the loops are of a U-tube design. Each loop utilizes two diagonally adjacent fuel element positions in the R2 test reactor, thus providing two test positions in the R2 core. One of the legs in each loop can be used for ramp tests. The U-tube is isolated from the reactor primary coolant by a gas gap containing CO_2. A diagram of the principle of the flow of loop 1 is shown in *Fig. 1.* Water is forced to circulate through the loops by pumps and is heated electrically by external heaters before it reaches the inlet tube. After the loop, the water passes two strainers, of which one is shielded, and a cooler. Pressurization is done by a boiling tank with electrical heaters.

2.2.3 **Ramp test facility**

In the present ramp test facility the fuel rod power during the test is controlled by variation of the 3He gas pressure in a stainless steel double mini-tube coil screen which surrounds the fuel rod test section [9]. The principle of operation of this system is because 3He absorbs neutrons in proportion to its density, which can be varied as required by proper application of pressure. The efficiency of the 3He neutron absorber system makes it possible to increase test rod power by a factor of 1.8-2.2 (depending on the fissile content of the fuel). The 3He absorber system is designed to achieve a 100% power increase within 90 s, when operating with the normal pressure variation (bellows system).

In order to achieve higher power increase, the reactor power must be increased before or simultaneously with the "3He ramping". This technique with combined ramp systems is called "double-step up-ramping". The technique makes it possible to increase the test fuel rod power by a factor of about 3. Ramp rates can be achieved in the range from 0.01 W /(cm* min) to about 3000 W/(cm*min). The ramp test facility is placed in one of the in-pile loops. The power (linear heat generation rate in the fuel rod) is measured calorimetrically by the use of two inlet thermocouples, two outlet thermocouples, a Venturi flow meter and a pressure gauge. The estimated uncertainty is at 2.3% when the most common rod lengths (0.3-1.4 m) are used. For fast ramps the discrepancy between the terminal power aimed at and that obtained is less than +/- 1 kW/ m. The axial thermal neutron flux distribution is measured by activation of cobalt wires in dummy rods and by 7 scanning of the ramp tested fuel rods.

Fuel rod failures in the loops are detected by a Cherenkov-type radiation sensor, which monitors the activity of the loop coolant water. The N_{16} background activity produced in the loop coolant water is decreased by the introduction of a delay time because the Cherenkov detector is positioned in the bypass circuit. The system detects fuel rod failure after 155 +/-10 s. The moment of failure is also registered instantaneously by the rod elongation measurement system as a sudden rod contraction and also often by the power measurement system as a small thermal "spike".

2.2.4 **Boiling capsule rigs**

The boiling capsule (BOCA) [9] facility is used for irradiations at constant power where fuel burn-up is accumulated under well-defined conditions of BWR and PWR fuel rods. *Fig. 1* shows a simplified flow chart and the in-pile part of a BOCA rig. The in-pile part of a BOCA rig consists of a bare stainless steel pressure thimble containing a shroud with flow entrance ports at the bottom and exit ports at the top. The lower part of this shroud is located in the reactor core region. A fuel test rod bundle consisting up to five rodlets is located inside the shroud. The BOCA is supplied with highly purified pressurized water with controlled water chemistry from a special pressurization system. Coolant movement and cooling are maintained by natural circulation.

Up to five BOCA rigs can be operated simultaneously in the reactor. Two independent pressurization systems are available, each capable of supplying three to five BOCA rigs with water. Each BOCA rig is connected to a separate outlet circuit. In order to make it possible to irradiate power reactor fuel with standard enrichment in the inpile loops and BOCA rigs in the R2 reactor, it is often necessary to decrease the thermal neutron flux. This is achieved with hafnium absorbers in the form of tubes or plates.

2.2.5 **Neutron flux in R2 reactor**

The maximum fast (above 1 MeV) neutron flux in a BOCA rig is 1.9 x 10 14 n /(cm ^{2} s) and the maximum thermal neutron flux is 2.0 x 10 14 n /(cm ^{2} s) [9]. The neutron flux can be selected to values between 100% and 40% of the maximum neutron flux by a proper choice of core position and core loading. The hafnium shield permits a further reduction to totally about 10% of the maximum neutron flux.

The neutron flux in the PWR-BWR loop 1 is 10% higher than the flux in a BOCA rig, while the maximum flux in the BWR loop 2 is 25% lower than the maximum flux in a BOCA rig. The neutron reduction system used with the loops is the same as for the BOCA rigs, except that the core position is fixed for the loops, resulting in a total possible neutron flux reduction to about 20% of the maximum neutron flux. The neutron flux distribution is somewhat softer than in a commercial LWR.

2.3 Studsvik PWR Super-Ramp Project

2.3.1 **Objective of the experiments**

The main technical objectives of the PWR sub-programme were the following [4]:

- establish through experiments the PCI failure threshold of standard design PWR test fuel rods on fast power ramping at burnup levels exceeding 30 and preferably 40 MWd/kgU;
- investigate whether or not a change in propensity or failure mode is obtained as compared to the failure behaviour at lower burnup levels;
- establish the possible increase in PCI failure power levels for candidate PCI remedy design fuel rods at selected burnup levels.

To meet these objectives, care was taken to record the power history in detail, and to determine the fuel rod changes based on thorough pre-irradiation characterization. Non-destructive examinations prior to ramping, measurements during ramping, and non-destructive and selected destructive examinations following the ramping were executed.

2.3.2 **Rod design**

The PWR sub-programme power ramped 28 individual test fuel rods of standard as well as modified designs.

Kraftwerk Union AG/Combustion Engineering (KWU/CE), as fuel suppliers, delivered 19 rods that have been base irradiated in the power reactor at Obrigheim, Germany. The rods formed four groups with the main characteristics summarized in Tab. 4.

Westinghouse (W) as a fuel supplier delivered 9 rods following base irradiation in the BR-3 reactor at Mol, Belgium. These rods formed the two groups summarized in Tab. 5.

The test matrix of the rods is given in Tab. 6 together with average values of design parameters. Test fuel fabrication and pre-irradiation characterization are reported in different documents. The main data are summarized in Tab. 7. Test fuel rod overall design and pellet details are shown in *Fig. 2*, *Fig. 3*, *Fig. 4*, *Fig. 5*.

2.3.3 **Detail of the experiment**

The following principal activities are included in both subprograms (PWR and BWR):

- design, fabrication and characterization of experimental fuel rods featuring certain design parameter characteristics;
- base irradiations of such experimental fuel rods in power producing reactors;
- pre ramp examinations of the base irradiated fuel rods;
- power ramp irradiations and ensuing non-destructive examinations of test fuel rods in the test reactor R2 a Studsvik;
- post ramp examinations of the test fuel rods in hot cells;
- data processing, reporting of test results and compilation of observations by the organization performing the work for each segment of the work scope;

The list of the measurement quantities carried out is reported in Tab. 8**.** Information about the two phases of the experiments is hereafter summarized.

Base irradiation

The KWU/CE test fuel rods were base irradiated in the commercial pressurized water reactor Obrigheim (KWO) in Germany.

Obrigheim Reactor characteristics are given in Tab. 9. The test fuel rods were irradiated as the five middle members of seven rods, one on top of the other, which together formed a segmented fuel rod. In the segmented rods the axial positions for individual rods were: XXX/S, XXX/1, XXX/2, XXX/3, and XXX/4 starting from the bottom.

The W test fuel rods were base irradiated in the semi-commercial pressurized water reactor BR-3 at Mol, Belgium. Reactor characteristics are given in Tab. 10.

Power ramp irradiation

The power ramping of the experimental fuel rods was performed in the R-2 reactor at Studsvik in the pressurized loop n°1 with forced circulation cooling simulating PWR conditions. The facilities used for the power ramping included the loop system, a sample exchange device, a He^3-absorber system for power control, and instruments for power measurement and fission products detection.
The power ramp tests were performed according to the following typical scheme:

- conditioning phase (from the end of the base irradiation until the power ramp phase): the objective was to adjust the rod conditions to the same conditioning level for all rods, thus equalizing the starting point of the ramp tests. This is done increasing linear heat rating with slow rates until a selected value (25kW/m) and than holding at this value for 24 h;
- ramping phase: a rapid increase of linear heat rate from the conditioning level to ramp terminal level;
- a holding phase at ramp terminal level of normally 12 h or until failure was evidenced by an activity increase in the fission product detection system;

Further details about ramping are available in *Fig. 6* and Tab. 11.

Main achievement from the experiment

Two out nineteen KWU rods went to failure during the ramping phase [4]. These rods were of remedy type with large grain size.

- PK1 and PK2 (standard type, 35 and 44 MWd/kgU respectively): the rods all sustained the power ramping to power level in the range of 41 to 49 kW/m and power changes in the range of 16 to 24 kW/m without failures. The rods reveal large deformations, restructuring effects, fission gas release especially the rods of PK2 group (that has the highest burnup).
- PK4 (standard type, Gd doped, 33 MWd/kgU): the rods all sustained the power ramping to power level in the range of 39 to 50.5 kW/m and power changes in the range of 14 to 25 kW/m without failures. The rods reveal large deformations, restructuring effects, fission gas release.
- PK6 (remedy type, large grain size, 36 MWd/kgU): a failure threshold of RTL 44 kW/m and power change of 18.5 kW/m was established. The fuel restructuring was modest and the fission

gas release was low compared to the other KWU rods. Significant bonding of fuel to cladding was found for these rods.

Seven out of nine W rods went to failure during the ramping phase [4].

- PW3 (standard type, 30 MWd/kgU): a failure threshold of RTL 37.5 kW/m and power change of 12.5 kW/m was established.
- PW5 (remedy type, annular pellets, 32 MWd/kgU): the rods all failed at power level in the range of 38 to 43 kW/m and power changes in the range of 13 to 18 kW/m. Hence no improvement in the PCI/SCC resistance compared to the standard solid design was found for the annular fuel pellets with remedy cladding tested.

In *Fig. 7*, *Fig. 8* and *Fig. 9* are reported the experimental failures, not failures as a function of burnup and RTL, power change and ramp rate respectively.

Power	50 MW (thermal)	Control rods	6 Cd–U rods
Moderator–coolant	H_2O	Maximum neutron flux in experimental positions	
Reflector	Be and D_2O		
Fuel material	U_2Si_3Al	Thermal	2.4×10^{14} n cm^{-2} s^{-1}
Enrichment	19.75%	Fast (>1 MeV)	2.5×10^{14} n cm^{-2} s^{-1}
Loading	≈12 kg ^{235}U	Primary coolant flow	1300 kgs^{-1}
Type of fuel element	MTR	Inlet temperature	30–40°C
Burn-up	≈60%		

Tab. 2 – R-2 Research Reactor: general data.

Loop	1	2
Type	PWR–BWR	BWR
Pressure (bar)	30–150	30–90
Coolant temperature (°C)	220–325	220–285
Coolant flow rate (kg s^{-1})	2.5–4.0	2.5–5.0
Maximum cooling capacity (kW)	150	400
Maximum neutron flux × 10^{14} n cm^{-2} s^{-1}		
Thermal	2.2	1.5
Fast (>1 MeV)	2.0	1.4
γ heating in stainless steel (W g^{-1})	3–12	2–9

Tab. 3 – R-2 Research Reactor: in-pile loops technical data.

Group	**N° of rods**	**Type**	**Nominal burnup** (MWd/kgU)
PK1	5	Standard "A"	35
PK2	5	Standard "A"	44
PK4	4	Standard "A" plus Gd_2O_3	33
PK6	5	Remedy "G", large grain	36

Tab. 4 – PWR Super-Ramp project: KWU rods main features.

Group	**N° of rods**	**Type**	**Nominal burnup** (MWd/kgU)
PW3	5	Standard	30
PW5	4	Remedy, annular pellets	32

Tab. 5 – PWR Super-Ramp project: W rods main features.

Variables	PK1	PK2	PK4	PK6	PW3	PW5
Rod Type	Standard "A"	Standard "A"	Standard "A" +Gd_2O_3 (4 %)	Remedy "G" large grain	Standard	Remedy annular pellets
Number of Rods	5	5	4	5	5	4
Base Irradiation						
Burnup (average in axial peak position) (MWd/kg U)	33 - 36	41 - 45	33 - 34	34 - 37	28 - 31	32 - 33
Linear Heat Rating (average in axial peak postion) (KW/m)	19 - 26	17 - 25	18 - 25	20 - 27	12 - 19	9 - 21
Rod Variables						
He Fill Pressure (bar)	22.5	22.5	22.5	22.5	13.8	13.8
UO_2 Stack Length (mm)	311	318	314	315	982	977
Overall Rod Length (mm)	388	390	390	390	1135	1136
Diametral Gap (µm)	197	145	169	146	165	165
Clad Variables						
Clad Heat Treatment	See Table 3.3					
Outer Diameter (mm)	10.76	10.75	10.77	10.74	9.51	9.51
Inner Diameter (mm)	9.31	9.28	9.28	9.29	8.35	8.35
Wall Thickness (mm)	0.73	0.74	0.74	0.73	0.58	0.58
Pellet Variables						
Powder Fabrication Process[1)]	AUC	AUC	AUC	DC	ADU	ADU
Initial U-235 Content (w %)	3.2	3.21	3.19	2.99	8.26	5.74
Pellet Form	Dished	Dished	Dished	Dished	Dished	Flat
Outer Diameter (mm)	9.11	9.14	9.11	9.14	8.19	8.19
Inner Diameter (mm)	-	-	-	-	-	2.17
Ratio Length/Diameter	1.25	1.24	1.19	1.21	1.63	1.66
Density (g/cm^3)	10.36	10.34	10.30	10.42	10.32	10.40
Density Increase after Densification Test (%)	0.4	0.7	0.7	none	0.3	0.3
Pore Formers	No	No	No	Yes	No	No
Average Grain Size (µm)	6.0	5.5	5.5	22	10.5	16.9

[1)] AUC = Ammonium-Uranyl-Carbonate, DC = Direct Conversion, ADU = Ammonium-Di-Uranate

Tab. 6 – PWR Super-Ramp project: test matrix of experimental rods.

Rod Group	PK1	PK2	PK4	PK6	PW3	PW5
Powder fabrication process[1]	AUC	AUC	AUC	DC	ADU	ADU
U-235 enrichment of Uranium (w %)	3.2	3.21	3.19	2.985	8.26	5.74
Gd-concentration (w % of UO_2 + Gd_2O_3)	-	-	4.09 ± 0.05	-	-	-
Density of green pellet compact (g/cm^3)	5.5-5.8	5.60	5.60	6.98[2]		
Sintering temperature (C^0)	1710	1700	1680	1700[2]		
Sintering time (h)	2.4	2.2	18	9.7[2]		
Final pellet density (g/cm^3)	10.360 ± 0.012	10.340 ± 0.019	10.295 ± 0.01	10.42 ± 0.04	10.32[3]	10.40[3]
Thermal densification test (temperature ^0C/time (h))	1700/2.2	1700/2.2	1680/2.2	1700/2.5	1750/10	1750/10
Density increase at thermal densification test (g/cm^3)	0.04	0.07	0.07	none	0.03	0.03
Outer pellet diameter (mm)	9.110 ± 0.006	9.138 ± 0.003	9.113 ± 0.004	9.144 ± 0.008	8.19	8.19
Inner pellet diameter (mm)	-	-	-	-	-	2.17
Pellet length (mm)	11.35 ± 0.60	11.34 ± 0.40	10.799 ± 0.065	11.1 ± 0.9	13.36	13.56
Average grain size (µm)	6.0	5.5	5.5	22	10.5	16.9
O/U ratio	2.00 ± 0.01	2.00 ± 0.01	2.037 ± 0.01	2.00 ± 0.01	1.998	1.997
Portion of open porosity of overall porosity (%)	50 ± 5	55.8 ± 3.1	2.1 ± 0.7	42.8 ± 7.8	See below[4]	
Portion of open porosity of pellet volume (%)	2.7 ± 0.3	3.16 ± 0.27	0.10 ± 0.03	2.1 ± 0.4		
Moisture content in finished rod (H_2O equivalent) (ppm)	2.7	3.5	1.0	2	4.7	5.5

1) AUC = Ammonium-Uranyl-Carbonate
DC = Direct Conversion
ADU = Ammonium-Di-Uranate

2) 1700 ^0C/7.5 h in cracked NH_3 then subsequently 1710 ^0C/2.2 h in wet hydrogen

3) Calculated from pellet weights and dimensions

4)

Rod group	(Porosity % pore distribution)					
	0-1 µm	1-2 µm	2-5 µm	5-10 µm	>10 µm	Total
PW3	0.88	0.61	0.52	0.32	2.99	5.32
PW5	0.70	0.85	1.06	0.54	1.51	4.66

Tab. 7 – PWR Super-Ramp project: UO2 pellet data.

Project Supplier	Studsvik		Pre-ramp examination					Ramping		Post-ramp examination							
rod No	rod No	rod No	VI[1]	ECT[2]	PROF[3]	GSCAN[4]	NRAD[5]	ELONG[6]	F/NF[7]	NRAD[5]	ECT[2]	PROF[3]	VI[1]	FGA[8]	BU[9]	CII[10]	MET[11]	SEM[12]
PK1/1	D455	1807	x	x	x			x	NF	x	x	x		x				
2	454	1806	x	x				x	NF	x	x			x		x	x	x
3	453	1805	x	x	x			x	NF	x	x	x		x				
4	452	1804	x	x				x	NF	x	x			x				
S	456	1808	x	x				x	NF	x	x							
PK2/1	D171	1812	x	x	x	x		x	NF	x	x	x		x				
2	170	1811	x	x		x		x	NF	x	x			x	x	x	x	x
3	169	1810	x	x	x	x		x	NF	x	x	x		x			13)	
4	168	1809	x	x	x	x			NF			x		x			x	
S	172	1813	x	x	x	x		x[15]	NF	x	x	x		x				
PK4/1	D251	1664	x	x	x				NF	x	x	x		x				
2	250	1663	x	x	x				NF	x	x	x		x				
3	249	1662	x	x					NF	x	x	x		x	x	x	x	x
S	252	1665	x	x				x	NF	x	x			x		x	x	
PK6/1	D281	1669	x	x	x				F	x	x	x	x					
2	280	1668	x	x	x				NF	x	x	x		x				
3	279	1667	x	x					NF	x	x	x		x		x	x	x
4	278	1666	x	x				x[15]	F		x		x					
S	282	1670	x	x				x	NF	x	x			x				
PW3/1	12-1	1731	x						F				x					
2	07-1	1732	x	x	x				NF	x	x	x		x				
3	10-1	1733	x						NF	x	x			x		x	x	x
4	21-1	1734	x	x	x	x			F		x	x	x		x		x	
S	14-1	1938	x						F									
PW5/1	04-8	1735	x	x			x		F		x		x					
2	09-8	1737	x	x		x	x		F	x	x		x		x			
3	02-8	1738	x	x	x		x		F		x	x	x			x	x[14]	x
4	07-8	1736	x	x	x		x		F		x	x	x					

1) VI = Visual Examination
2) ECT = Eddy Current Testing
3) PROF = Profilometry
4) GSCAN = Gamma-Scanning
5) NRAD = Neutron Radiography
6) ELONG = Rod elongation
7) F = Failure, NF = No Failure
8) FGA = Fission Gas Analysis
9) BU = Burnup Determination
10) CII = Clad Inside Inspection
11) MET = Metallography
12) SEM = Scanning Electron Microscopy
13) Met also of an additional sample from base irradiated, not ramped rc
14) Three MET performed
15) The elongation detector did not work

Tab. 8 – PWR Super-Ramp project: Project measurement schedule.

Characteristic at 100% reactor power	Obrighein power reactor
Average reactor thermal power	1045 MWth
Average rod power (linear heat rate)	17.1 kW/m
Coolant temperature at core inlet	283 °C
Coolant temperature at core outlet	312 °C
Coolant velocity at 300°C	3.39 m/s
Mass flow rate	6833 kg/s
Average system pressure	14.5 MPa
Active length of core	2.65 m

Tab. 9 – PWR Super-Ramp project: Obrighein reactor main data (KWU rods base irradiation).

Characteristic at 100% reactor power	BR-3 power reactor
Average reactor thermal power	40.9 MWth
Coolant temperature at core inlet	252-257 °C
Coolant temperature at core outlet	264-269 °C
Mass flow rate	9.4 kg/s
Average system pressure	14.0 MPa
Active lenght of core	1.00 m

Tab. 10 – PWR Super-Ramp project: BR-3 power reactor main data (W rods base irradiation).

Rod group	Rod Label	Conditioning terminal level [W/m]	Hold time of conditioning [h]	Ramp Terminal level [W/m]	Ramp rate [W/mh]	Hold time at RTL [min]
PK1	PK1/1	25	24	41.5	540	720
	PK1/2	25	24	44	480	720
	PK1/3	25	24	47.5	510	720
	PK1/4	25	24	47.5	570	720
	PK1/S	25	24	42	360	720
PK2	PK2/1	25	24	41	510	720
	PK2/2	25	24	46	570	720
	PK2/3	25	24	49	510	720
	PK2/4	25	24	44	510	1
	PK2/S	25	24	44	510	720
PK4	PK4/1	25	24	39	480 *	720
	PK4/2	25	24	44.5	510	720
	PK4/3	25	24	50.5	660	720
	PK4/S	25	24**	43	510	720
PK6	PK6/1	25	24	45	540	55
	PK6/2	25	24	40	540	720
	PK6/3	25	24	43	540	720
	PK6/4	25	24	44	600	60
	PK6/S	25	24	41	600	720
PW3	PW3/1	25	24	40	600	22
	PW3/4	25	24	37.7	540	12
	PW3/S	25	24	40.5	600	17
PW5	PW5/1	25	24	42.7	540	118
	PW5/2	25	24***	40.3	540	26
	PW5/3	25	24	38.2	540	38
	PW5/4	25	24	38	510	72

* Ramp rate was 120 W/mh in the range 25 / 28.5 W/m
** Conditioning time was 26 hours than it was stopped and resumed for 13 hours
*** Conditioning time was 23 hours than it was stopped and resumed for 7 hours

Tab. 11 – PWR Super-Ramp project: Ramping data.

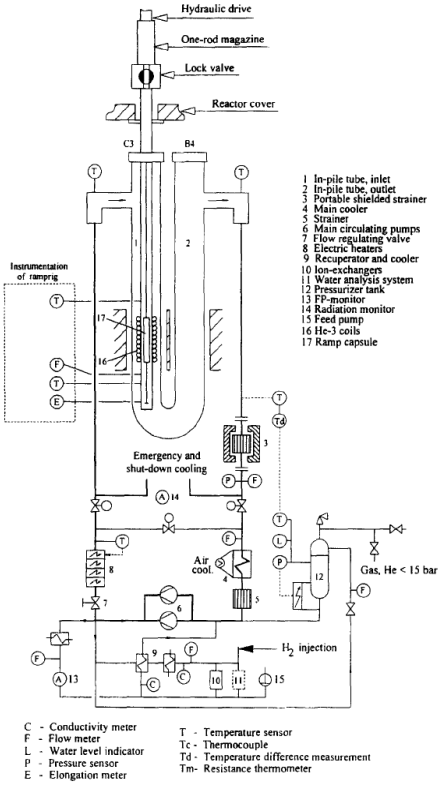

(a) Diagram of loop 1: simplified flow chart with ramp test rig.

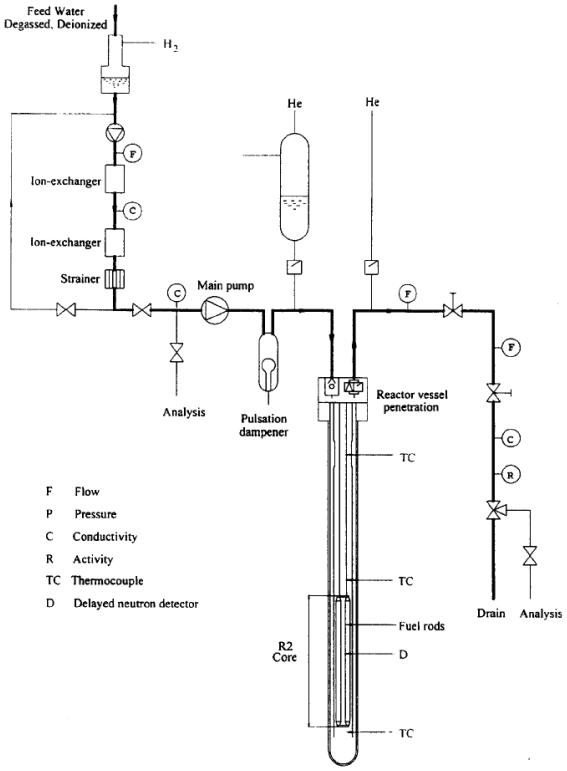

(b) BOCA rig: simplified flow chart showing in pile part.

Fig. 1 – The Studsvik R2 Research Reactor.

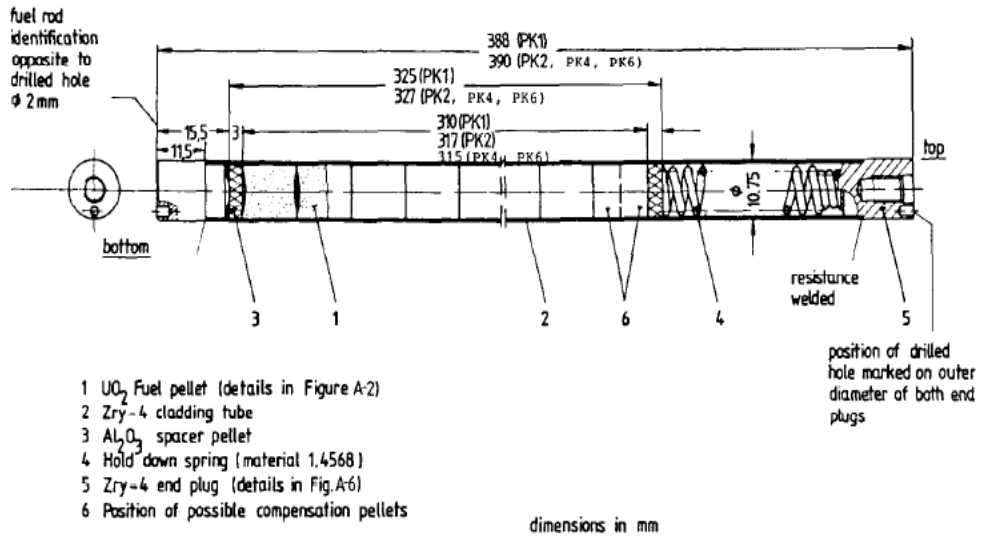

Fig. 2 – PWR Super-Ramp project: overall design of the KWU test fuel rod.

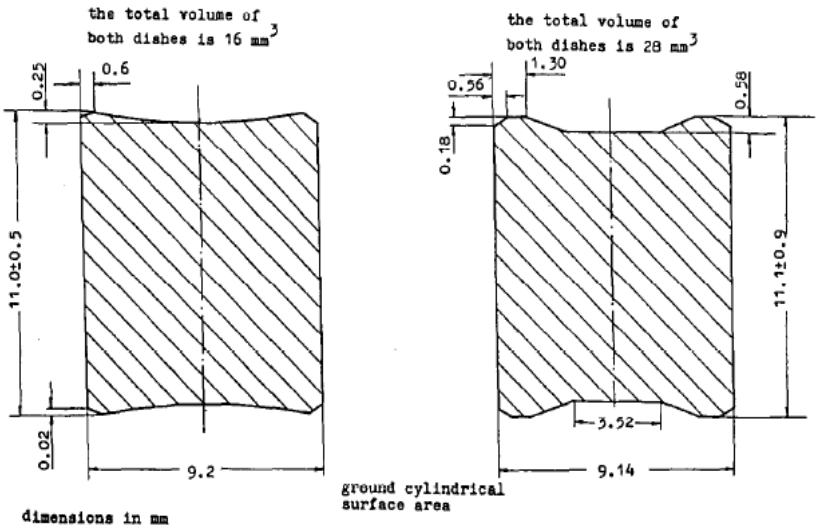

A. UO_2 Fuel Pellet (PK1, PK2),
UO_2/Gd_2O_3 Fuel Pellet (PK4)

B. UO_2 Fuel Pellet (PK6)

Figure 3.2 KWU/CE Test Fuel Pellet Design.

Fig. 3 – PWR Super-Ramp project: KWU test fuel, pellet design.

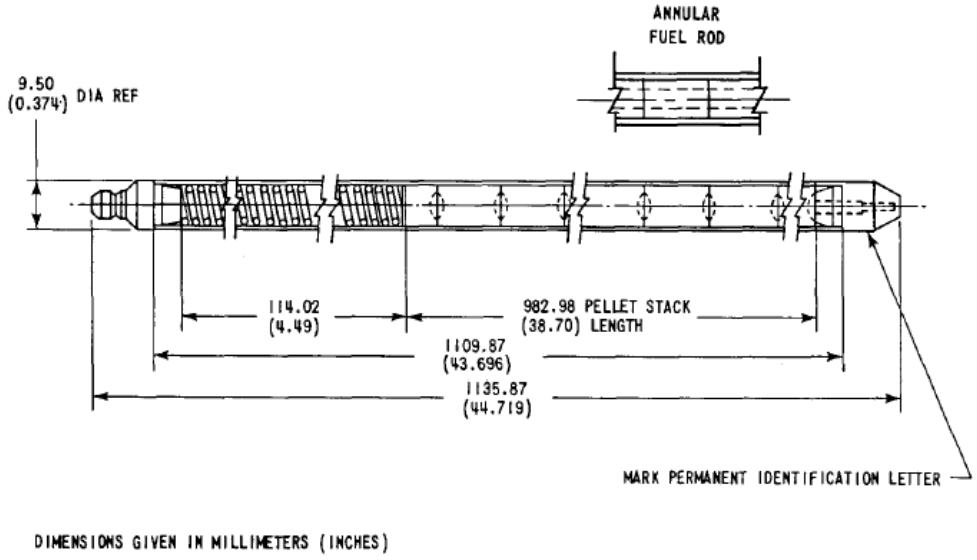

Fig. 4 – PWR Super-Ramp project: W test fuel rod: overall design.

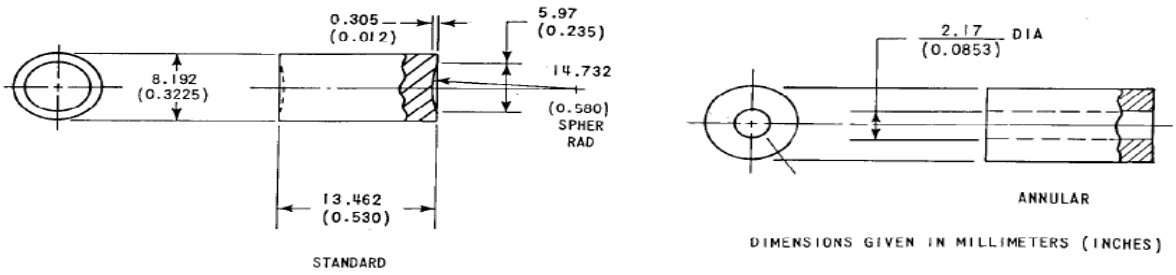

Fig. 5 – PWR Super-Ramp project: W test fuel, pellet design.

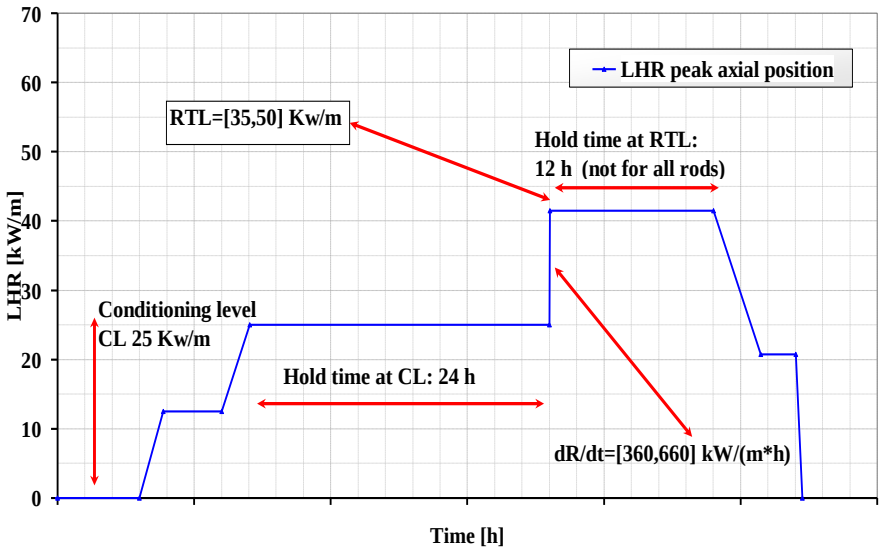

Fig. 6 – PWR Super-Ramp project: outline of the ramping phases.

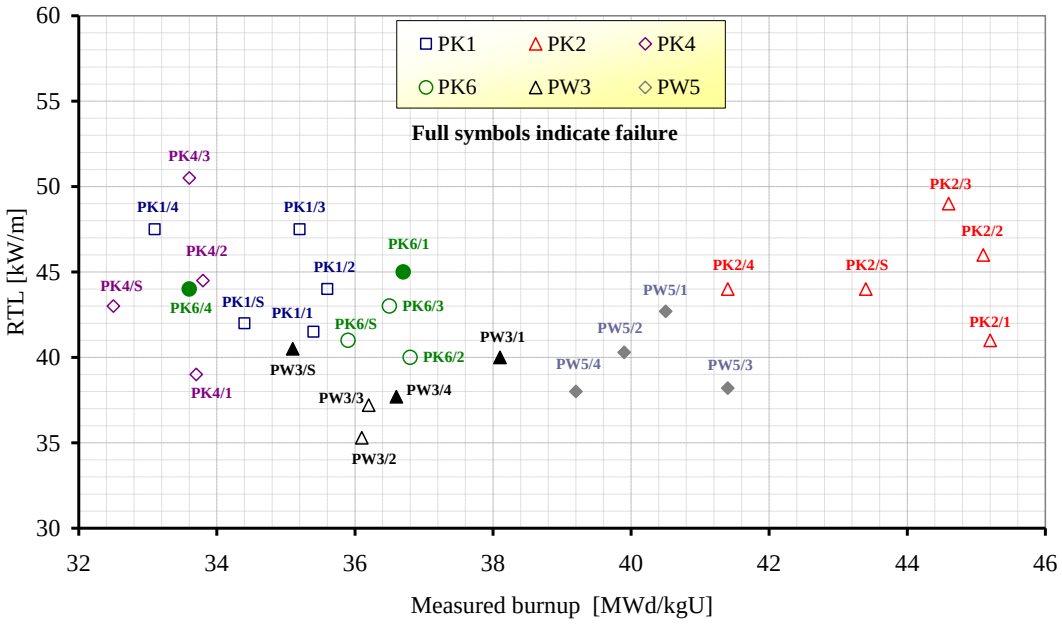

Fig. 7 – PWR Super-Ramp: experimental failures as function of burnup and RTL.

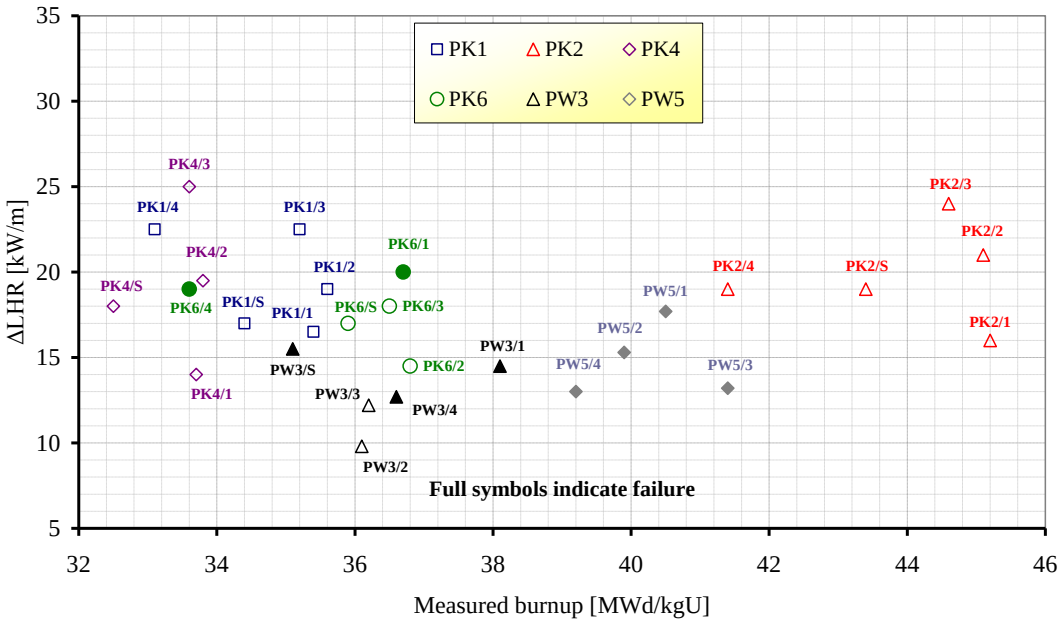

Fig. 8 – PWR Super-Ramp: experimental failures as function of burnup and power change.

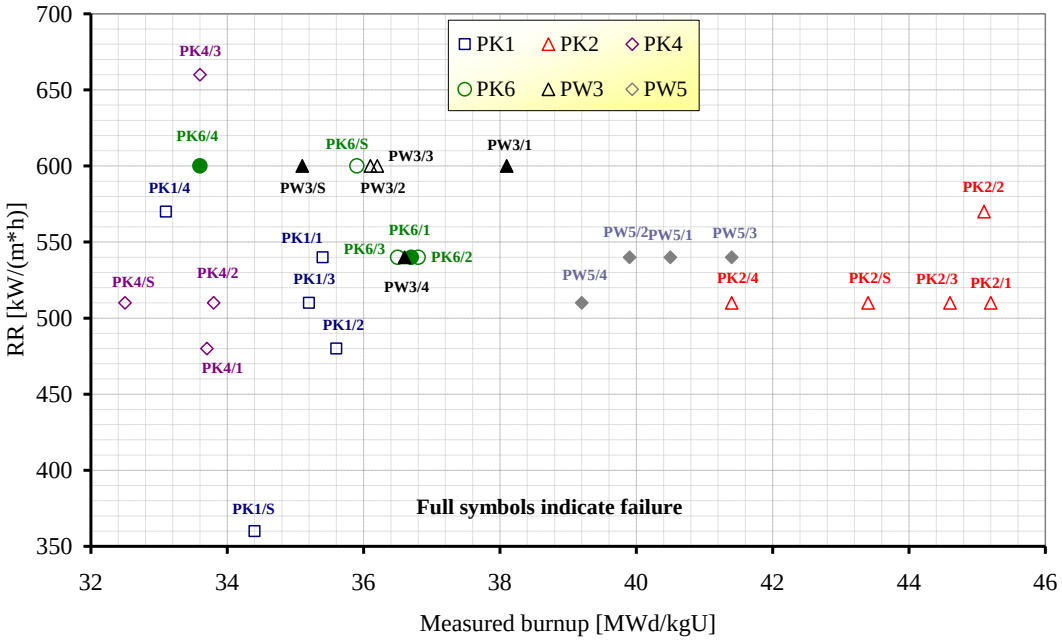

Fig. 9 – PWR Super-Ramp: experimental failures as function of burnup and ramp rate.

3 Development and setup of the TRANSURANUS models

3.1 Studsvik PWR Super-Ramp Project

The activity is performed using TRANSURANUS code, version "v1m1j11", with the deterministic option, steady state thermal and mechanical analysis. The version of the manual is "v1m1j06". The boundary conditions were prepared using a program written in PERL language.

3.1.1 **Description of the input decks**

Input decks were prepared for 19/19 KraftWerk Union AG/Combustion Engineering (KWU/CE) rods and for 7/9 Westinghouse (W) fuel rods. Two W rods, PW3/2 and PW3/3, are not modeled because ASCII data were not in agreement with experimental specifications. In particular, ASCII data showed a ramp terminal level grater than the experimental ramp specifications reported in Tab 3.9 of STIR 32 report [4].

The reference input deck for KWU rods is reported in Appendix B for rod PK1/1; the reference input deck for W rods is obtained starting from the KWU reference input. The input deck has been prepared respecting the information available in the code manual [3]. The models selected are generally the ones standard for the transient to be simulated. Only the active part of the fuel is accounted for the simulation. The active part has been divided into 3 axial slices of different length for KWU rods and into 6 axial slices of different length for W rods, according to the experimental data available [6]. For the reference calculations, the nominal geometrical values were used when available, the measured values are considered when nominal values are not specified (gas plenum length). The input deck of each rod within KWU group differs from the others in:

- boundary conditions: burnup, linear heat rate, ramp terminal level, cladding temperature histories;
- geometry: pellet diameter, cladding inner and outer diameter, gas plenum length;
- physical proprieties: enrichment, UO_2 grain size (PK6 rods are of large grain size), gadolinium content (PK4 rods contain Gadolinia), porosity.

The input deck of each rod within W group differs from the others in:

- boundary conditions: burnup, linear heat rate, ramp terminal level, ramp rate, clad temperature histories;
- geometry: pellet diameter, cladding inner and outer diameter, gas plenum length, kind of pellet standard (PW3 are standard while PW5 are annular);
- physical proprieties: enrichment, UO_2 grain size, porosity.

The KWU rods differ from W rods principally in:

- base irradiation performed into two different reactors.
- fuel rods height: W rods are about three times longer than KWU rods.

Summaries of the main data distinguishing the different inputs are reported from Tab. 12 to Tab. 15.

Group label	Rod No	Rod Label	Gas plenum length [mm]	Clad outer diam. [mm](1)	Clad Inner diam. [mm](1)	Pellet outer diam. [mm](2)	Pellet inner diam. [mm](2)	Clad grain size [µm](3)	UO2 grain size [µm](2)	Gd_2O_3 content [w%](2)	U235 enrich. [w%](2)
PK1	1	PK1/1	32.0	10.76	9.31	9.110	0	10.5	6	0	3.2
	2	PK1/2	32.2								
	3	PK1/3	32.4								
	4	PK1/4	32.3								
	5	PK1/S	32.1								
PK2	6	PK2/1	32.6	10.75	9.28	9.138	0	9.5	5.5	0	3.21
	7	PK2/2	33.0								
	8	PK2/3	32.5								
	9	PK2/4	32.6								
	10	PK2/S	32.8								
PK4	11	PK4/1	32.4	10.77	9.28	9.113	0	9.5	5.5	$4.09^{+/-0.05}$	3.19
	12	PK4/2	32.8								
	13	PK4/3	32.4								
	14	PK4/S	32.8								
PK6	15	PK6/1	33.1	10.74	9.29	9.144	0	12.0	22	0	2.985
	16	PK6/2	32.5								
	17	PK6/3	33.0								
	18	PK6/4	33.0								
	19	PK6/S	32.9								
PW3	20	PW3/1	117.78	9.51	8.35	8.19	0		10.5	0	8.26
	21	PW3/2	119.32								
	22	PW3/3	118.66								
	23	PW3/4	104.90								
	24	PW3/S	116.48								
PW5	25	PW5/1	120.94	9.51	8.35	8.19	2.17		16.9	0	5.74
	26	PW5/2	121.36								
	27	PW5/3	121.48								
	28	PW5/4	121.88								

(1) From table 3.1 of STIR report
(2) From table 3.2 of STIR report
(3) From table 3.3 of STIR report
(4) From table 3.4 of STIR report

Tab. 12 – PWR Super-Ramp: main fuel rods data.

Group label	Nominal Burn-up [MWd/kgU]
PK1	25
PK2	44
PK4	33
PK6	36
PW3	30
PW5	32

Tab. 13 – PWR Super-Ramp: nominal burn-up.

Group label	Slice 1 Height [mm]	Slice 2 Height [mm]	Slice 3 Height [mm]
PK1 PK2 PK4	104	80	128
PK6	90	80	145

Tab. 14 – PWR Super-Ramp: slices height for KWU rods.

Rod label	Slice 1 Height [mm]	Slice 2 Height [mm]	Slice 3 Height [mm]	Slice 4 Height [mm]	Slice 5 Height [mm]	Slice 6 Height [mm]
PW3/1	169	169	13	209	209	209
PW3/4	171	171	13	211	211	211
PW3/S	170	170	14	209	209	209
PW5 group	169	169	14	208	208	208

Tab. 15 – PWR Super-Ramp: slices height for W rods.

3.1.2 **Selection of the boundary conditions**

The boundary conditions implemented for the analysis are:

- linear heat rate at 3 or 6 axial position;
- cladding temperature histories at same position of linear heat rate;
- fast neutron flux (>1 MeV);
- pressure.

Linear heat rate (LHR) and temperatures are those at the given time which have been constant over the interval time step, i.e. the data are in histogram format. The rate of increase/decrease between different constant linear heat rate spans has been selected as 6 kW/ (m*h). Inclination between two values of constant linear heat rate is calculated on the basis only of the peak linear heat rate position. In case of step too small to apply the above-mentioned method, the measured slope of the database is implemened.

The power ramp has been "constructed" according to ASCII files, together with Table 3.9 of STIR 32 report, i.e. considering the ASCII files using the selected "6 kW/(m*h)" except for the ramp in which the rate, the conditioning time and ramp hold time have been taken directly from Table 3.9 of STIR 32 report. These data are summarized in Tab. 11. According with ITU inputs the duration of the ramp is prolonged beyond the ASCII data if the final temperature at the end of irradiation is not 20° C (cold conditions). This hypotesys is necessary in order to compare the experimental measures (executed in cold conditions) with the calculated.

Comparisons between different sources for LHR history in base irradiation and in ramp are reported in *Fig. 10* and *Fig. 11* for rod PK2/3 as example.

Comparisons between different sources for temperature history in base irradiation and in ramp are reported in *Fig. 12* and *Fig. 13* for rod PK2/3 as example. Details of the LHR boundary conditions are reported in Appendix **A** (*Fig. A - 1* to *Fig. A - 25*).

Fast neutron fluence in base irradiation (KWU rods) was available from Table 3.7 of STIR32 Report. According to these data, average fast neutron flux was calculated considering the time of the end of base irradiation. For W rods, Table 3.8 of STIR 32 Report gives neutron fast flux average value at each base irradiation cycle, a weighted average value between those data is implemented in TU code.

Finally, a pressure of 14.5 MPa has been selected for KWU rods while 14.0 MPa has been selected for W rods. The choice of those values respects the experimental base irradiations conditions.

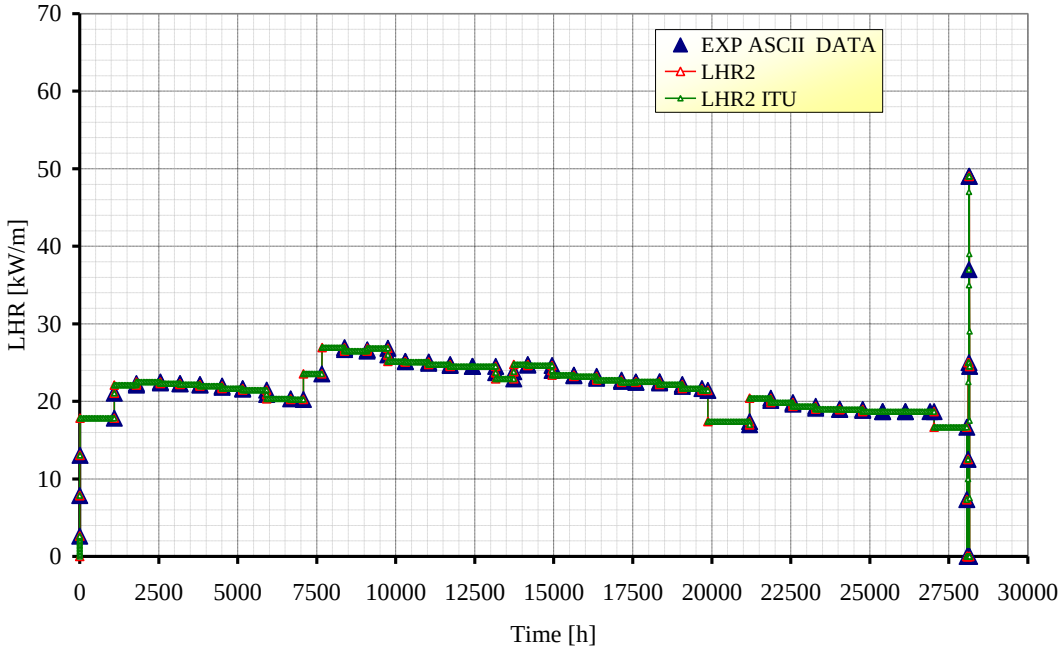

Fig. 10 – PWR Super-Ramp (rod PK2/3), base irradiation: maximum axial LHR.

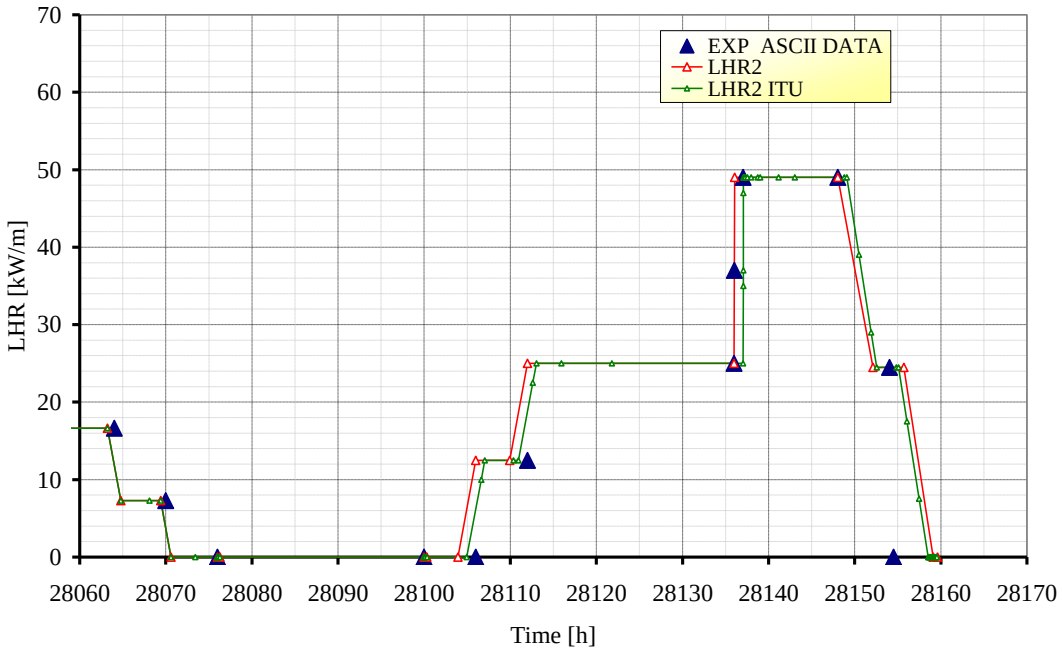

Fig. 11 – PWR Super-Ramp (rod PK2/3), power ramp: maximum axial LHR.

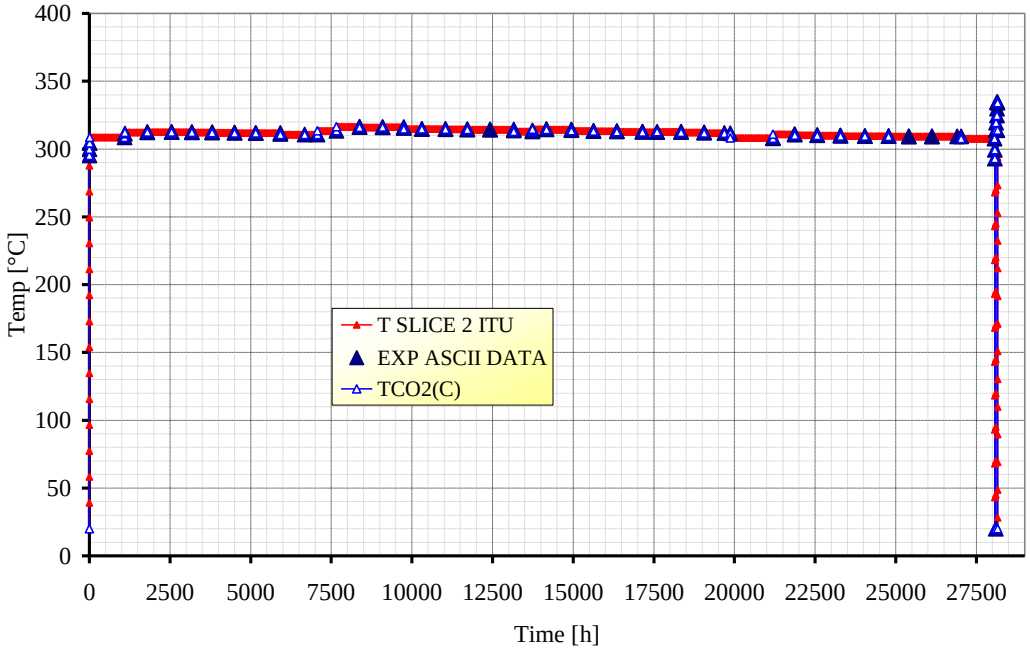

Fig. 12 – PWR Super-Ramp (rod PK2/3), base irradiation: maximum axial external cladding temperature.

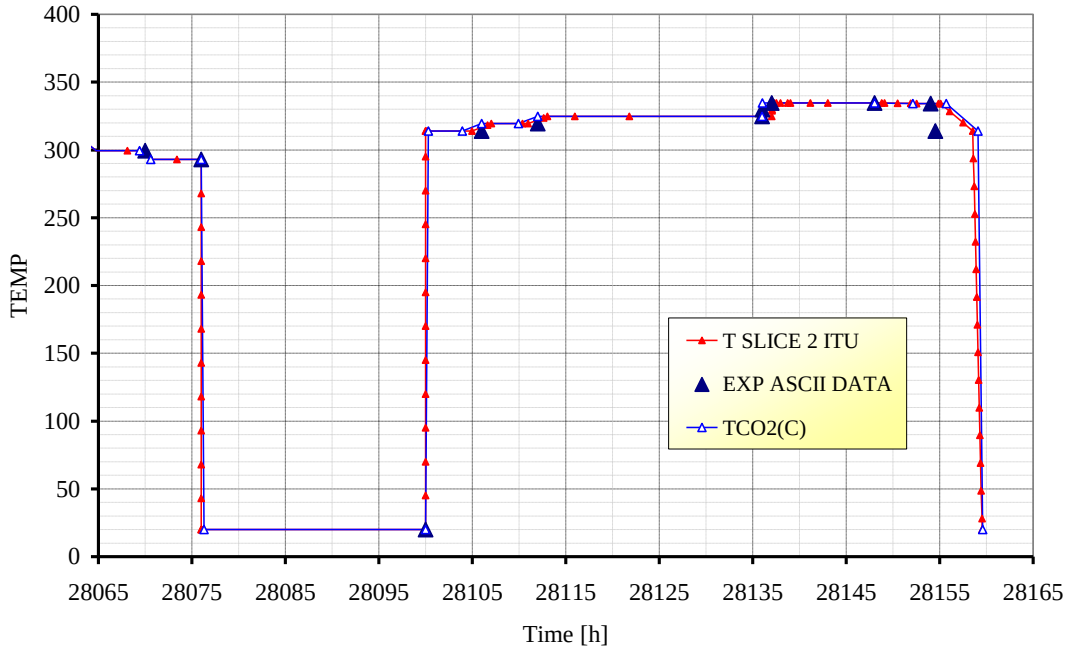

Fig. 13 – PWR Super-Ramp (rod PK2/3), power ramp: maximum axial external cladding temperature.

4 Fuel cladding failures under power ramp conditions by PCI

During irradiation, fuel-cladding gap size may close giving rise to an inversion of the tensional state in the tangential direction within the cladding [13][14][15]. This is due to the differential thermal expansion between fuel and cladding, the external pressure load applied to the cladding, the gaseous-solid FP formation and swelling in the fuel and the temperature gradient in the fuel that is responsible for the typical hour-glassing shape of the pellets. Prolonged PCI can lead to a cladding local permanent deformation called ridge. Primary ridges appear in the contact surfaces between the deformed pellet (the hourglass pellet ends) and the cladding. PCI is influenced by fuel behavior, cladding behavior, gap behavior and external imposed conditions.

During power ramps, PCI conditions are often reached and the results may be the cladding failure due to PCI\SCC mechanism. Cladding failure is dependent from conditions related to the irradiation history and to conditions related to the perturbation. PCI/SCC consists on: cracks formation (caused by PCI), cracks dimensional increase (caused by iodine chemical attack), and crack propagation trough the cladding (influenced by thermo-mechanical conditions and crack dimensions).

4.1 Phenomena and parameters relevant to PCI

Several external conditions and intrinsic material properties influence PCI. In this classification, fuel, gap, and cladding should not be treated separately because of the large unlinearities of the phenomena involved.

The main phenomena/parameters that influence PCI directly related to the pellet are:

- swelling (solid and gaseous);
- densification;
- relocation;
- thermal conductivity;
- grain growth;
- fuel initial grain size;
- fuel density.

The main phenomena/parameters that influence PCI directly related to the gap are:

- gap conductance;
- gap initial size.

The main phenomena/parameters that influence PCI directly related to the cladding are:

- creep;
- swelling;
- cladding thermal conductivity.

4.2 Parameters relevant for fuel cladding failure under power ramp conditions

During power ramps after a burnup threshold is overpassed, PCI conditions may be reached. The most important parameters that influence cladding failure due to PCI/SCC related to time prior irradiation or irradiation history are:

- initial cladding elastic and plastic fields;
- fuel central temperature evolution;
- long time PCI conditions occurred previous ramp (if applicable);
- burn-up;
- fission gas release;
- iodine release;
- linear heat rate during irradiation (maximum and average values);
- local neutron fast flux during irradiation (particularly in the peak axial position);
- cladding outer corrosion;
- cladding inner corrosion.

External conditions that influence cladding failure related to the perturbation caused by the power ramps are:

- ramp rate;
- ramp terminal level;
- linear heat rate change during ramp;
- ramp terminal level duration;
- axial form factor of LHR during the ramp.

4.3 Outline of relevant TU code options

This section is reported, for sake of completeness, on the basis of the information available in TU manual (Ref. [3]).

4.3.1 Fuel conductivity correlations for LWRs with UO_2 fuel

According with the TU manual [3] the fuel conductivity correlations, suitable for the implementation in the fuel rod performance codes have two contributions, both temperature dependent:

- conduction through lattice vibrations (phononic term): $\lambda_{phonon}=1/(a+bT)$ where a, b are constant and T is temperature [K]. It is the dominant contribute at lower temperatures
- conduction through free electrons: $\lambda_{electronic}= c*T^3$ where c is a constant or $\lambda_{electronic}=(c_1/T^2)*e^{d/T}$ where c_1 and d are constants. It contributes at high temperatures.

Beside the dependence on the temperature, the thermal conductivity of UO_2 depends on the porosity (P), the oxygen to metal ratio O/M (stoichiometry) and the burn-up.

- Porosity in a ceramic material invariably decreases the thermal conductivity. In general the effect of porosity is taken into account by a correction factor (fp): $\lambda(P) = \lambda_{100}*fp$. In which λ_{100} is intended conductivity at 100% dense material.

- Hypo- and hyper-stoichiometric fuel has a lower thermal conductivity that stoichiometric fuel. It is taken into account as a corrective factor proportional to the deviation x to the stoichiometric value 2 in the form: a_x*x where a_x is a constant.
- The introduction of solid FPs and the formation of fission gas bubbles decrease the thermal conductivity λ so the burn-up effect is degradation of fuel conductivity proportional to the burn-up.

Recently, a new dependence of λ was found which results from an obviously structural change of the UO_2 fuel near the surface at high burn-up, the so-called "High Burnup Structure" (HBS). It acts as a heat transfer barrier due the Pu radial redistribution. It is a not completely clear mechanism that occurs beyond 68 MW/kgU (this value is intended a local value).

In TU there are several correlations for simulating LWRs UO_2 fuel conductivity: correlations 18, 19, 20 (old standard), 21 (new standard), 22, 23, 24, 28. They are implemented by the option MODFUEL(j=6).

Reference correlation implemented (correlation 21)
The correlation implemented is the new standard correlation 21. It has been fitted to data from ITU[°][3]. The correlation takes into account the High Burnup Structure (HBS), as well as the influence of gadolinium.

$$\lambda = \{1/(a+a_1*bu+a_2*Gd+b_1*bu*Tp+b_2*Gd*Tp+b*T) + (c/T^2)*e^{d/T}\}*(1-P)^{2.5} \quad \text{Eq. 1}$$

[W/mK]

where:
a, a_1, a_2, b, b_1, b_2, c, d are constants
bu is the local burnup [MWd/kgU]
Gd is the the local gadolinium content [%w]
T is the the local absolute temperature [K]
Tp is defined as min (1923,T)
P is the local porosity.

The term b_1*bu*Tp takes into account HBS; the first expression accounts also for phononic term and burnup effect, the second considers conduction by mean of free electron and, finally, they are multiplied by a factor that simulates porosity effects.

4.3.2 Fuel swelling correlations for LWRs with UO_2 fuel

Swelling is defined as the fractional increase in the volume of the solid with respect to the initial volume Vo of the as-fabricated fuel [3], or by:

$$[\Delta V/V](t) = (V(t) - Vo)/Vo \quad \text{Eq. 2}$$

Fuel swelling take into account of two terms: solid swelling and gaseous swelling:

$$\Delta V/V = (\Delta V/V)^{sol} + (\Delta V/V)^{gas} \quad \text{Eq. 3}$$

the fractional increase in the volume due to swelling is expressed via swelling strains $\varepsilon_{swe,i}$ (i = r, t, a = radial, tangential, axial):

$$\varepsilon_{swe,i}(t) = \varepsilon_{swe,i}(t0) + \Delta\varepsilon_{swe,i}tot \quad \text{Eq. 4}$$

$$\Delta\varepsilon_{swe,i}^{tot} = f[\Delta(\Delta V/V)] \quad \text{Eq. 5}$$

With f = 1/3 if the swelling rate can be considered isotropic.

There are several correlations in TU for considering the fuel swelling for LWRs. They are: correlations 18, 19, 20 (recommended), 21. They are selected by mean of the option MODFUEL(j=4).

Reference correlation implemented (correlation 20)
The correlation implemented is the standard correlation 20 developed by K. Lassmann [3] from correlation 19 in which gaseous swelling contribute was modified and integrated from this steady state equation:

$$(\Delta V/V)^{gas} = c*a(T)/k *(1-e^{-k*bu}) \quad \text{Eq. 6}$$

where:
$(\Delta V/V)^{gas}$ fractional gaseous swelling
c, a(T), k are model parameters (c depends on stress, a from temperature)

Integration of previous equation is done in this manner:

$$\Delta(\Delta V/V)^{gas} = \Delta(\Delta V/V)^{gas}_{max} * (1-e^{\Delta t/\tau}) \quad \text{Eq. 7}$$

where:
$\Delta(\Delta V/V)^{gas}$ increment of fractional increase in volume due to gaseous FPs in a time step with a burnup increment Δbu
$\Delta(\Delta V/V)^{gas}_{max}$ is defined as $\Delta(\Delta V/V)^{gas}_{max} = (\Delta V/V)^{gas}_{n+1} - (\Delta V/V)^{gas}_{n}$
n,n+1 are related respectively to time t_n and time t_{n+1}
τ is the time constant = 1/D
D is the diffusion coefficient.

Solid swelling was considered as follow:

$$\Delta(\Delta V/V)^{sol} = B*\Delta bu \quad \text{Eq. 8}$$

where:
Δbu is the burnup increment during time step $\Delta t = t^{n+1} - t^n$
$\Delta(\Delta V/V)^{sol}$ is the increment of fractional increase in volume due to solid FPs in a time step with a burnup increment Δbu
B is a model parameter.

4.3.3 **Fuel pellet fragments relocation models for LWRs**

Pellet cracking and relocation can be separated into two mechanisms [3][16]:

- mechanism1: the elastic strain prior to cracking is redistributed, i.e. the pellet volume increases and the stress level in the pellet are reduced.
- mechanism2: depending on the geometrical details of the rod, e.g. the gap size, relocation (i.e. a gross movement of fuel fragments), occurs.

Detailed models based on first principles in mechanics are available for mechanism1, whereas the mechanism2 by its nature can be treated only empirically. Unfortunately, in most situations, the second mechanism is by far the most important and this is the reason of the big uncertainties encountered in simulating relocation. The most important models correlate the radial relocation with the as fabricated gap size g_o and the linear power q. In some cases, burnup dependence is also considered. There are six relocation models for LWRs available in TU [3]: IRELOC 2, 3, 4, 5, 6, 8. The ITU recommended models are IRELOC 8 and IRELOC 5.

Reference model implemented

The reference model implemented is IRELOC 5, the modified KWU-LWR model, ITU calibration 1997. This model calculates relocation increment according with the simple FEMAXI correlation [16]:

$$u^{rel} = 0.3 * g_o \qquad \text{Eq. 9}$$

where

g_o is the as fabricated gap size normalized to the as fabricated pellet outer radius

$u^{rel}_{\ o}$ is the radial deformation at outer surface of the fuel due to radial relocation

This model applies once at the beginning of the calculation, the axial relocation is also considered as dependent by the ratio free volume/total pellet volume, the axial forces and the radial relocation. This option is strictly correlated with the number of cracks (NCRACK input variable); as usual, this number range between 4-6 (recommended range).

4.3.4 **Fuel grain growth: reference model implemented**

Fuel grain growth is treated in TU code by one model only [3]:

- *IGRNSZ 0:* No grain growth considered.
- *IGRNSZ 1*: Grain growth model according with Ainscough and Olsen theory (standard option).

In this activity grain growth is considered, the model is developed according to Ainscough equation:

$$dR_{gr}/dt = k[(1/R_{gr}) + (1/R_{MAX})] \qquad \text{Eq. 10}$$

where:

R_{gr} is mean grain radius

R_{MAX} is the maximum radius at which the growth stops

k is the grain growth rate (m^2/s), which is dependent from radial temperature distribution in the pellet.

4.3.5 **Fission gas release models**

FGR phenomenon is addressed in Ref [17]. The equations to be solved are [3]:

- to simulates intragranular behavior (grain matrix):

$$\partial Cs/\partial t = D\cdot[\partial 2Cs/\partial r2 + (2/r)\cdot\partial Cs/\partial r] - g\cdot Cs + b\cdot Cb + \beta \quad \text{Eq. 11}$$

$$\partial Cb/\partial t = g\cdot Cs - b\cdot Cb \quad \text{Eq. 12}$$

where:

$D(t)$ is the gas atom diffusion coefficient;
$C_s(r,t)$ is the local concentrations of gas in solution in the fuel matrix;
$C_b(r,t)$ is the local concentrations of gas in solution in bubbles;
g is the probability per unit time of gas atoms in solution being captured by a bubble;
b is the probability per unit time of gas atom in bubble being re-dissolved to the matrix;
$\beta(t)$ is the rate at which gas is produced.

- to simulates intergranular behavior (grain boundary):

$$C^{sat}_{gb} = [4\cdot r\cdot f(\theta)\cdot f_c/(3\cdot k\cdot T\sin 2\Theta)]\cdot(2\cdot\gamma/r + P_{ext}) \quad \text{Eq. 13}$$

where:

C^{sat}_{gb} is the number of gas atoms per unit area of grain boundary;
r is the bubble radius;
$f(\theta)$ is a factor that considers that the bubbles are lenticular-shape and not spherical;
f_c represents the fraction of grain face area occupied by bubbles;
k is the Boltzamann constant;
T is temperature
$2\cdot\Theta$ is the angle under which the lenticular bubble meets the grain boundary
P_{ext} is the external pressure.

In TU code the choice of the diffusion coefficient to simulate the intragranular behavior is performed by three options selected by the keyword FGRMOD.

- *FGRMOD 4* selects the URGAS algorithm with the diffusion coefficients of Hj. Matzke (thermal) and a-thermal diffusion coefficient according to data of R. White. This model option should be used together with an option for an intragranular fission gas release model (IGRBDM).
- *FGRMOD 6* selects the URGAS algorithm with the diffusion coefficients of Hj. Matzke (thermal) and a constant a-thermal diffusion coefficient. This model option should be used together with an option for an intragranular fission gas release model (grain boundary model grbdm1 or grbdm2). This model is the recommended TRANSURANUS model.
- *FGRMOD 9* selects the URGAS algorithm with diffusion coefficients of T. Turnbull. This model option should be used together with an option for an intragranular fission gas release model (grain boundary model grbdm1 or grbdm2).

The options for treating the FGR behavior at the grain boundary (intergranular equation) available in TU are four and are selected by the keyword IGRBDM:

- *IGRBDM 0:* Fission gas behavior at grain boundaries not treated
- *IGRBDM 1:* Simple grain boundary fission gas behavior model (standard option)
- *IGRBDM 2:* Simple grain boundary fission gas behavior model
- *IGRBDM 3:* New model developed according to modified Koo model for ramps simulations

Finally there are seven options for the selection of the algorithm by which the diffusion equation is solved (selected by the keyword IDIFSOLV):

IDIFSOLV 0: Diffusion equation is solved by the URGAS-algorithm
IDIFSOLV 1: Diffusion equation is solved by the FORMAS-algorithm with 1 exponential term
IDIFSOLV 2: Diffusion equation is solved by the FORMAS-algorithm with 2 exponential terms
IDIFSOLV 3: Diffusion equation is solved by the FORMAS-algorithm with 3 exponential terms
IDIFSOLV 4: Diffusion equation is solved by the FORMAS-algorithm with 4 exponential terms
IDIFSOLV 5: Diffusion equation is solved by the FORMAS-algorithm with 5 exponential terms
IDIFSOLV 6: Diffusion equation is solved by the FORMAS-algorithm with 6 exponential terms.

Reference model implemented
In this activity, the selected options are FGRMOD6, IGRBDM3, and IDIFSOLV0 [3].

FGRMOD 6

The diffusion coefficient D_{eff} is given by the Madzke correlation:

$$D_{eff} = D_{thermal} + D_{athermal}\ [m2/s] \qquad \text{Eq. 14}$$

$$D_{thermal} = a_0 \cdot e^{-(k0/T)}\ [m2/s] \qquad \text{Eq. 15}$$

$$D_{a\text{-}thermal} = 10^{-25}[m2/s] \qquad \text{Eq. 16}$$

where:
k_0= 40262 [K];
$a_0=5 \cdot 10^{-8}$ [m^2/s];

effective diffusion coefficient is given by:

$$D_{eff} = D \cdot b/(b+g) \qquad \text{Eq. 17}$$

where:
g is the probability per unit time of gas atoms in solution being captured by a bubble
b is the probability per unit time of gas atom in bubble being re-dissolved to the matrix.

IGRBDM 3

IGRBDM 3 introduces a correction to the equations implemented in IGRBDM 1 in order to considers that the threshold concentration of gas at grain boundary ($C_{sat,gb}$) depends also by temperature (constant/T).

IDIFSOLV 0

Diffusion equation is solved by the URGAS-algorithm.

Models considered in the sensitivities
The validation of FGR models implemented in TU code is documented in Ref. [17].

FGRMOD4

The diffusion coefficient (D_{eff}) is given by Eq. 9 and the thermal diffusion term by Eq. 10 [3]. It differs from the reference option for the a-thermal part of the coefficient chosen according to White and Tucker:

$$D_{a\text{-}thermal} = 1.086 \cdot 10^{-15} \cdot e^{-16506/T} \text{ [m2/s]} \qquad \text{Eq. 18}$$

where:
T is the temperature in [K];

FGRMOD9

The single gas atom diffusion coefficient (D) is given by T. Turnbull et al [3].

$$D = D_1 + D_2 + D_3 \qquad \text{Eq. 19}$$

$D_1 = 7.6 \cdot 10^{-10} \cdot e^{-35000/T}$ [m^2/s] is the intrinsic high-temperature component;
$D_2 = 3.22 \cdot 10^{-16} \cdot (R)^{0.5} \cdot e^{-13800/T}$ [m^2/s] is an irradiation enhanced thermal component where R represents the rating in W/gU*;*
$D_3 = 6 \cdot 10^{-23} \cdot R$ [m^2/s] is the a-thermal term according to R.J. White.

4.3.6 **Fuel densification models for LWRs**

There are several options available in TU for treating the densification [3]. They are selected by the keyword IDENSI. The models applicable to LWR are:

- *IDENSI 0*: densification is not considered.
- *IDENSI 2*: empirical model for LWR and FBR. This model needs
  - the input of the minimum porosity DENPOR at the end of thermal irradiation induced densification and
  - the time constant DENBUP (burnup in MWd/tU, at which irradiation induced densification is terminated).
- *IDENSI* 3: Assmann-Stehle model for UO_2 in a LWR. This model needs several input data:
  - PFEIN (initial porosity of fine pores),
  - PGRO1 (fabrication porosity of coarse pores, Class 1),
  - PGRO2 (fabrication porosity of coarse pores, Class 2),
  - PGRO3 (fabrication porosity of coarse pores, Class 3),
  - RGRO1 (fabrication radius of the coarse pores, Class 1 [mm]),
  - RGRO2 (fabrication radius of the coarse pores, Class 2 [mm]),
  - RGRO3 (fabrication radius of the coarse pores, Class 3 [mm]) and
  - DENPOR.
- *IDENSI* 7: MATPRO LWR models FUDENS/FHOTPS. This model needs the input of the minimum porosity DENPOR at the end of thermal and irradiation induced densification. According with the TU manual this model option is not yet fully tested.

Reference model implemented
The reference model implemented is IDENSI 2 in which densification is treated according with this empirical correlation [3]:

$$P(bu) = P_{\infty} + (P_0 - P_{\infty})* e^{-(5bu/bu0)} \quad \text{Eq. 20}$$

where:
P(bu) is the sinter porosity
P_{∞} represents the minimum porosity (input data DENPOR)
P_0 is the fabrication porosity (input data POR000)
bu is the burnup
bu_0 is a burnup model constant.

4.3.7 **Gap conductivity models**

The fuel-cladding temperature difference $\Delta\theta_{f,cl}$ is defined by:

$$\Delta\theta_{f,cl} = q''_{f,cl}/h \quad \text{Eq. 21}$$

where:
$q''_{f,cl}$ is the heat flux density between fuel and cladding, it is defined as $q''_{f,cl} = = q'/2*\pi*r_{f0}$
q' is the linear power
r_{f0} is the outer fuel radius
h represents the heat transfer coefficient between fuel and cladding (gap conductance).

The heat transfer coefficient h depends on:

- gap width or contact pressure between fuel and cladding;
- gas pressure and composition;
- surface characteristics of cladding and fuel;

The gap conductance model incorporated in the TRANSURANUS code is the well-documented URGAP model. The original URGAP model from 1979 was revised and recalibrated in 1986 using an extended database consisting of approximately 1000 data. Four options are available in TU to simulate gap conductance [3] they are labeled as IHGAP:

- *IHGAP 0:* standard Option gas Bonding thermal conductivity of mixture according to Lindsay and Bromley. Accommodation coefficients are taken into account
- *IHGAP 1*: gap conductance is prescribed; no call of URGAP-Model
- *IHGAP 3*: as standard option but without considers accommodation coefficients
- *IHGAP 4*: specific model gas bonding, thermal conductivity of mixture according to Tondon and Saxena. Accommodation coefficients are taken into account
- *IHGAP 5*: as option 4, accommodation coefficients are not taken into account.

Reference model implemented
In 1991, the TRANSURANUS standard LWR thermal conductivities of the fuel and the cladding were modified [3]. The new correlation for Zircaloy gives approximately 10% higher values, whereas the thermal conductivity of the fuel has not changed significantly. Nevertheless, it was felt that the extremely sensitive gap conductance model, which depends on these material properties,

should be refitted. All four model options, i.e. IHGAP = 0, 3, 4 and 5 were fitted individually and finally the URGAS model option IHGAP = 0 was chosen as recommended.

The analyses have been carried out selecting the recommended gap conductivity, option IHGAP 0.

4.3.8 **Zircaloys (cladding) conductivity correlations**

In TU there are several correlations to simulate Zircaloy conductivity [3]: 19, 20 (standard), 21, 22. The conductivity model is selected with the option MODCLAD (j=6).

Reference correlation implemented

The correlation implemented as reference is the standard correlation 20. The correlation is identical with the MATPRO correlation 19 that was taken from the MATPRO handbook [3]:

$$\lambda = (7.51 + 2.09*10^{-2}*T - 1.45*10^{-5}*T^2 + 7.67*10^{-9}*T^3) \quad \text{Eq. 22}$$

[W/mK]

T is the cladding temperature [°C].

4.3.9 **Zircaloys (cladding) swelling correlations**

In general, the correlations for the cladding depend on the neutron fluence (Φ_t), the temperature T and on other parameters [3].

Considering that swelling data are obtained under steady-state conditions, (i.e. the temperature T and the other parameters are constant); any application under varying conditions is somewhat speculative [3].

Under slowly varying conditions, it seems reasonable to assume that the fractional volume increase is expressed by:

$$(\Delta V/V) = \partial/\partial t(\Delta V/V)\cdot dt \quad \text{Eq. 23}$$

Since *ΔV/V* is given as a function the increment of the fractional volume increase, *Δ(ΔV/V)* is given by:

$$\Delta(\Delta V/V) = (\Delta V/V)\cdot\{(\Phi_t),T_{\Delta t},P_{\Delta t}\} - (\Delta V/V)\cdot\{(\Phi_t)_n,T_{\Delta t},P_{\Delta t}\} \quad \text{Eq. 24}$$

$$(\Phi_t)_{n+1} = (\Phi_t)_n + \Delta(\Phi_t) \quad \text{Eq. 25}$$

$$\Delta(\Phi_t) = \Phi_{\Delta t}\cdot\Delta t \quad \text{Eq. 26}$$

where the index Δt indicates average values during the time step Δt.

There are several correlations considering the fuel swelling that are selected by MODCLAD (j=4): correlations 17 and 18 are for ZR-4 claddings (PWRs), correlations 19, 20 (standard), 21 are for Zr-2 (BWRs) and Zr-4 (PWRs) claddings.

Reference correlation implemented
The correlation implemented is the standard correlation 20. This correlation was given by Duncombe [3] for Zircaloy in an annealed state or with a small amount of cold work. The strains due to irradiation growth (radial, tangential, axial) are given by:

$$\varepsilon_i = [a*(\Phi_t) + b*(1-e^{-(\Phi t)/c})]*(1 - 3*f_i)$$

$$i = r, t, a \qquad \text{Eq. 27}$$

a, b, c, f_r, f_t f_a are constants.

4.3.10 **Cladding outer corrosion models**

Subroutine OUTCOR calculates the outer cladding corrosion [3]. The following LWRs models are included:

The MATPRO model CORROS for BWR and LWR conditions, the EPRI/C-E/KWU waterside corrosion model for PWR conditions, and the EPRI code comparison corrosion model for LWR conditions. The effect of the outer cladding corrosion is twofold. Firstly, the corrosion layer may increase the thermal resistance of the cladding (thermal effect) and secondly, corrosion means that the cladding thickness of the original material decreases (mechanical effect). Through input options, either the thermal effect alone, or both the thermal and the mechanical effect can be taken into account.

Under varying conditions, i.e. when linear rating, flux, coolant temperature etc. are time dependent, the application of rate equations is not clearly defined in all models. Two approaches are made to cope with this problem: **model a**, where the thickness of the oxide layer S_{ox} determines the transition point *tp* and **model b**, in which the corrosion rate beyond transition is always assumed if, once under specific conditions, the transition point has been reached.

Model a: Within a time step Δti the temperature $T_{interface,i}$ at the boundary between cladding and oxide layer (metal-oxide interface) is assumed to be constant. At time t, the thickness of the oxide layer is $S_{ox}(t)$. If the thickness of the oxide layer at the transition point S_{ox} [*tp* ($T_{interface,i}$)] is less than $S_{ox}(t)$, then the corrosion rate until transition is assumed. If not, the corrosion rate beyond transition applies. In *Fig. 14* the transition oxide thickness is represented as function of the interface temperature.

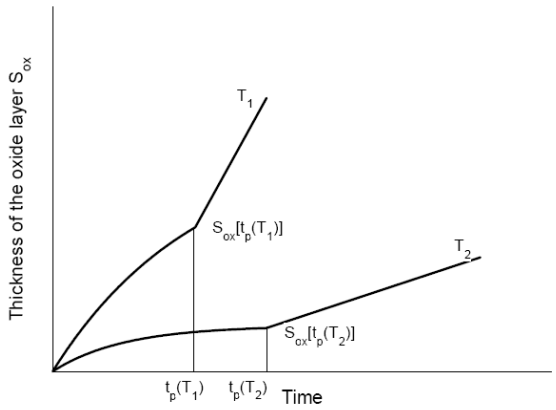

Fig. 14 – Thickness of the oxide at which transition occurs at different interface temperatures.

There are 50 outer corrosion models available in TU [3]. They are selected by the keyword ICORRO.

The models for BWR cladding outer corrosion simulation are:

- ICORRO 1: MATPRO model (BWR conditions); only thermal effect is considered.
- ICORRO 3: MATPRO model (BWR conditions); thermal effect and the weakening of the cladding (mechanical effect) are considered.

The models for PWR cladding outer corrosion simulation are:

- ICORRO 2: MATPRO model (PWR conditions); only thermal effect is considered.
- ICORRO 4: MATPRO model (PWR conditions); thermal effect and the weakening of the cladding (mechanical effect) are considered.
- ICORRO 11: EPRI/C-E/KWU waterside corrosion model (PWR conditions); model assumption a) for varying conditions, only thermal effect is considered.
- ICORRO 12: EPRI/C-E/KWU waterside corrosion model (PWR conditions); model assumption b) for varying conditions, only thermal effect is considered.
- ICORRO 13: EPRI/C-E/KWU waterside corrosion model (PWR conditions); model assumption a) for varying conditions, thermal effect and the weakening of the cladding (mechanical effect) are considered.
- ICORRO 14: EPRI/C-E/KWU waterside corrosion model (PWR conditions); model assumption b) for varying conditions, thermal effect and the weakening of the cladding (mechanical effect) are considered.

Reference models implemented
The reference simulations concern two different reactor types: BWR and PWR so two different options are selected, ICORRO 3 and ICORRO 12 respectively. No indications are given about the implemented equation because due to the complexity and specificity this activity would request a work finalized only on outer cladding corrosion.

4.3.11 **Cladding creep correlations**

There are two correlations to simulate cladding creep strain in TU for Zircaloy that are selected in by Modclad (j=7): correlations 18, 20 (standard) [3].

Reference correlation implemented

The standard option (correlation 20) for Zircaloy cladding creep is used in the reference calculations. This correlation calculates the effective creep rate according to the Lassmann-Moreno model [3]. It considers two components of steady state creep as thermal creep and dislocation climb:

$$\dot{\varepsilon}_{eff} = \dot{\varepsilon}_{th} + \dot{\varepsilon}_{climb} \qquad \text{Eq. 28}$$

$$\dot{\varepsilon}_{th} = 1.083 \cdot 10^{5} \cdot e^{(-1700/T)} \cdot \sinh(\sigma_{eff}/60) \qquad \text{Eq. 29}$$

$$\dot{\varepsilon}_{climb} = 1.0885 \cdot 10^{-28} \cdot \sigma_{eff}^{4} \cdot \Phi + 4.2466 \cdot 10^{-23} \cdot \sigma_{eff} \cdot \Phi \qquad \text{Eq. 30}$$

where

$\dot{\varepsilon}_{eff}$ is the effective strain rate [1/h];
σeff is the effective stress [MPa];
T is the temperature [K];
Φ is the fast neutron flux [n/(cm^2·s)].

The thermal component depends from temperature and effective stress while, the climb component, depends from neutron fast flux and effective stress.

4.3.12 **Cladding failure model**

The occurrence of fuel cladding failure for PCI/SCC is calculated in TU code by the failure subroutine SPAKOR [3].

The stress-corrosion cracking (SCC) model SPAKOR is that of Mattas, Yaggee and Neimark. The model is based on the observation that iodine SCC failures usually begin as an intergranular fracture, which becomes a "cleavage and fluting" fracture at some point in crack growth. It is assumed that the intergranular portion of the failure is due to chemical attack, which is independent of applied stress, while the cleavage and fluting portion of the failure can be described by linear elastic fracture mechanics. The time to failure (t_f) can be divided into the time required to chemically grow an intergranular crack (t_{ch}) and the time required to propagate the crack to failure by cleavage and fluting (t_{cf}):

$$t_f = t_{ch} + t_{cf} \qquad \textit{Eq. 31}$$

The chemical crack-growth rate da/dt is assumed to have an initial value A_0, and to decrease exponentially as the crack depth increases:

$$da/dt = A_0 \cdot e^{-a/B} \qquad \textit{Eq. 32}$$

where

a is the crack depth, and
B is a rate constant.

Previous equation can be integrated and put into an incremental form:

$$a(t) = B \cdot ln[A_0 \cdot \Delta t/B + e^{a \cdot (t - \Delta t)/B}] \qquad Eq.\ 33$$

Chemical crack growth is assumed to continue until critical stress intensity for cleavage and fluting, $K_{I\text{-}SCC}$, is reached. At this point, cleavage and fluting fracture initiates and continues up to failure:

$$da/dt = K^4/C \quad Eq.\ 34$$

where
K is the stress intensity factor ($K^2 = \sigma^2 \cdot y^2 \cdot a$),
C is a constant,
y is a geometric factor, and
σ is the applied hoop stress.

The equation in incremental form is:

$$a(t) = [a \cdot (t - \Delta t) \cdot C] / [C - a \cdot (t - \Delta t) \cdot \sigma^4 \cdot y^4 \cdot \Delta t] \qquad Eq.\ 35$$

For steady state conditions, the times t_{ch} and t_{cf} can be obtained in closed form from Eqs. 24, 26.

Chemical crack growth is assumed to initiate if the following conditions are satisfied:

- The burn-up must exceed a critical value (5000 MWd/tU).
- The cladding temperature must exceed a critical value (270 °C).
- The strain rate in the cladding must exceed a critical value, which is temperature dependent.
- The hoop stress must be positive.

The SPAKOR model evaluates the incremental formulations Eqs. 62 and 64 as well as a global cumulative damage concept, where the cumulative damage fraction D is given by:

$$D(t) = \Sigma_i \Delta t_i / t_f \qquad Eq.\ 36$$

t_f is the time to failure under the conditions in time step Δt_i.

Zircaloy properties (yield strength σys and rupture strength σrs) need to be known precisely in order to apply the model correctly. At present, the approximate values are σys = 560MPa, σrs = 690MPa. Cladding sensibility to SCC in TU code is represented by the failure subroutine that shows which conditions must be reached to have cladding failure by SCC. This subroutine is SPAKOR [3].

4.4 Selection of relevant TU code options

The "Reference" TU options described above are summarized in Tab. 16 distinguishing among the correlation model related to fuel pellet, gap, cladding and fission gas release. The criteria adopted in devolving the "Reference" input decks are:

- choice of models or correlations recommended in the TU handbook version 2006 (when indicated);

- choice of models or correlations implemented as usual (if no recommendation are given in the handbook);
- choice of boundary conditions directly indicated in the experimental report or in the related ASCII files.

PWR Super-Ramp: "Reference" input decks			
Parameter	**Reference option**	**Description**	**Other options**
Fuel conductivity	Correlation 21 (recommended)	New correlation fitted to data from ITU, it takes into account the High Burnup Structure (HBS), as well as the influence of gadolinium.	18, 19, 20, 22, 23, 24, 28.
Fuel swelling	Correlation 20 (recommended)	Developed by K. Lassmann from correlation 19. The gaseous swelling contribute was modified and integrated from this steady state equation	18, 19, 21
Number of radial cracks in the pellet	6 radial cracks	The parameter ncracks treats the stochastic number of radial cracks in the fuel at the beginning, standard recommendations indicate that from 4 to 6 initial cracks can be applied	--
Pellet fragment relocation	Model ireloc 5	Modified KWU-LWR model, ITU calibrated according with the simple FEMAXI correlation.	2, 3, 4, 6, 8
Fuel grain growth	Model igrnsz 1 (recommended)	Grain growth model of Ainscough and Olsen	0
Fuel densification	Model idensi 2 (recommended)	Empirical model for LWR and FBR. This model needs the input of the minimum porosity DENPOR at the end of thermal and irradiation induced densification and the time constant DENBUP (burnup in MWd/tU, at which irradiation induced densification is terminated).	0, 3, 7
Gap conductivity	Model ihgap 0 (recommended)	Standard Option: gas Bonding thermal conductivity of mixture according to Lindsay and Bromley. Accommodation coefficients are taken into account	1, 3, 4, 5
Cladding conductivity	Correlation 20 (recommended)	Identical with the MATPRO correlation 19 that was taken from the MATPRO handbook	19, 21, 22
Cladding swelling	Correlation 20 (recommended)	This correlation was given by Duncombe for Zircaloy in an annealed state or with a small amount of cold work	17, 18, 19, 21
Cladding outer corrosion	Model icorro 13	EPRI/C-E/KWU waterside corrosion model (PWR conditions); model assumption a) for varying conditions, thermal effect and the weakening of the cladding (mechanical effect) are considered.	2, 4, 11, 12, 14
Cladding creep	Correlation 20 (recommended)	Effective creep rate according to the Lassmann-Moreno	18
Fission gas release	Models: **fgrmod6 (recommended)**, **igrbdm3**,**Idifsolv0**	*FGRMOD 6:* URGAS algorithm with the diffusion coefficients of Hj. Matzke (thermal) and a constant athermal diffusion coefficient. *IGRBDM 3:* New model developed according to modified Koo model for ramps simulations *IDIFSOLV 0:* Diffusion equation is solved by the URGAS-algorithm	Fgrmod: 4,9 Igrbdm: 0, 1, 2 Idifsov: 1, 2, 3 4,5,6

Tab. 16 – PWR Super-Ramp: "Reference"input decks, options related to PCI assessment.

5 Validation of TRANSURANUS code against PWR Super-Ramp experiment

5.1 Reference results

The section presents the analyses of the results by TU code version "v1m1j11". The aim is to validate the capability of TU code in predicting the PCI failures against the PWR Super-Ramp database. The database comprises the data of twenty-eight fuel rods; twenty-six have been initially modeled and simulated through suitable input decks. The two remaining rods have not been modeled. The burn-up values range between 30 and 45 MWd/kgU. Two different rods type belongs to the database: KWU rods and W rods.

The validation of the PCI/SCC failure criterion and the reliability of the SPAKOR subroutine implemented in the code are the main concerns. The analysis of the results involves the main phenomena, which characterize power ramp tests and are involved or may influence the cladding failure behavior. Therefore, systematic comparisons is performed for the burn-up (section 5.1.1), the cladding diameter changes, namely cladding creep-down and expansion (section 5.1.2), the rod elongation (section 5.1.3), the uranium oxide grain size (section 5.1.4), the cladding outer corrosion (section 5.1.5), the FGR (5.1.6), the cladding stress (section 5.1.7) and the failure predictions (section 5.1.8).

Sensitivity calculations on fission gas release models (section 5.2) are performed in order to address the influence of the options available in TU or to tests different interpretations of the boundary conditions. The impact of selected parameters and/or code options on the results and the limits of the models implemented in the code are investigated. Finally, in section 5.3 an "Improved" input deck is investigated. It is based on the results obtained from the sensitivity analyses permormed in Ref. [36].

5.1.1 **Burn-up analysis**

The determinations of burn-up were performed on samples from four rods using the Nd-148 method. The other experimental data are estimated based on the measurements executed. The measured data agreed within 8% with the estimeted values based on neutron physics and reactor records [4].

Fig. 15 shows the comparisons between the calculated and the experimental values of the burn-up at end of the irradiation. The figure distinguishes with different colors the rods belonging to different homogeneous groups. The bands of ±10% and ±5% are also reported and it will be referred as the acceptability threshold. The objective of the analysis is to verify the correctness of the imposed LHR in the code simulations as well as the reliability of the experimental data reported in Ref. [4].

The achieved TU code results show a slight general underestimation of the burn-up. In particular, they are all bounded by the experimental data ±10%, with the exception of the rod PK1/S that overestimates the burn-up of 25%. More in detail, the burn-up calculations of the KWU and W rods, namely the groups PK1 (5 rods), PK2 (5 rods), PK4 (4 rods), PK6 (5 rods), PW3 (3 rods) and PW5 (4 rods) are affected by errors in the order of 5% (that is also the accuracy of the measurement reported in figure). Few exceptions are observed which are: the rods PK1/S, already mentioned, and the rods identified as PK1/4 and PK4/S. The anomalous behavior of rod PK1/S is due to unconformity of the experimental data.

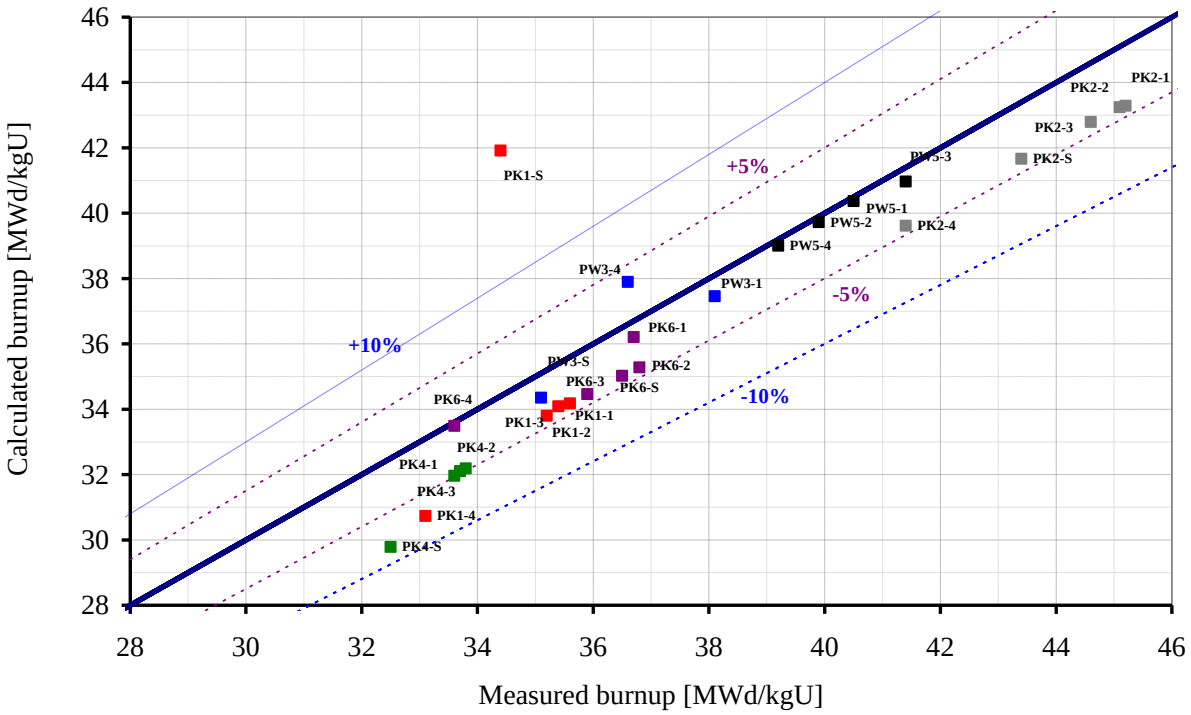

Fig. 15 – PWR Super-Ramp experiment versus TU v1m1j11 code results: burn-up at end of the irradiation ("Reference").

5.1.2 **Cladding diameter change analysis**

The analysis of the results concerns the comparisons of the cladding diameter changes evaluated at the end of the fuel irradiation (PTR) and at the end of the ramp phase (AR). The analyses address two different phenomena occurring in the cladding: the creep-down (PTR) and the diameter increase (AR).

The experimental data of the **cladding creep-down** are available in Ref. [4] and are related to 9 out of 19 and 3 out of 7 KWU and W rods, respectively. The results are summarized in Tab. 17, for each rod is reported the burn-up, the average fast flux, the average linear heat rate in base irradiation, the measured and calculated cladding maximum creep down and the error (percentage). The experimental values represent the cladding maximum creep down obtained from the greatest difference between several diameter measurements performed prior to irradiation (PTI) and prior to ramp (PTR), considered in cold conditions (20°C). In particular, they are evaluated on the bases of 2x(7x3) measurements that means 2 times at 7 axial elevations and 3 angular positions. The measurement accuracy is ±5 microns.

Analogously, the maximum diameter decrease (PTI-PTR Max) calculated by TU code and reported in *Tab. 17* is obtained as:

$$D^{Max}\,[TU_{CALC}\,(PTI\text{-}PTR)] = [D^{Max}\,(T = 20°C;\, t = PTI) - D^{Min}\,(T = 20°C;\, t = PTR)]$$

The summary of the analyses at PTR are reported in *Fig. 16.* The code results show a systematic under-prediction. The errors are bounded by the line corresponding to -50% for the groups PK1, PK2, PK4, PW3 and PW5. The simulations of the rods PK6, fabricated with larger grain size, evidence errors between 60% and 65%. It should be noted that average linear heat rate of W rods is quite less than KWU rods and so the creep down (related to temperature) is less as absolute value in

respect to KWU rods. The rod PK2/3 experiences the best prediction: the result is close to the experimental measure plus its uncertainty (+/-5µm).

The differences are correlated with the limits of the code in the geometrical modeling. First of all, the schematization is one-dimensional, plane and axisymmetric and characterized by plain strain condition. In addition to this, local variation of the geometry cannot be modeled (e.g. ridges). Finally, the maximum diameter changes are calculated based on 3 or 6 positions, whereas in the experiments the measures are taken in 7 axial and 3 azimuthal positions (21 measurement points per each rod at each time).

The experimental data of the **cladding diameter increase** during the power ramp are available in Ref. [4] and are related to 9 out of 19 and 3 out of 7 KWU and W rods, respectively. The results are summarized in Tab. 18 where for each rod it is reported the ramp rate, the RTL, two different measurements of the diameter increase (between the ridges and at the ridge), the average and maximum diameter increase calculated and finally the errors. The quantities assumed as more representative and therefore compared in Tab. 18 (column 9) are the maximum diameter increase (calculation) and the average diameter increase between the ridges (experiment). It should be noted that all measures represent cladding diameter increase obtained from several diameter measurements performed PTR and AR, considered in cold conditions (20°C). The average and maximum diameter increases are evaluated in the calculation with the formulas below.

$$D^{Max}\,[TU_{CALC}\,(AR\text{-}PTR)] = [D^{Max}\,(T = 20°C;\ t = AR) - D^{Min}\,(T = 20°C;\ t = PTR)]$$
$$D^{Avg}\,[TU_{CALC}\,(AR\text{-}PTR)] = [D^{Avg}\,(T = 20°C;\ t = AR) - D^{Avg}\,(T = 20°C;\ t = PTR)]$$

Fig. 17 summarizes the code results, which are in general under-predicted. The best prediction is experienced by the KWU rods PK1/3, PK4/2 and PK2/S. This can be correlated with the erroneous prediction of failures. Indeed, the cladding expansion occurs during the power decrease and is connected with pellet cracking, fragment relocation and volume increases caused by gaseous porosity expansion when gap opens. In the case of W rods large underestimation is observed.

The general under-estimation is connected with the limitation already briefly discussed above. Moreover, it should be remarked that the real deformation of the fuel involves the formation of primary and secondary ridges, as discussed in section 4.1. This phenomenon is clearly not modeled in TU code.

Rod group	Rod Label	PTR time [hrs]	Avg. LHR [&] [kW/m]	Measured Burn-up [MWd/kgU]	EXP PTI-PTR max decrease [µm]	TU Calc. PTI-PTR max decrease [µm]	Error %
PK1	PK1/1	21006.5	23.00	35.4	85	54	-37
	PK1/3	21034.0	22.80	35.2	75	54	-28
PK2	PK2/1	28098.0	21.98	45.2	85	67	-21
	PK2/3	28100.0	21.72	44.6	75	69	-8
	PK2/S	28097.0	21.17	43.4	90	70	-23
PK4	PK4/1	21192.0	19.92 [21.41] [$]	33.7	95	59	-38
	PK4/2	21194.6	19.96 [21.46]	33.8	85	66	-23
PK6	PK6/1	22014.4	21.92 [23.56]	36.7	95	37	-61
	PK6/2	21224.1	23.82	36.8	95	33	-65
PW3	PW3/4	23801.9	14.87 [18.16]	36.6	70	37	-47
PW5	PW5/3	23680.4	15.09 [18.43]	41.4	50	36	-29
	PW5/4	23679.9	14.27 [17.54]	39.2	50	33	-33

[&] Calculated from ASCII data.
[$] In bracket the avg. linear heat rate in peak axial position, if not indicated is intended that no axial difference appears in LHR.

Tab. 17 – PWR Super-Ramp experiments versus TU v1m1j11 results: summary of the cladding creep down analysis during base irradiation ("Reference").

1	2	3	4	5	6	7	8	9
Rod group	Rod Label	Ramp Rate [kW/m/h]	RTL [kW/m]	EXP AR-PTR (between ridges) [µm]	EXP AR-PTR (at ridge) [µm]	TU Calc. AR-PTR avg. [µm]	TU Calc. AR-PTR max [µm]	Error (Column #8 - #5) %
PK1	PK1/1	540	41.5	6	28	0.82	1.71	-71.5
	PK1/3	510	47.5	36	69	10.42	33.25	-7.6
PK2	PK2/1	510	41	36	71	14.87	18.33	-49.1
	PK2/3	510	49	101	135	37.84	51.14	-49.4
	PK2/S	510	44	10	33	4.69	8.05	-19.5
PK4	PK4/1	480	39	8	29	0.21	0.23	-97.1
	PK4/2	510	44.5	11	41	4.29	14.77	34.3
PK6	PK6/1	540	45	34	44	1.99	3.45	-89.9
	PK6/2	540	40	29	37	2.65	5.16	-82.2
PW3	PW3/4	540	37.7	28	42	0.027	0.13	-99.5
PW5	PW5/3	540	38.2	37	46	0.024	0.16	-99.6
	PW5/4	510	38	32	32	0.014	0.14	-99.6

Tab. 18 – PWR Super-Ramp experiments versus TU v1m1j11 results: summary of diameter increase analysis during power ramp ("Reference").

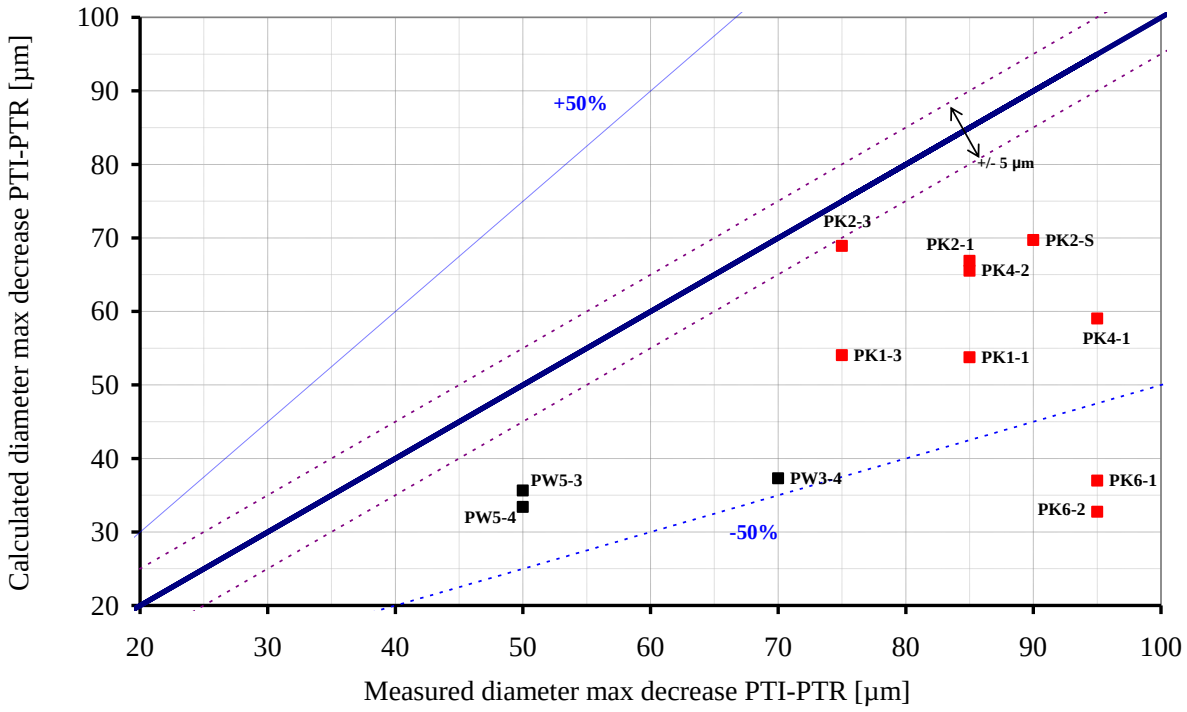

Fig. 16 – PWR Super-Ramp experiments versus TU v1m1j11 results: cladding creep down ("Reference").

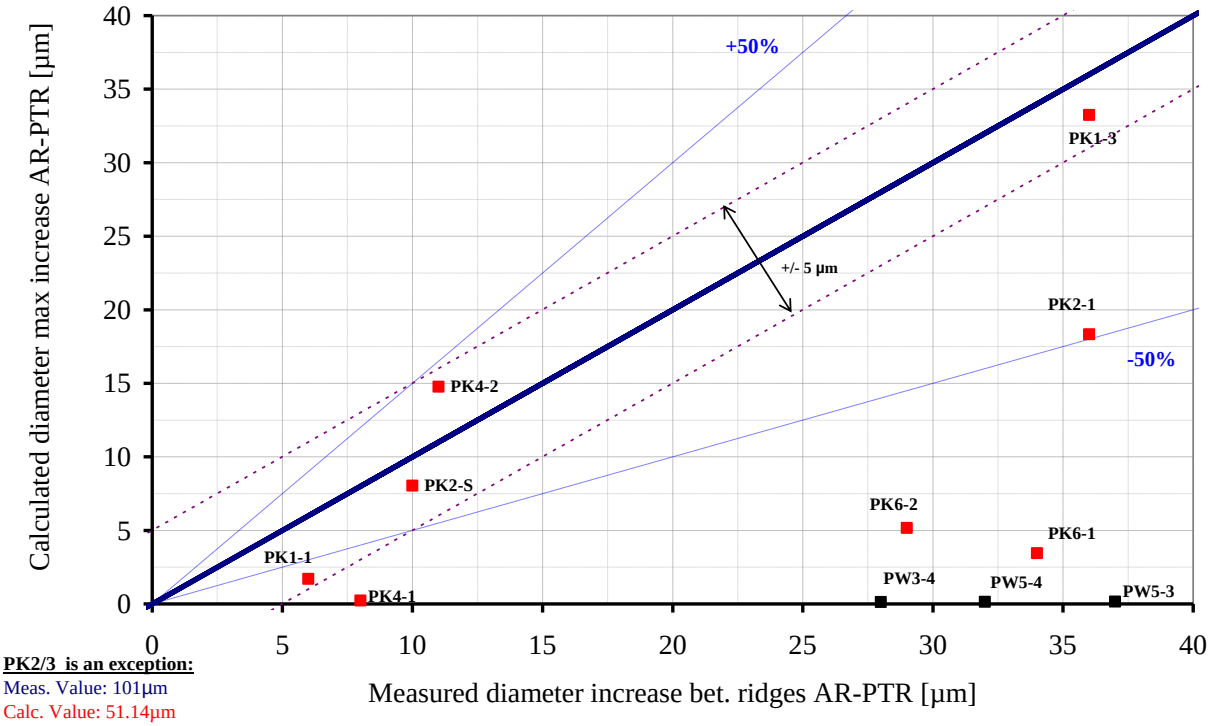

Fig. 17 – PWR Super-Ramp experiments versus TU v1m1j11 results: cladding diameter increase during power ramp ("Reference").

5.1.3 **Cladding outer corrosion analysis**

The measurement of the cladding outer oxidation layer thickness is performed by SEM (scanning electron microscopy) [4]. The available experimental data (Ref. [4]) consider measures taken in longitudinal rod sections, KWU rods, or in transverse sections, W rods. In the case of the rod PW5/3 three different axial positions are considered. The experimental data represent an average value between several measurements; the range of variations of the measurements is also available. Each datum is provided with its reference axial elevation. The results are summarized in Tab. 20, Tab. 21 and *Fig. 18*.

The model implemented in TU for the evaluation of cladding outer corrosion is ICORRO 13 (EPRI type). Details about the TU external corrosion models are available in Ref. [3]. TU calculations show an under-estimation of the outer oxidation layer, both for KWU and W as well. The rods PK2/4 and PK6/3 experience the worst predictions. TU simulations show that oxidation thickness is axially uniform with the exception of rods PK4/3 and PK4/S. These rods differ from the others because the LHR is not axially constant. This implies, following the break-away point, an increase of the difference of the oxidation thickness in axial direction. The two mechanism of corrosion are observable in the code results (see also *Fig. 14*). The break away point, only KWU rods, is calculated in the range of 12000 to 19000 hrs of irradiation (Tab. 19). On the contrary, for the W rods, the time trends of the cladding outer corrosion does not experience the break away occurrence. This is explained with the different coolant temperature during the base irradiation. In particular, the KWU rods were base irradiated in a commercial reactor having coolant temperature higher than W rods.

The influence of the water chemistry can play a role in the explanation of the general difference between calculated and measured values. This boundary condition cannot be taken into account by TU code.

Rod Label	TU Calc. Time[$] of break away point [hrs]	TU Calc. Corresponding burnup[$] [MWd/kgU]
PK1/2	12800	22.1
PK2/2	14100	23.0
PK2/4	15300	22.5
PK4/3	11900	15.0
PK4/S	17500	24.7
PK6/3	13100	22.9
[$] Qualitative values		

Tab. 19 – PWR Super-Ramp: TU Calculated burnup at break away point transition time for KWU rods ("Reference").

Rod Label	EXP Outer oxidation layer thickness [µm]	TU Calc Outer oxidation layer thickness [µm]	Error %	EXP Local ramp power [kW/m]	EXP Hold time at ramp terminal level [hrs]
PK1/2	18[$] (10-24)[$$]	8.91	-51	42 - 43	12
PK2/2	30 (19-38)	14.14	-53	42 - 43	12
PK2/4	65 (60-72)	12.31	-81	42 - 43	**1 min**
PK4/3	22 (12-30)	12.53	-43	**50.5**	12
PK4/S	7 (3-15)	4.57	-35	42 - 43	12
PK6/3	32 (26-36)	9.07	-72	42 - 43	12
[$]Avg. value of the measurements [$$] In bracket the range of measured data					

Tab. 20 – PWR Super-Ramp: summary of oxidation layer data for KWU rods ("Reference").

Rod Label	TU Calc Outer oxidation layer thickness [µm]	EXP Outer oxidation layer thickness [µm]	Error %
PW3/4	1.56	2.5 (2-3)	-38
PW5/3 B	1.53	3.8	-60
PW5/3 I	1.58	3.5 (3-4)	-55
PW5/3 T	1.61	4	-60

Tab. 21 – PWR Super-Ramp: summary of oxidation layer data for W rods ("Reference").

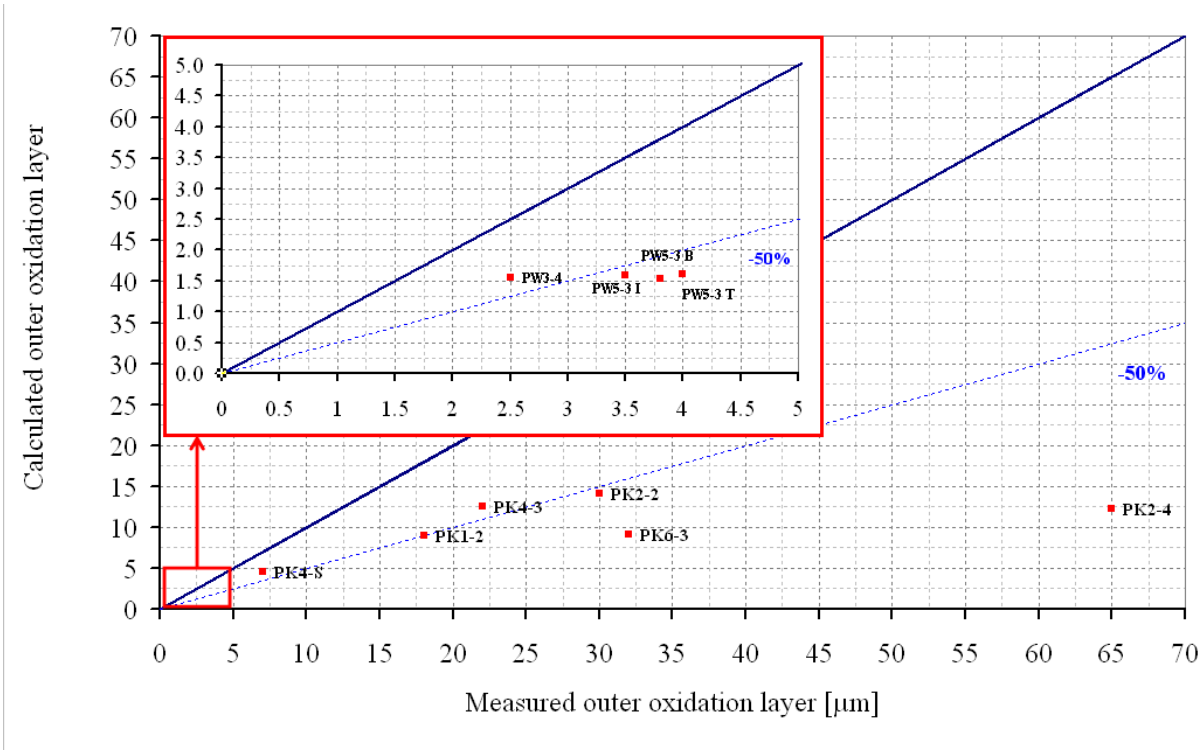

Fig. 18 – PWR Super-Ramp experiments versus TU v1m1j11 results: cladding outer oxidation layer ("Reference").

5.1.4 **Grain size analysis**

The experimental purpose of metallographic examinations was to compare four different rod types, one rod of each group at the similar local ramp power, and equal ramp holding time (12 hrs). Therefore, they were cutted at an axial position corresponding to 42-43 kW/m in local power ramp. Rod PK2/4 was measured in order to compare the impact of a lesser ramp terminal level holding time (only 1 minute) and rod PK4/3 was measured in order to compare the impact of a higher local ramp power (50.5 kW/m). Details are available in Tab. 23.

This analysis addresses the prediction of the grain size in the fuel pellet at the end of the irradiation. The option selected for the grain growth is the model of Ainscough and Olsen (IGRNSZ 1). No other options are available, see Ref. [3]. The experimental data (Tabs 3.12 and 3.13 of Ref. [4]) are available with the same measurement[1] approach described above (section 5.1.3).

In accordance with [36], a corrective multiplication factor of 1.50 is applied to PK1, PK2 and PK4 groups. Different corrections are applied to the other measures because of the substantial agreement to be reached at the periphery region (*Fig. 21*). This last assumption is based on Ref. [35]. The correlation between average grain size (*G*) and mean intercept length (*MIL*) is expressed as:

$$G = MIL*Fs*Fd$$

Where *Fs* is dependent from grain shape, it is equal to 1.50, 1.775, 2.12, 2.25 for sphere (our case), tetrakaidecahedron, rhombicdodecahedron, and cube shapes respectively. The constant *Fd* is usually equal to 1 when the grains are uniform in the size; with broadening of size distribution it becomes smaller then 1 down to 0.3 (*Fig. 19*). No experimental data are available to calculate *Fd*. Therefore,

[1] The measure of the grain size is carried out with a Reichert telatom microscope with a magnification up to 1000. The distribution of the grain size can be determined by an attached linear analysis equipment from which the results can be evaluated analytically.

a simple approach is used: the measured values at pellet pheriphery are used to calibrate *Fd* assuming that no substantial deviations from the initial grain size affects this measure (see Tab. 22); the acceptability band is fixed at +/-25% based on conservative judgement.

The results of the analyses are reported in *Fig. 20*, *Fig. 21*, Tab. 23 and Tab. 24 below. The experimental measurements provide data of the grain size at pellet centre and pellet periphery. The code results provide information regarding the grains size trend as function of the pellet radius.

KWU rods results (*Fig. 20)* reveal that the code generally underestimates the grain size at centre pellet in the case of the rods. The comparisons at the periphery of the pellet highlight a general accordance with the measured values. In the case of the rod PK4/3, the experimental datum shows the formation of columnar grain type in the centre of the pellet, since the size of the grain (MIL), is about 50 micron. The restructuring effect is qualitatively predicted by TU code. The case of the rod PK6/3, manufactured with larger grain size, is less affected by this phenomenon accordingly in the code simulation and in the experimental measures as well.

Since PK4/2 section for experimental analysis overlaps two TU slices, an alternate value (using the calculated value in the other overlapped TU slice) has been included in table Tab. 23 (square brackets) and in *Fig. 20* (green triangle) showing a much better occordance with experimental data.
In the case of the W rods the code always under predicts the grain size. TU calculations show that there is no difference in grain size as a function of the radius and the restructuring effects are negligible. However, this is qualitatively in agreement with the experimental data and can be explained by the lowest fuel central temperature that doesn't reaches the recrystallizing temperature value.

Rod **Label**	**Initial average grain size** **[µm]**	**EXP** **Grain size at pellet periphery AR** **[µm]**	**Deviation** **(possible Fs*Fd)** **[Initial / EXP AR]**
PK1/2	6.00	4.80	1.25
PK2/2	5.50	4.40	1.25
PK2/4	5.50	3.80	1.48
PK4/3	5.50	3.70	1.49
PK4/S	5.50	3.20	1.72
PK6/3	22.00	23.00	0.96
PW3-4	10.50	13.00	0.81
PW5-3-B	16.90	17.00	0.99
PW5-3-I	16.90	18.00	0.94
PW5-3-T	16.90	19.00	0.89

Tab. 22 – PWR Super-Ramp experiments grain size at the beginning and MLI AR at pellet pheriphery.

Rod Label	**EXP Grain size at pellet centre [µm]**	**TU Calc. Grain size at pellet centre [µm]**	**Error %**	**EXP Grain size at pellet periphery [µm]**	**TU Calc. Grain size at pellet periphery [µm]**	**Error %**	**EXP Local ramp power [kW/m]**	**EXP Hold time at ramp terminal level**
PK1/2	54.00	42.90	-21	7.20	6.00	20	42 - 43	12 hrs
PK2/2	19.20	15.48	-19	6.60	5.50	20	42 - 43	12 hrs
PK2/4	12.45	61.29[11.98]	392[-4]	5.70	5.50	4	42 - 43	**1 min**
PK4/3	75.00	41.31	-45	5.55	5.50	1	**50.5**	12 hrs
PK4/S	39.00	62.02	59	4.80	5.50	-13	42 - 43	12 hrs
PK6/3	25.00	22.11	-12	23.00	22.00	5	42 - 43	12 hrs

Tab. 23 – PWR Super-Ramp experiments versus TU v1m1j11 results: KWU rods, summary of grain size data ("Reference").

Rod Label	EXP Grain size at pellet centre [µm]	TU Calc Grain size at pellet centre [µm]	Error %	EXP Grain size at pellet periphery [µm]	TU Calc Grain size at pellet periphery [µm]	Error %	EXP Experimental purpose
PW3/4	13.00	10.50	-19	13.00	10.50	24	Compared with PW5/3 I
PW5/3 B	21.00	16.90	-20	17.00	16.90	1	Study of a crack
PW5/3 I	18.00	16.90	-6	18.00	16.90	7	Compared with PW3/4
PW5/3 T	23.00	16.90	-26	19.00	16.90	12	Compared with PW3/3

Tab. 24 – PWR Super-Ramp experiments versus TU v1m1j11 results: W rods, summary of grain size data ("Reference") .

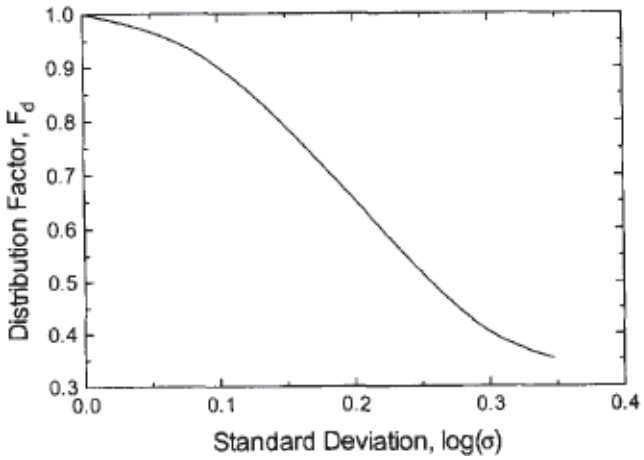

Fig. 19 – Variation of the distribution factor, Fd, as function of log(σ) for log normally distributed grain (σ indicates the standard deviation associated to the grain distribution).

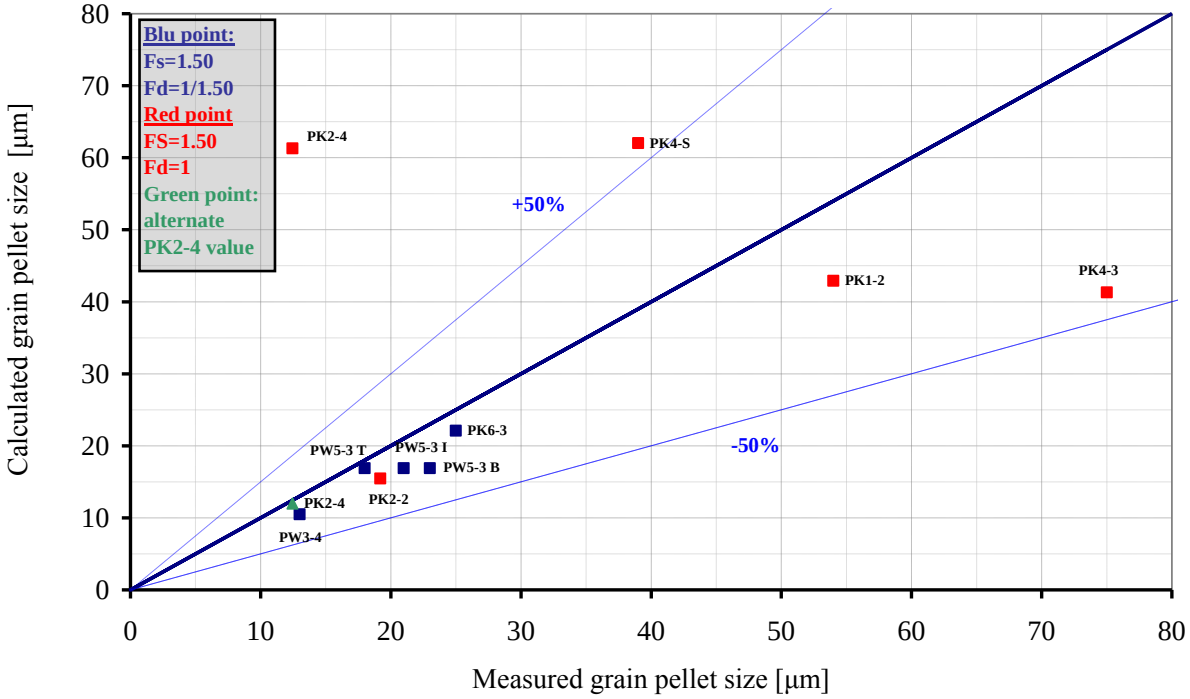

Fig. 20 – PWR Super-Ramp experiments versus TU v1m1j11 results: grain size at centre of the pellet ("Reference").

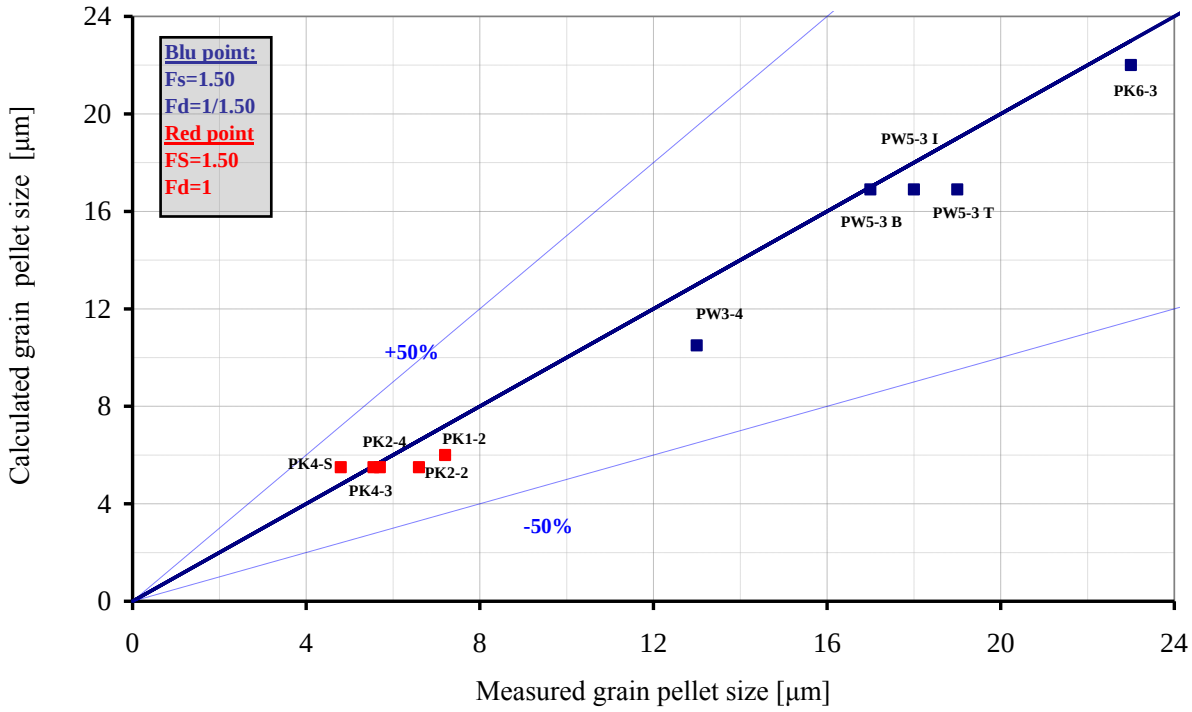

Fig. 21 – PWR Super-Ramp experiments versus TU v1m1j11 results: grain size at periphery of the pellet ("Reference").

5.1.5 **Rod elongation**

The analysis is addressed to cladding length change during base irradiation. Experimental data, carried out in laboratory hot cells are available only for W rods [4]. The length is measured between the top of the upper and a surface of the lower edges. The results obtained are corrected at 20°C and the uncertainty in measures is ±0.1mm.

The results are reported in Tab. 25, *Fig. 22*. They are characterized by an under prediction larger than 50%. This is connected with the error observed in the creep down results in section 5.1.2.

Rod group	Rod Label	EXP Rod length increase in BI [mm]	TU Calc. Rod length increase in BI [mm]	Error %
PW3	**PW3-4**	4.06	1.42	-65.0
PW5	**PW5-3**	3.46	1.44	-58.3
	PW5-4	3.6	1.35	-62.4

Tab. 25 – PWR Super-Ramp experiments versus TU v1m1j11 results: W rods, summary of the cladding elongation data ("Reference").

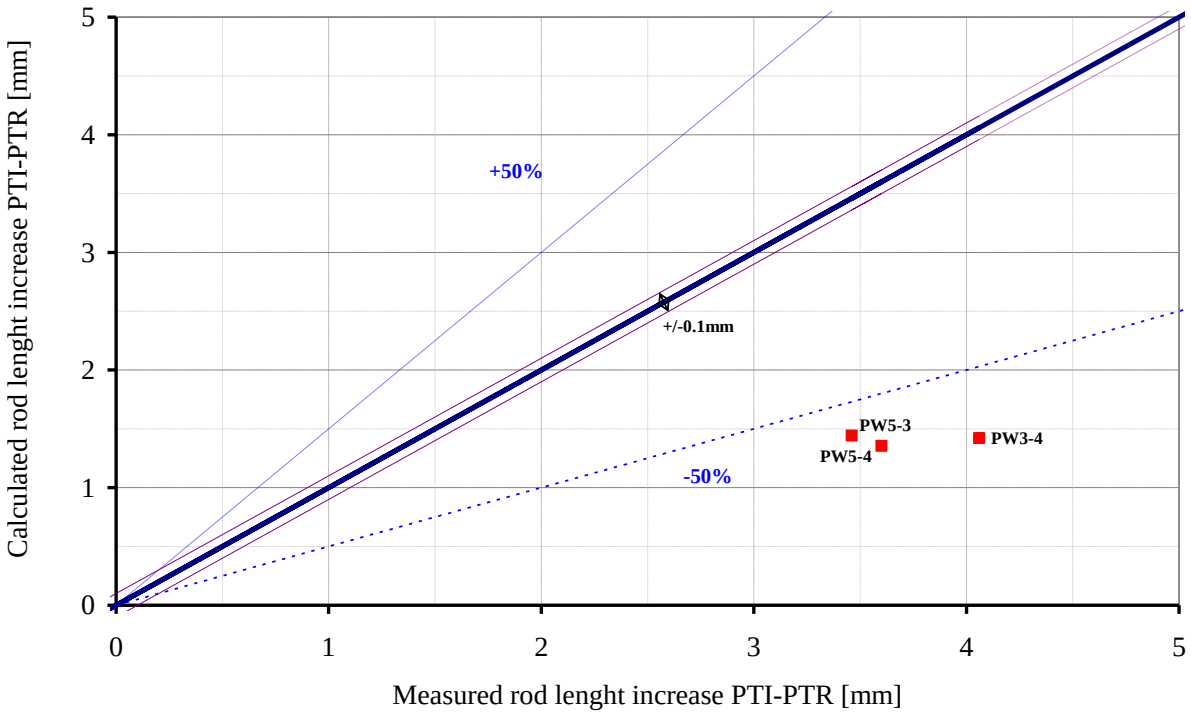

Fig. 22 – PWR Super-Ramp experiments versus TU v1m1j11 results: W rods, cladding elongation at the end of the base irradiation ("Reference").

5.1.6 **FGR analysis**

The reference simulation shows different predictions (*Fig. 23*):

- PK1 group results over predicted; the range of FGR is between 5 and 25%.
- PK2 group is generally slightly under predicted with the exception of PK2/S rod, this rod was ramped at a temperature 50° C lesser than the others. In this case, the range of FGR spreads between 10 up to 45 % (simulation and experiment).
- PK4 group results slightly under predicted with the exception of rod PK4/S that shows the worst under prediction (about -60%). The range of FGR is embedded in 10-30% (experiment and simulation)
- PK6 and PW3 (PW3/2 and PW3/3 are here attached) groups highlight low values of FGR (less than 10%) both in the experiment and calculation. The trend is generally under predicted.

In the figure is reported also the experimental accuracy (+/-8%).

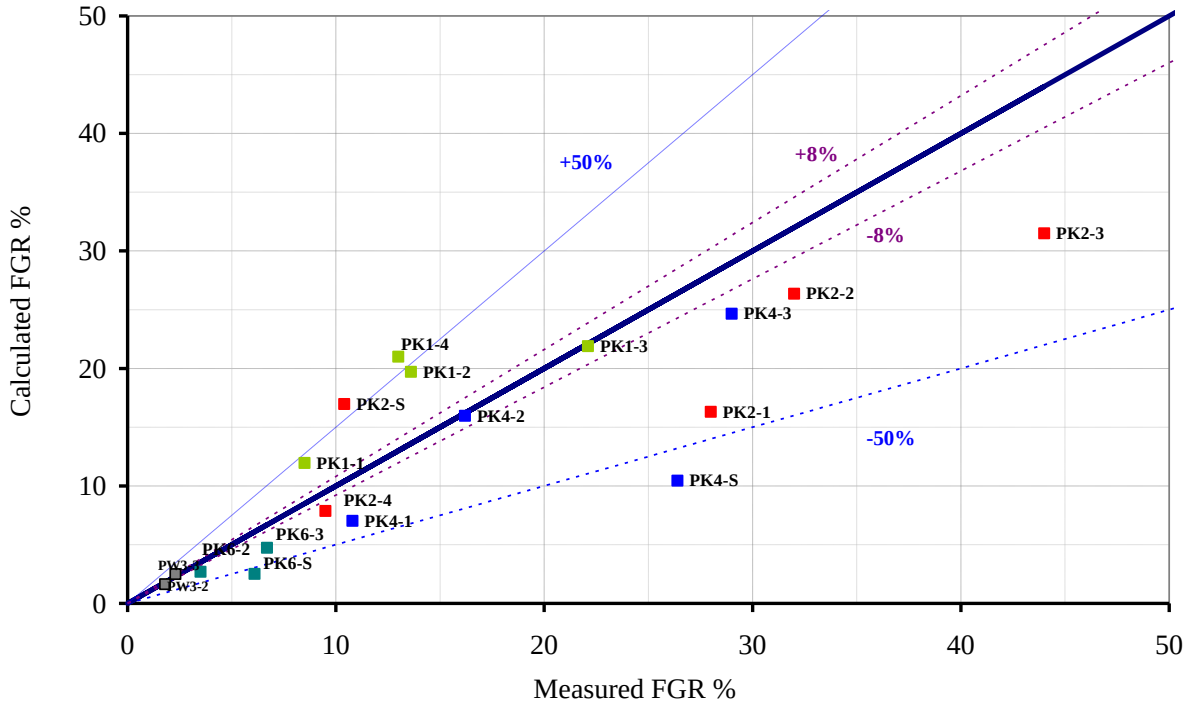

Fig. 23 – PWR Super-Ramp experiments versus TU v1m1j11 results: FGR analysis.

5.1.7 **Cladding stress analysis**

The parameters trends reported in *Fig. 24* and *Fig. 25* are related to the TU code results. No experimental data are available for the comparison. However, the code results are considered to provide relevant information for understanding when the SPAKOR subroutine, which is in charge to calculate the cladding failure for PCI/SCC, is activated. Chemical crack growth is assumed to initiate if the following conditions are satisfied (more details are available in Ref. [4] and section 4.3.12):

- Creation of a crack.
- The burn-up must exceed a critical value,
- The cladding temperature must exceed a critical value,
- The strain rate in the cladding must exceed a critical value, which is temperature dependent,
- The hoop stress must be positive.

The analysis is focused on two KWU rods: PK1/1 and PK6/1. *Fig. 24* and *Fig. 25* report the linear heat rate the gap width and the cladding hoop stress (all in peak axial position). When the failure occurs (*Fig. 25*), it is reported with a black dot. In these figures it is highlighted the transition between the negative and the positive hoop stress occurring when the gap is closed.

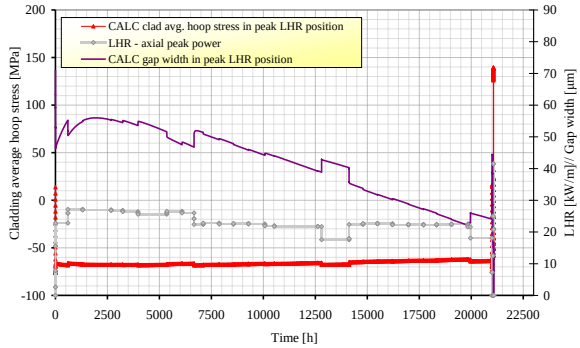

(a) overall

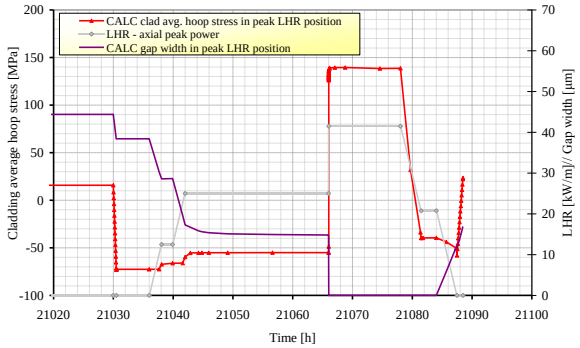

(a) Zoom on ramp phase

Fig. 24 – PWR Super-Ramp experiments versus TU v1m1j11 results: rod PK1/1, PWR Super-Ramp, cladding avg. hoop stress, gap size and LHR versus time ("Reference").

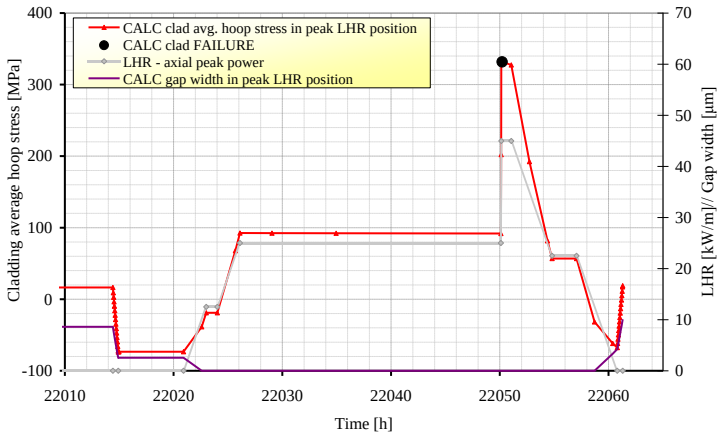

Fig. 25 – PWR Super-Ramp experiments versus TU v1m1j11 results: rod PK6/1, PWR Super-Ramp, cladding avg. hoop stress, gap size and LHR versus time (zoom on ramp phase, "Reference").

5.1.8 **Failure prediction**

The rod failures in the R-2 reactor are detected by a Cerenkov-type radiation sensor, which monitors the activity of the loop coolant water. The detector is installed in a by-pass circuit thus giving a delay time from failure to detection in the order of 155 ±10 s. In some cases, the moment of failure is registered by the power measurement system as a small thermal spike of very short duration, probably caused by an improvement of gap conductance when a crack penetrates the cladding. The rod elongation measuring system, if said system is used for the rod during ramping, may also reveal the rod failure moment. More details are available in Ref. [4]

In Tab. 26 and Tab. 27 cladding failure by PCI/SCC is analyzed, some parameters discussed in section 4.1, are also reported. TU predictions are compared with experimental results [4]. The choice of two distinct tables reflects the fact that, for KWU rods (Tab. 26), a conservative over-estimation of the failure propensity is predicted by TU code comparatively with the experimental failures while, for W rods, an under-estimation of failure propensity is observed (Tab. 27).

The code failure thresholds of each experimental group are reported (*Fig. 26*) in terms of ramp terminal level versus burn up. These thresholds are also identified experimentally for the groups PK6, and PW3 and 5 while are bounded for the other groups. The analysis of the experimental data and of the code results brought to the observations reported hereafter.

- The failure thresholds of the groups PK1, PK2, and PK4 are above the ramp terminal level limit of about 50 kW/m (corresponding to a power change of 25 kW/m), for burnup values between 30 and 45 MWd/kgU. The failure thresholds calculated by the "reference" calculations are lower. Rod PK1/S as to be considered an exception because of the calculated and measured burnup. The ramp test of this rod is conducted at low temperature (comparatively with the other PK1 rods). For these reasons, it is not considered embedded in the calculated threshold.
- Difficulties are observed in predicting the group PK2, which is characterized by the lower gap width and higher burnup. The calculated threshold resulted too conservative compared with the experimental one.
- The presence of Gadolinia (group PK4) shows a negligible influence in the rod failures, both in the experiments and in the TRANSURANUS simulation as well.
- The large grain size (group PK6) causes a reduction of the threshold limit, which was found in the experiment equal to 44 kW/m at about 35 MWd/kgU. The TRANSURANUS simulations qualitatively reproduce this effect, even though it underestimates this threshold of about 10 kW/m or more.
- The remedy cladding and annular pellets have no effect on the cladding failures (groups PW3 and PW5). The experimental data evidenced a failure threshold of 37.5 kW/m for burnup from 35 to 42 MWd/kgU. The TRANSURANUS simulations reveal that the calculated threshold is beyond the experimental especially for group PW3 (see *Fig. 26*). In the group PW3 two different calculated threshold can be identified: 41.5 – 43 KW/m for PW3/2 and PW3/3 rods and 62.5 – 69 KW/m for the others.

Rod group	Rod Label	Initial gap Width [µm]	Initial pellet grain size [µm]	Avg. LHR in BI [kW/m]	Avg. Neutron Fast flux [n/cm^{2}s]	Meas. Burnup [MWd/kgU]	RTL [kW/m]	RR [W/mh]	Hold Time [min]	EXP F/NF[1]	TU Ref. F/NF	TU PCI [hrs] [£]
PK1	PK1-1	100	6	23.00[&]	7.64E+13	35.4	41.5	540	720	**NF**	NF	21066
	PK1-2	100	6	23.04	7.64E+13	35.6	44	480	720	**NF**	**F** [2]	21069
	PK1-3	100	6	22.80	7.64E+13	35.2	47.5	510	720	**NF**	**F**	21070
	PK1-4	100	6	20.73	7.64E+13	33.1	47.5	570	720	**NF**	NF	22475
	PK1-S	100	6	21.11	5.72E+13	34.4	44	360	720	**NF**	NF	28133
PK2	PK2-1	71	5.5	21.98	7.99E+13	45.2	41	510	720	**NF**	**F**	21602
	PK2-2	71	5.5	21.95	7.99E+13	45.1	46	570	720	**NF**	**F**	21354
	PK2-3	71	5.5	21.72	7.99E+13	44.6	49	510	12	**NF**	**F**	21504
	PK2-4	71	5.5	20.14	7.99E+13	41.4	44	510	1	**NF**	**F**	23725
	PK2-S	71	5.5	21.17	7.99E+13	43.4	44	510	720	**NF**	**F**	22475
PK4	PK4-1	83	5.5	19.92 [21.41][$]	8.23E+13	33.7	39	480	720	**NF**	NF	21227
	PK4-2	83	5.5	19.96 [21.46]	8.23E+13	33.8	44.5	510	720	**NF**	**F**	21225
	PK4-3	83	5.5	19.46 [21.30]	8.23E+13	33.6	50.5	660	720	**NF**	**F**	21228
	PK4-S	83	5.5	18.10 [19.86]	8.23E+13	32.5	43	510	720	**NF**	NF	21228
PK6	PK6-1	73	22	21.92 [23.56]	7.68E+13	36.7	45	540	55	**F**	F	11479
	PK6-2	73	22	23.82	7.96E+13	36.8	40	540	720	**NF**	**F**	11407
	PK6-3	73	22	23.64	7.96E+13	36.5	43	540	720	**NF**	**F**	11508
	PK6-4	73	22	20.52 [21.83]	7.68E+13	33.6	44	600	60	**F**	F	11863
	PK6-S	73	22	23.20	7.96E+13	35.9	41	600	720	**NF**	**F**	11725

[&] Average value calculated from ASCII data
[$] Average value in peak axial position calculated from ASCII data
[£] Qualitative values
1 F/NF: failure / not failure
2 Blue color indicates wrong prediction in a conservative way

Tab. 26 – PWR Super-Ramp experiments versus TU v1m1j11 results: KWU rods, failure/ not failure ("Reference").

Rod group	Rod Label	Initial gap width [μm]	Initial grain size [μm]	Av.ge LHR in BI [kW/m]	Av.ge Neutron Fast flux [n/cm²s]	Meas. Burnup MWd/kgU	RTL [kW/m]	RR [W/mh]	Hold Time [min]	EXP F/NF[1]	TU F/NF	TU PCI [hrs]
PW3	PW3-1	80	10.5	14.66 [17.92]	3.30E+13	38.1	40	600	22	F	NF[2]	22780
	PW3-2	80	10.5	--	--	36.1	35.6	600	720	NF	NF	23701
	PW3-3	80	10.5	--	--	36.2	37.5	600	720	NF	NF	22973
	PW3-4	80	10.5	14.87 [18.16]	3.33E+13	36.6	37.7	540	12	F	NF	21768
	PW3-S	80	10.5	13.55 [16.53]	3.12E+13	35.1	40.1	600	17	F	NF	23730
PW5	PW5-1	80	16.9	14.86 [18.15]	3.30E+13	40.5	42.7	540	118	F	NF	19475
	PW5-2	80	16.9	14.63 [17.86]	3.25E+13	39.9	40.4	540	26	F	NF	20532
	PW5-3	80	16.9	15.09 [18.43]	3.40E+13	41.4	38.2	540	38	F	NF	18216
	PW5-4	80	16.9	14.27 [17.54]	3.06E+13	39.2	38	510	72	F	NF	23018

[&] Average value obtained from ASCII data
[$] Average value in peak axial position obtained from ASCII data

1 F/NF: failure / not failure
2 Red color indicates wrong prediction in a not conservative way

Tab. 27 – PWR Super-Ramp experiments versus TU v1m1j11 results, failure/not failure ("Reference").

Rod group	EXP RTL threshold [kW/m]	TU Reference RTL threshold [kW/m]
PK1	>47.5	[43.5-51]
PK2	>49	[33.5-39].
PK4	>51	[44-52]
PK6	44	[33-38.5]
PW3	37.5	[41.5 - 69]*
PW5	37.5	[44.5-46]

* [41.5 – 43] for PW3/2 and PW3/3
[62.5 – 69] for the others.

Tab. 28 – PWR Super-Ramp experiments versus TU v1m1j11 results: ramp terminal level failure thresholds ("Reference").

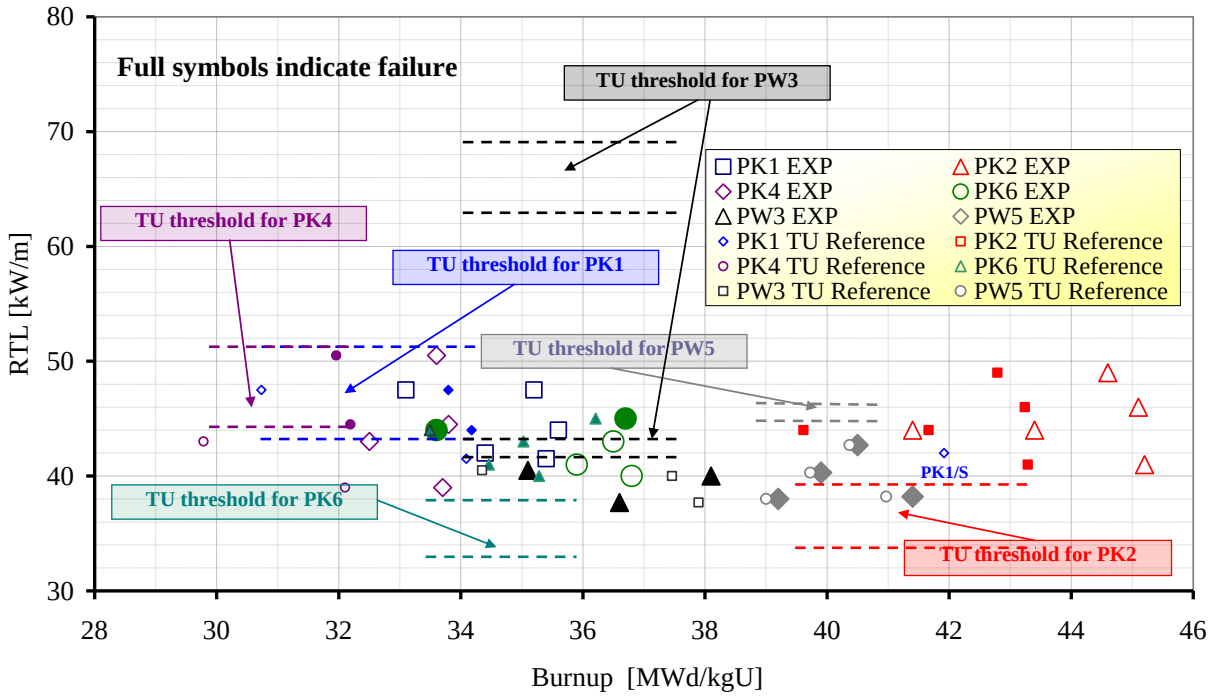

Fig. 26 – PWR Super-Ramp experiments versus TU v1m1j11 results: comparison between experimental results and TU simulations ("Reference").

5.2 Sensitivity analysis

5.2.1 **Fission gas release models**

The objective of the sensitivities is to verify the influence of the FGR models on the failure predictions. The "Reference" calculations are performed with FGRMOD 6 to treat intragranular bubbles gas behavior. It uses the URGAS algorithm with the diffusion coefficients of Hj. Matzke (thermal) and a constant athermal diffusion coefficient; the sensitivities concern:

- FGRMOD 4: URGAS algorithm with the diffusion coefficients of Hj. Matzke (thermal) and athermal diffusion coefficient according to data of R. White.
- FGRMOD 9: URGAS algorithm with diffusion coefficients of T. Turnbull.

The "Reference" model that considers intergranular gas bubbles behavior is IGRBDM 3, the new model to treat the grain boundary FGR during power ramps. Three sensitivities are performed with the "Reference" model for intragranular behavior (FGRMOD 6) and setting the intergranular behavior to:

- IGRBDM 0: Fission gas behavior at grain boundaries not treated
- IGRBDM 1: Simple grain boundary fission gas behavior model (standard option)
- IGRBDM 2: Simple grain boundary fission gas behavior model

The solving algorithm used in the "Reference" simulation is Idifsolv 0: diffusion equation is solved by the URGAS-algorithm. The analyses are performed with the "Reference" models for intragranular and intergranular behaviors (FGRMOD 6, IGRBDM3 respectively) and changing the solving algorithm to:

- IDIFSOLV 6: Diffusion equation is solved by the FORMAS-algorithm with 6 exponential terms.

The effect of the gas intergranular behavior is analyzed in *Fig. 27* comparing four different models. With the exception of the IGRBDM0 that assumes FGR without grain boundaries trapping in the other cases the predictions are lower compared to the reference one. IGRBDM 1 and IGRBDM 2 seem better represent the FGR of group PK1 while make worst the predictions in the other cases.

The effect of the gas intragranular behavior is analyzed in *Fig. 28* comparing three different models. The sensitivities highlight an increase of the calculated FGR comparatively with the reference case. Model FGRMOD4 better represent the behavior of PK2 and PK4 groups (PK1 result over predicted, PK6 and PW3 that have low FGR are predicted as in the reference). Model FGRMOD9 largely over predicts the FGR. Best estimate predictions can be reached choosing different models, the result obtained are presented in Fig. *29*, they are bounded in +/- 20%.

The results of the simulation are not considered relevant in term of failure prediction because they are similar to those of Tab. 26 and Tab. 27. Some models predicts the correct not failures of one rod (PK1/2).

Rod group	Rod Label	Measured Burnup [MWd/kgU]	EXP F/NF	TU Ref. F/NF	TU Idifsolv6 F/NF	TU Igrdbm0 F/NF	TU Igrdbm1 F/NF	TU Igrbdm2 F/NF	TU Fgrmod4 F/NF	TU Fgrmod9 F/NF
PK1	PK1-1	35.4	NF	NF	NF	NF	NF	NF	NF	NF
	PK1-2	35.6	NF	F	NF	F	NF	NF	F	F
	PK1-3	35.2	NF	F	F	F	F	F	F	NF
	PK1-4	33.1	NF	NF	NF	NF	NF	NF	NF	NF
	PK1-S	34.4	NF	NF	NF	NF	NF	NF	NF	NF
PK2	PK2-1	45.2	NF	F	F	F	F	F	F	F
	PK2-2	45.1	NF	F	F	F	F	F	F	F
	PK2-3	44.6	NF	F	F	F	F	F	F	F
	PK2-4	41.4	NF	F	F	F	F	F	F	F
	PK2-S	43.4	NF	F	F	F	F	F	F	F
PK4	PK4-1	33.7	NF	NF	NF	NF	NF	NF	NF	NF
	PK4-2	33.8	NF	F	F	F	F	F	F	F
	PK4-3	33.6	NF	F	F	F	F	F	F	F
	PK4-S	32.5	NF	NF	NF	NF	NF	NF	NF	NF
PK6	PK6-1	36.7	F	F	F	F	F	F	F	F
	PK6-2	36.8	NF	F	F	F	F	F	F	F
	PK6-3	36.5	NF	F	F	F	F	F	F	F
	PK6-4	33.6	F	F	F	F	F	F	F	F
	PK6-S	35.9	NF	F	F	F	F	F	F	F
PW3	PW3-1	38.1	F	NF	NF	NF	NF	NF	NF	NF
	PW3-4	36.6	F	NF	NF	NF	NF	NF	NF	NF
	PW3-S	35.1	F	NF	NF	NF	NF	NF	NF	NF
PW5	PW5-1	40.5	F	NF	NF	NF	NF	NF	NF	NF
	PW5-2	39.9	F	NF	NF	NF	NF	NF	NF	NF
	PW5-3	41.4	F	NF	NF	NF	NF	NF	NF	NF
	PW5-4	39.2	F	NF	NF	NF	NF	NF	NF	NF

Tab. 29 – PWR Super-Ramp experiments versus TU v1m1j11 results: sensitivity analysis concerning FGR – Failure prediction.

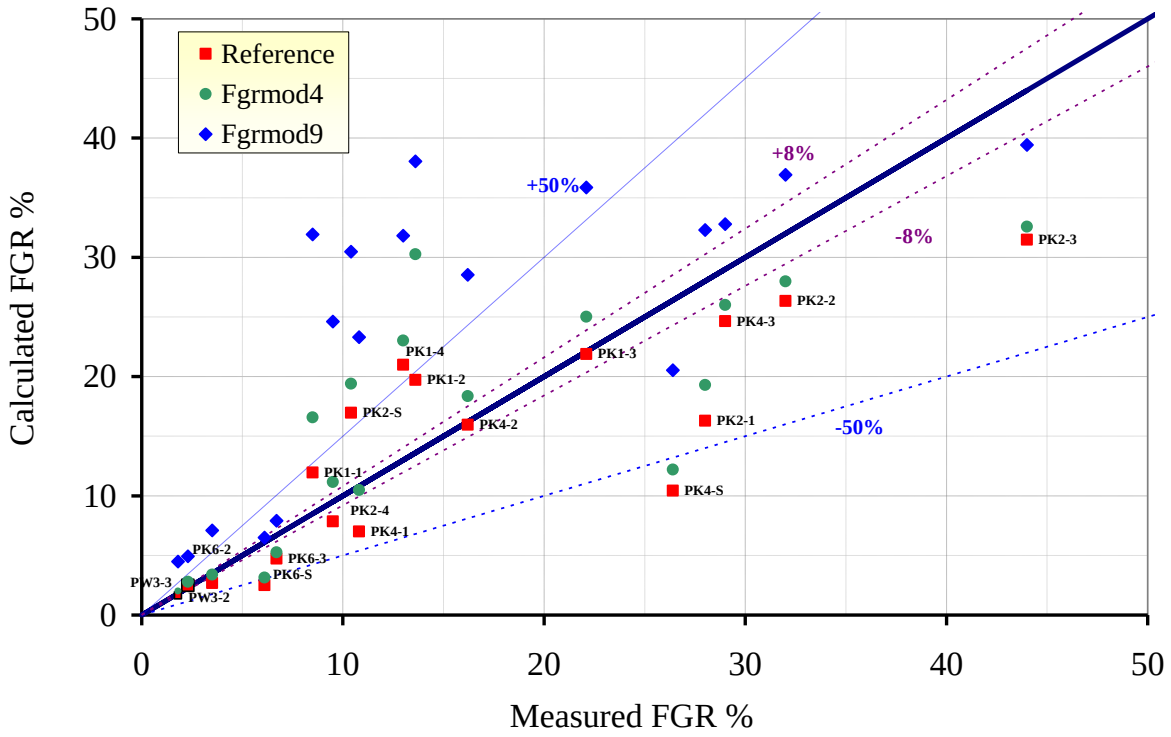

Fig. 27 – PWR Super-Ramp experiments versus TU v1m1j11 results: sensitivity analysis addressing the influence of FG intergranular model.

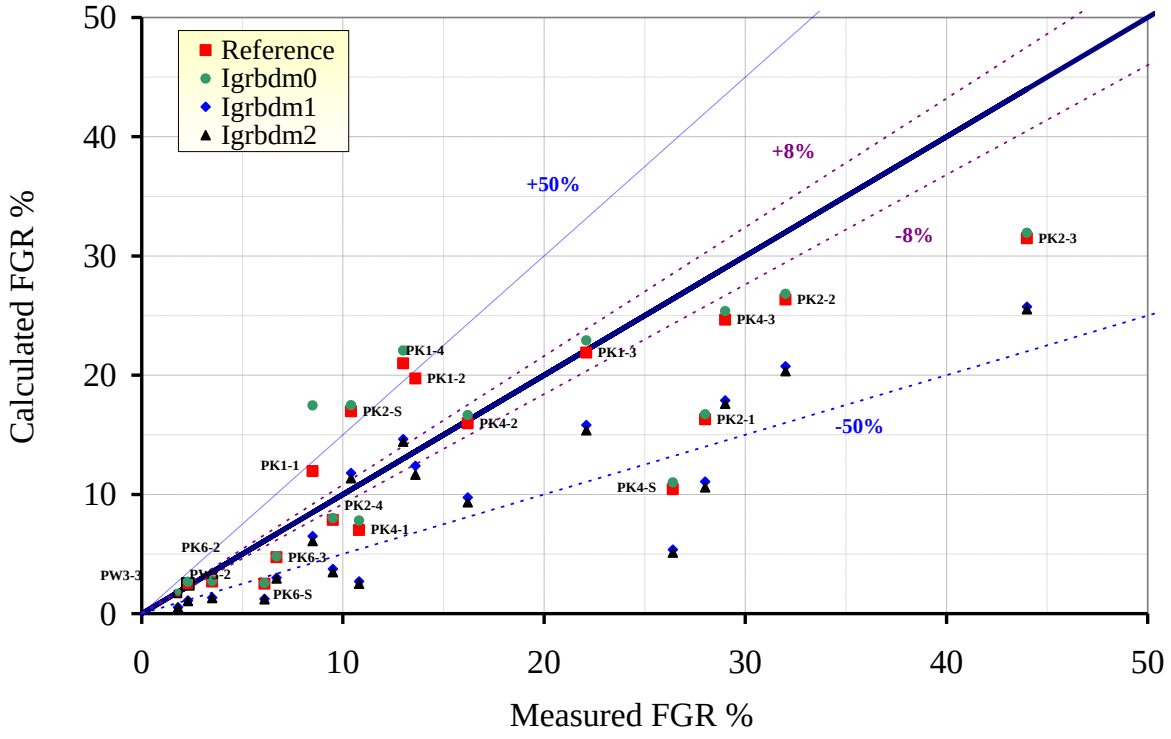

Fig. 28 – PWR Super-Ramp experiments versus TU v1m1j11 results: sensitivity analysis addressing the influence of FG intragranular model.

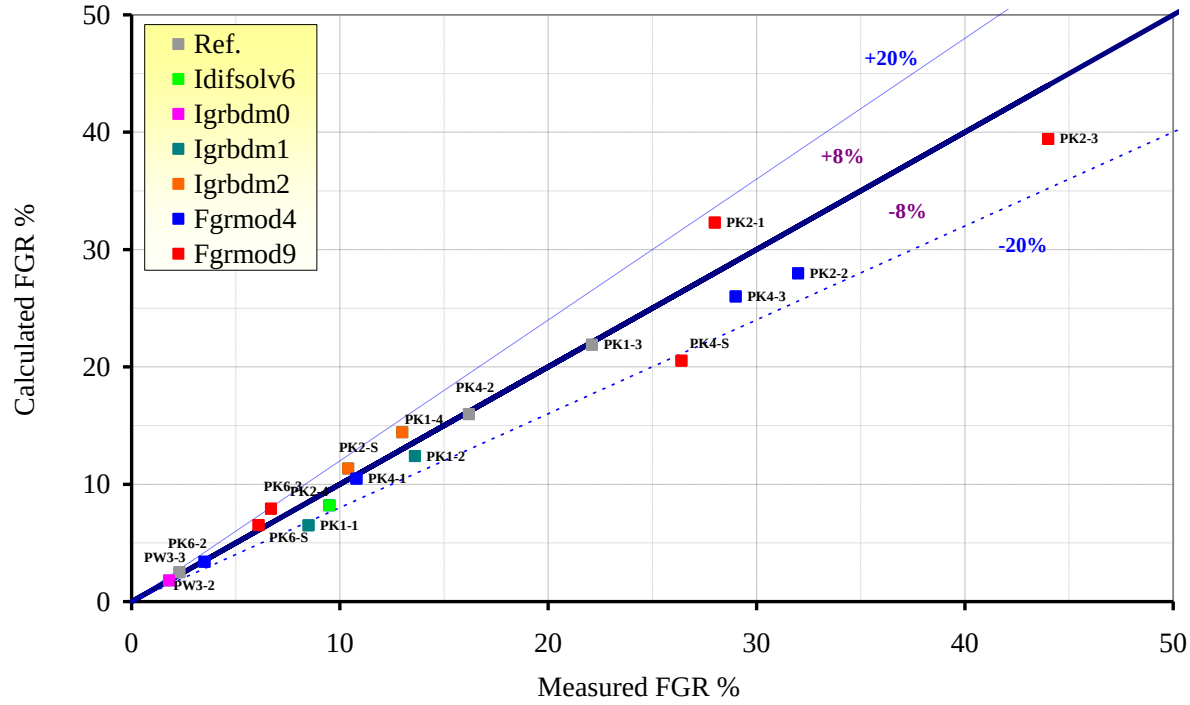

Fig. 29 – PWR Super-Ramp experiments versus TU v1m1j11 results: best estimate FGR models.

5.3 "Improved" input decks

An "Improved" input for KWU rods is proposed in Tab. 30. it is based on the results obtained from the sensitivity analyses performed in [36]. (see also Refs. [32] and [33]).

An "improved" input-deck may be necessary to take into account the different designs and irradiation conditions among the six groups (PK1, PK2, PK4, PK6, PW3, PW5). In fact, as reported in the PWR SUPER-RAMP final report (*Djurle, et al., 1984*) *"...it is to be expected that differences in design, material, fabrication procedure and base irradiation history may influence the rod behaviour during ramping and the achieved rod data. However, within each group of rods consistent data may be expected..."*. In particular is reported that: "*A comparison between PK and PW rods does not to seem meaningful due to the large differences in design and heat rating.*"

Differences are also in the rod lengths, in the active lengths of the NPP cores used for the base irradiation (W rods are more than two times longer than KWU and are irradiated in a research reactor core of similar length, while KWU rods are irradiated in a commercial core six time longer) and in the base irradiation conditions (about 10 kW/m of difference). The application of the different models was, also, justified because the observation of different behaviors of "some" KWU rods, due to the differences above.

- The Reference fuel conductivity correlation has been changed to the old recommended. It is correlated with the HBS width of the more irradiated rods: it results several time lesser than the pellet radial dimension so the old correlation (that do not consider HBS) is applied.
- The relocation model has also been changed. The modified FRACPON-3 model (ireloc 8, recommended) applied in the "Improved" input decks seems to be more appropriate comparatively with the simple model ireloc 5 that considers relocation as a function of the initial gap in cold conditions only.

In particular it has been observed that with the reference relocation and conductivity models the failure of rods PK1/3, PK4/2, PK2/4, PK4/3 occur after the ramp, when the LHR decrease. According to [36]:

- The radial gap stays closed during the ramp
- It opens when power decrease, at this point FG are released
- The gaseous porosity when gap opens is relaxed and expands causing gap reclosure, fuel central temperature increase (due to conductivity degradation), the clad is forced to expand until its failure in semi-cold conditions.

The principal responsible for gaseous swelling is the relocation model while fuel conductivity degradation due to high porosity is responsible for fuel temperature increase.

In Tab. 31 the "Improved" input for W rods is reported. It is based, mainly, on the sensitivity analyses performed on the boundary conditions and swelling correlations.

- The constant axial shape of the fast neutron flux implemented in the "Reference" calculation is fixed axially variable as cosine in the "Improved" (see [36]).
- The relocation model has been changed.
- The fuel swelling correlation implemented (only for PW5 group) in the "Improved" input is the simple correlation 18. It is related to the better predictions achieved in both failures and cladding

dimensional changes as demonstrated in [36]. This results may be connected to the radial temperature profile that influence the reference swelling model and, to the design (annular pellet) is quite low to simulate the real swelling. It must be mentioned that the simple correlation Swell 18 is appropriate for normal operation and usually underpredicts the swelling if applied to ramp situation (FGR from ramp is neglected).

- The EPRI cladding waterside corrosion model implemented in the "Reference" calculation is changed to the MATPRO model in the "Improved". It is connected with the different behavior observed for the W rods (comparatively to the KWU) [36].

In Tab. 32 the results obtained from the "Improved" input decks are compared with the original one ("Reference"). The new simulations show that 20 out of 28 rods are predicted as in the experiment, the 8 erroneous predictions are of conservative type, the results include PW3/2 and PW3/3 rods.

The code failure thresholds of each experimental group are reported (*Fig. 30* and Tab. 33) in terms of ramp terminal level versus burn up, PW3/2 and PW3/3 are included. The analysis of the experimental data and of the code results brought to the observations reported hereafter.

- The failure thresholds of the groups PK1, and PK4 are above the ramp terminal level limit of about 50 kW/m. The "Improved" results increased these thresholds (comparatively to the "Reference" results), allowing a better estimate of the not failed rods.
- Difficulties are observed in predicting the group PK2 (both "Reference" and "Improved" simulations), which is characterized by the lower gap width and higher burnup. The calculated threshold resulted too conservative compared with the experimental one. Rod PK2/S has to be considered an exception. It is ramped at 50°C below as normal, for this reason the "Improved" calculation predicts that it does not fail although it is beyond the calculated PK2 threshold. A check addressed to this rod reveals that it fails if the normal temperature is applied during the ramp phases.
- The large grain size (group PK6) causes a reduction of the threshold limit, which was found in the experiment equal to 44 kW/m at about 35 MWd/kgU. This effect is qualitatively reproduced by the TRANSURANUS simulations, even though it underestimates this threshold of about 10 kW/m (both "reference" and "improved" analyses).
- The remedy cladding and annular pellets have no effect on the cladding failures (groups PW3 and PW5). The experimental data evidenced a failure threshold of 37.5 kW/m for burnup from 35 to 42 MWd/kgU. The TRANSURANUS simulations demonstrate that the failure threshold calculated is well predicted when the assumption of the axial neutron fast flux with cosine approximation is applied ("Improved" results).

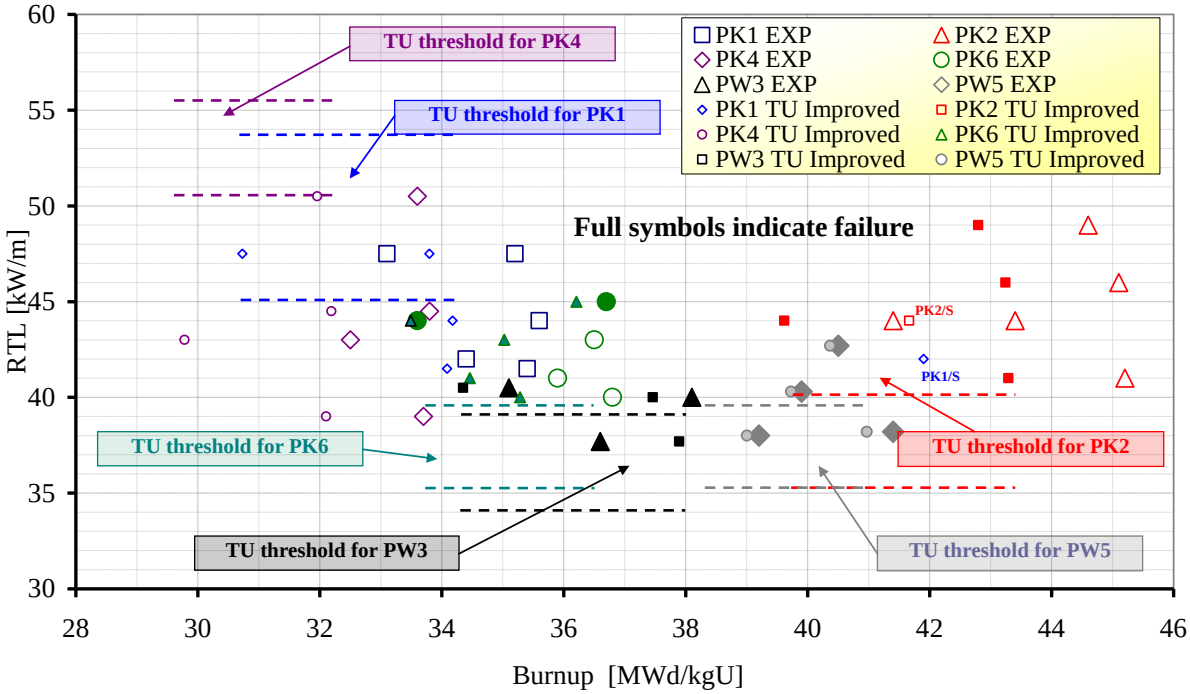

Fig. 30 – PWR Super-Ramp experiments versus TU v1m1j11: comparison between experimental results and "Improved" TU simulation.

PWR Super-Ramp KWU rods			
Input parameter	**Reference**	**Improved**	**Description**
Fuel conductivity	Correlation 21 (recommended)	Correlation 20	Old standard $(U,Gd)O_2$ correlation
Fuel swelling	Correlation 20 (recommended)	Correlation 20 (recommended	Developed by K. Lassmann from correlation 19. The gaseous swelling contribute was modified and integrated from this steady state equation --
Pellet fragment	Model ireloc 5	Model ireloc 8	Modified FRAPCON-3 model
Fuel grain growth	Model igrnsz 1 (recommended)	Model igrnsz 1 (recommended)	Grain growth model of Ainscough and Olsen
Fuel densification	Model idensi 2 (recommended)	Model idensi 2 (recommended)	Empirical model for LWR and FBR. This model needs the input of the minimum porosity DENPOR at the end of thermal and irradiation induced densification and the time constant DENBUP (burnup in MWd/tU, at which irradiation induced densification is terminated).
Gap conductivity	Model ihgap 0 (recommended)	Model ihgap 0 (recommended)	Standard Option: gas Bonding thermal conductivity of mixture according to Lindsay and Bromley. Accommodation coefficients are taken into account
Cladding conductivity	Correlation 20 (recommended)	Correlation 20 (recommended)	Identical with the MATPRO correlation 19 that was taken from the MATPRO handbook
Cladding swelling	Correlation 20 (recommended)	Correlation 20 (recommended)	This correlation was given by Duncombe for Zircaloy in an annealed state or with a small amount of cold work
Cladding outer corrosion	Model icorro 13	Model icorro 13	EPRI/C-E/KWU waterside corrosion model (PWR conditions); model assumption a) for varying conditions, thermal effect and the weakening of the cladding (mechanical effect) are considered
Cladding creep	Correlation 20 (recommended)	Correlation 20 (recommended)	Effective creep rate according to the Lassmann-Moreno
Fission gas release	Models: **fgrmod6 (recommended)**, **igrbdm3**,**Idifsolv0**	Models: **fgrmod6 (recommended)**, **igrbdm3**,**Idifsolv0**	*FGRMOD 6:* URGAS algorithm with the diffusion coefficients of Hj. Matzke (thermal) and a constant athermal diffusion coefficient. *IGRBDM 3:* New model developed according to modified Koo model for ramps simulations *IDIFSOLV 0:* Diffusion equation is solved by the URGAS-

Tab. 30 – PWR Super-Ramp experiments versus TU v1m1j11 results: KWU rod, comparison addressing parameter that influence PCI/SCC: "Reference" vs "Improved" input decks.

PWR Super-Ramp W rods			
Input parameter	**Reference**	**Improved**	**Description**
Neutron fast flux	Axially constant	Axially variable as cosine	Boundary condition
Fuel conductivity	Correlation 21 (recommended)	Correlation21 (recommended)	New standard correlation. It has been fitted to data from ITU.
Fuel swelling	Correlation 20 (recommended)	Correlation 18	Simple correlation gives the total swelling rate for LWR fuel including matrix swelling due to solid and gaseous fission products (PW5 only)
Pellet fragment	Model ireloc 5	Model ireloc 8	Modified FRAPCON-3 model
Fuel grain growth	Model igrnsz 1 (recommended)	Model igrnsz 1 (recommended)	Grain growth model of Ainscough and Olsen
Fuel densification	Model idensi 2 (recommended)	Model idensi 2 (recommended)	Empirical model for LWR and FBR. This model needs the input of the minimum porosity DENPOR at the end of thermal and irradiation induced densification and the time constant DENBUP (burnup in MWd/tU, at which irradiation induced densification is terminated).
Gap conductivity	Model ihgap 0 (recommended)	Model ihgap 0 (recommended)	Standard Option: gas Bonding thermal conductivity of mixture according to Lindsay and Bromley. Accommodation coefficients are taken into account
Cladding conductivity	Correlation 20 (recommended)	Correlation 20 (recommended)	Identical with the MATPRO correlation 19 that was taken from the MATPRO handbook
Cladding swelling	Correlation 20 (recommended)	Correlation 20 (recommended)	This correlation was given by Duncombe for Zircaloy in an annealed state or with a small amount of cold work
Cladding outer corrosion	Model icorro 13	Model icorro 2	MATPRO model (PWR conditions); only thermal effect is considered
Cladding creep	Correlation 20 (recommended)	Correlation 20 (recommended)	Effective creep rate according to the Lassmann-Moreno
Fission gas release	Models: **fgrmod6 (recommended)**, **igrbdm3**,**Idifsolv0**	Models: **fgrmod6 (recommended)**, **igrbdm3**,**Idifsolv0**	*FGRMOD 6:* URGAS algorithm with the diffusion coefficients of Hj. Matzke (thermal) and a constant athermal diffusion coefficient. *IGRBDM 3:* New model developed according to modified Koo model for ramps simulations *IDIFSOLV 0:* Diffusion equation is solved by the URGAS-

Tab. 31 – PWR Super-Ramp experiments versus TU v1m1j11 results: W rods, comparison addressing parameter that influence PCI/SCC: "Reference" vs "Improved" input decks.

Rod group	Rod Label	EXP F/NF	TU Reference F/NF	TU Improved F/NF
PK1	PK1-1	NF	NF	NF
	PK1-2	NF	F	NF
	PK1-3	NF	F	NF
	PK1-4	NF	NF	NF
	PK1-S	NF	NF	NF
PK2	PK2-1	NF	F	F
	PK2-2	NF	F	F
	PK2-3	NF	F	F
	PK2-4	NF	F	F
	PK2-S	NF	F	NF
PK4	PK4-1	NF	NF	NF
	PK4-2	NF	F	NF
	PK4-3	NF	F	NF
	PK4-S	NF	NF	NF
PK6	PK6-1	F	F	F
	PK6-2	NF	F	F
	PK6-3	NF	F	F
	PK6-4	F	F	F
	PK6-S	NF	F	F
PW3	PW3-1	F	NF	F
	PW3-2	NF	NF	NF
	PW3-3	NF	NF	F
	PW3-4	F	NF	F
	PW3-S	F	NF	F
PW5	PW5-1	F	NF	F
	PW5-2	F	NF	F
	PW5-3	F	NF	F
	PW5-4	F	NF	F

Tab. 32 – PWR Super-Ramp experiments versus TU v1m1j11 results: comparison between "Reference" and "Improved" input decks.in predicting failures / not failures.

Rod group	EXP RTL threshold [kW/m]	TU Reference RTL threshold [kW/m]	TU Improved RTL threshold [kW/m]
PK1	>47.5	[43.5-51]	[44.5-54.5]
PK2	>49	[33.5-39].	[35 – 40]
PK4	>51	[44-52]	[50-57]
PK6	44	[33-38.5]	[35–39]
PW3	37.5	[41.5 - 69]*	[35-38]
PW5	37.5	[44.5-46]	[35-39]

Tab. 33 – PWR Super-Ramp experiments versus TU v1m1j11 results: ramp terminal level failure thresholds.

6 Conclusions

The capability of TRANSURANUS version "v1m1j11" code in predicting the phenomenon of the pellet clad interaction is assessed against PWR Super-Ramp Project. The experiment addresses the behavior of 26 PWR fuel rods, including preceding base irradiation, during the over-power ramping. The burn-up values range between 30 and 45 MWd/kgU. The approach to the analysis was performed in this manner:

1. preparation of the "Reference" input decks based on [36],
2. execution of FGR sensitivity analyses,
3. preparation of the "Improved" input decks based on the major results obtained in the sensitivity analyses performed in [36].

The main conclusions are hereafter summarized.

- Burnup analysis: the "Reference" calculations show a general agreement between measured and calculated values. The burnup results under-predicted with an error lesser then 10%. Only rod PK1/S shows an over-prediction close to 25%, further analysis indicates that the ASCII data of this rod are not in agreement with the data of the PK1 group.
- Diameter change analysis: the code results show a systematic under-prediction of the *creep down* in both the cases "Reference" and "Improved", the errors are bounded by the line corresponding to -50% with the exception of group PK6 (large grain size). Cladding *diameters increase* are in general under-predicted. The best prediction ("Reference" case) is experienced by the KWU rods PK1/3, PK4/2 and PK2/S. This can be correlated with the erroneous prediction of failures. Similar results are achieved by the "Improved" calculations, with the exception of the noticeable improvement of the W rods, modeled imposing cosine axial shape to the neutron fast flux.
- Outer corrosion analysis: the general trend is under-prediction ("Reference"). Two different behaviors are visible comparing KWU and W rods. The first reaches the break away point while the second never reaches this point, the experimental measures seems to confirm this prediction and it is correlated with the different cladding temperatures during base irradiation. In the "Improved" input this fact is taken into account, a different corrosion model is applied to W rods and better results are obtained for these rods.
- Grain size analysis: similar results are obtained in both "Reference" and "Improved" simulations. KWU rods are both under-estimated, the error range from up to 50%. W rods are always under-predicted; the error is less than 30%. Different behavior is observed between the two types of rods: KWU rods shows radial grain change effect while, the contrary is for W rods. The experiment seems to confirm this prediction (W rods don't reach UO_2 recrystallization temperature).
- Rod length change analysis: the data are available for W rods only and show a large under-prediction of the rod length increase during base irradiation.

- Fission gas release: FGR obtained from the Reference and the Improved simulations results bounded +/-50% comparatively to the experiment. Assuming best estimate models +/-20 error can be reached.
- Failure/not failure prediction: the prediction of the failures of KWU rods is correct for 7 out of 19 rods in the "Reference" simulation. The analysis of the results demonstrates that the code resulted conservative, over predicting the fuel failures. On the contrary, the 7 W rods failed in the experiment were predicted not failed by the code ("Reference"). The "Improved" input decks allows to predict correctly 12 out of 19 rods KWU and 7 out of 7 W rods. The errors are all of conservative type.
- Comparison with the main experimental results.
  - Not any experimental failure threshold were identified for groups PK1, PK2, PK4. The failure thresholds calculated by the "Reference" calculations are too conservative, the "Improved" results increases these thresholds, allowing a better estimate of the not failed rods especially for groups PK1 and PK4.
  - The large grain size (group PK6) causes a reduction of the threshold limit, which was found in the experiment equal to 44 kW/m at about 35 MWd/kgU. This effect is qualitatively reproduced by the TRANSURANUS simulations, even though it underestimates this threshold of about 10 kW/m (both "Reference" and "Improved" analyses).
  - The remedy cladding and annular pellets have no effect on the cladding failures (groups PW3 and PW5). The experimental data evidenced a failure threshold of 37.5 kW/m for burnup from 35 to 42 MWd/kgU. The TRANSURANUS simulations demonstrate that the failure threshold calculated is well predicted when the assumption of the axial neutron fast flux with cosine approximation is applied ("Improved" results).

Therefore, the conclusion is that the PCI failure criterion implemented in TRANSURANUS code (SPAKOR soubroutine) in the case of PWR fuel (PWR KWU and Westinghouse, from 30 to 45MWd/kgU) and Zircaloy-4 cladding, predicts the rod failures due to PCI conservatively.

REFERENCES

[1] *Lassmann K.*, **TRANSURANUS: a fuel rod analysis code ready for use**, Journal of Nuclear Material 188 (1992) 295-302.

[2] *Van Uffelen P.*, **Modeling of Nuclear Fuel Behavior**, **Publications Office,** JRC Publications, Report EUR 22321 EN, European Commission, 2006.

[3] *Lassmann K., A. Schubert, P. Van Uffelen, Cs. Gyory, J. van de Laar*, **Transuranus Handbook Version "v1m1j06"**, EC, JRC, ITU, July 2006**.**

[4] *Djurle S., et al.*, **The Super-Ramp Project, Final report of the Super-Ramp project**", STIR-32, Studsvik AB Atomenergi, Studsvik, Sweden, 1984.

[5] *Mogard H., et al.*, **The Studsvik Inter-Ramp Project", Final Report of the Inter-Ramp Project**, STIR-53, Studsvik AB Atomenergi, Studsvik, Sweden, 1979.

[6] *OECD/NEA*, **The Public Domain Database on Nuclear Fuel Performance Experiments for the Purpose of Code Development and Validation, International Fuel Performance Experiments (IFPE)**, http://www.nea.fr/html/science/fuel/ifpelst.html.

[7] *Chantoin P., E. Sartori, J.A. Turnbull*, **The Public Domain Database on Nuclear Fuel Performance Experiments (IFPE) for the Purpose of Code Development and Validation**, ANS, Topical Meeting on Light Water Reactor Fuel Performance, Portland, Oregon, 2-6 March 1997.

[8] *Killeen J.C., E. Sartori, J.A. Turnbull*, **Experimental Data on PCI and PCMI within the IFPE Database**, Proceedings of Seminar on Pellet-clad Interaction in Water Reactor Fuels, Aix-en-Provence, France, 9-11 March 2004.

[9] *Grounes M., H. Tomani, A. Lassing, M. Carlsson*, **Fuel R&D at Studsvik I. Introduction and experimental facilities**, Studsvik nuclear AB S-611 82 Nikoping Sweden.

[10] *Adorni M., A. Del Nevo, F. Oriolo, F. D'Auria, P. Van Uffelen*, **Assessment of TRANSURANUS Fuel Performance Code Against Studsvik Inter-Ramp BWR Database**, Proceedings of the 17th International Conference on Nuclear Engineering, Portorož, Brussels, Belgium July 12-16, 2009, pp. 1-10.

[11] *IAEA International Nuclear Safety Group*, **Basic safety principles for NPPs**, INSAG-3 report, IAEA, Vienna, Austria, March 1988)

[12] *IAEA International Nuclear Safety Group*, **Basic safety principles for nuclear power plants**, INSAG-12 report, 75-INSAG-3 rev.1, IAEA, Vienna, Austria, 1999.

[13] *Bailly H., D. Menessier, C. Prunier*, **The Nuclear Fuel of Pressurized Water Reactors and Fast Neutron Reactors**, Collection du Commissariat a l'Energie Atomique, Lavoisier Pub., Intercept, Paris, Andover, 1999,.

[14] *Cox B.*, **Pellet clad interaction (PCI) failures of Zirconium alloy fuel cladding**, J Nucl.Mater 172, 249-292 (1990).

[15] *M. Gartner, G. Fischer*, **Survey of the power ramp performance testing of KWU's PWR UO2 fuel**, J.Nucl.Mater., 149, 29-40 (1987).

[16] *Lassmann, H Blank*, **Modeling of fuel rod behavior and recent advances of TU code,** Nuclear Engineering and design 106(1988) 291-313 North-Holland, Amsterdam.

[17] *Adorni M., A. Del Nevo, F. D'Auria, L. Luzzi*, **Verification of TRANSURANUS Code Version V1M1J07 and V1M1J08 against BWR Inter-Ramp Experiment**, Gruppo di Ricerca Nucleare San Piero a Grado, DIMNP, UNIPI, NT631(08) Rev. 1, 2008.

[18] *Olander D. R.*, **Fundamental Aspects of Nuclear Reactors Fuel Elements**, Department of Nuclear Engineering University of California, Berkeley. 1 January 1976.

[19] *Golinelli C., M. J. L. Guillet*, **MOX in France. Status and Prospects**, IAEA Technical Committee Meeting on Recycling of Pu and U in Water Reactor Fuel, Windermere, 1995.

[20] *American National Standard Institute*, **Nuclear Safety Criteria For The Design Of Stationary PWR Plants**, AISI No.18.2, 1973.

[21] *ARN regulatory guide*, **Radiological Criteria relating to accidents in nuclear power plants**, ARN AR 3.1.3, República Argentina, 2002

[22] *OECD/CSNI/PWG2 Task Force*, **Fuel Safety Criteria Technical Review**, OECD NEA/CSNI/R(99)25, Paris, July 2000.

[23] *OECD/NEA/CSNI Member Countries*, **Fuel Safety Criteria in NEA Member Countries: Compilation of Responses Received from Member Countries**, OECD NEA/CSNI/R(2003)10, Paris, July 2003.

[24] *Djurle S. et al.*, **The International OVER-RAMP Project at Studsvik**, Proceedings of ANS Topical Meeting on Fuel Performance, VA, USA, April 1982.

[25] *Denis A., A. Soba*, **Simulation of pellet-cladding thermomechanical interaction and fission gas release**, Nuclear Engineering and Design, Volume 223, Issue 2, August 2003, Pages 211-229.

[26] OECD Nuclear Science, Pellet-clad Interaction in Water Reactor Fuels, Seminar Proceedings, Aix-en-Provence, Published by OECD Publishing, France, 9-11 March 2004.

[27] *ITU Fuel Modeling Team*, **Direct communication**, Meeting ITU-GRNSPG/UNIPI, JRC-ITU Karlsruhe, 8 June 2009.

[28] *G. Pastore, P. Botazzoli, V. Di Marcello, L. Luzzi*, **Simulation of Power Ramp Tested LWR Fuel Rods by Means of the TRANSURANUS Code**, Proceeding of Top Fuel 2009, Paris France, 6-10 September 2009.

[29] *Adorni M, D. Rozzia, A. Del Nevo, F. D'Auria*, **Capabilities of TRANSURANUS Code in Simulating Power Ramp Tests from the IFPE Database**, Proceedings of OECD/NEA Workshop Nuclear Fuel Behavior during RIA, Paris, France, 9-11 September 2009.

[30] *Pastore G., P. Botazzoli, V. Di Marcello, L. Luzzi*, **Assessment of the prediction capability of the TRANSURANUS fuel performance code on the basis of power ramp tested LWR fuel rods**, Proc. of the 8th Conf. on WWER Fuel Performance, Modelling and Experimental Support, Burgas, Bulgaria, 26 September 4 October 2009.

[31] *D. Rozzia*, **Modeling of PCI during Power Ramp in Water Reactor Fuel,** Master Degree, UNIPI 12-10-2009.

[32] *D. Rozzia, Adorni M, A. Del Nevo, F. D'Auria,* **Capabilities of TRANSURANUS Code in Simulating Power Ramp Tests from the IFPE Database**, Proceeding of International Conference of Nuclear Energy for New Europe (NENE), Bled, Slovenia N. 108, pp. 1–12.

[33] *Rozzia, D., et al*, **Capabilities of TRANSURANUS Code in Simulating Power Ramp Tests from the IFPE Database**, Nucl. Eng. Des. (2010), doi:10.1016/j.nucengdes.2010.04.027.

[34] *Van Uffelen P.* **Direct communication with ITU. Obj. Re: Final report BWR-INTERRAP**, e-mail received 20 October 2010, 7.16pm

[35] *Joo-Wan H., Doh-Yeon K.* Analysis of the proportionality constant correlating the mean intercept length to the average grain size, Acta metal. Mater. Vol. 43, No. 8 pp. 3185-3188, 1995.

[36] *D.Rozzia, M. Adorni, A.Del Nevo, F. D'Auria*. **Capabilities of Transuranus code in simulating power ramp tests from the IFPE database: PWR super-ramp experiment**, Gruppo di Ricerca Nucleare San Piero a Grado, DIMNP NT647(10) Rev.0, March 2010.

APPENDIX A: PWR Super-Ramp boundary conditions implemented

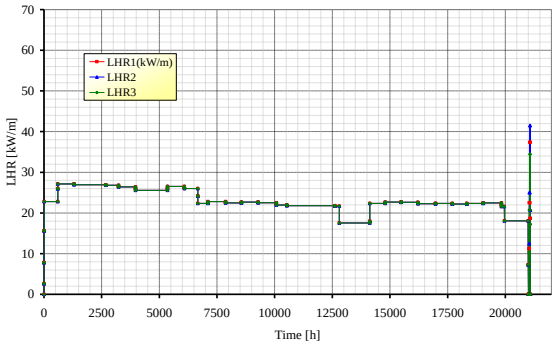

(a) LHRs in total irradiation in 3 axial positions

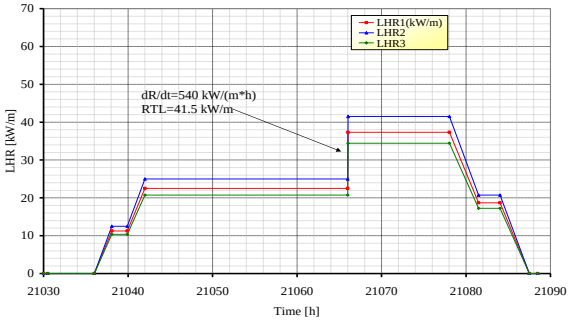

(b) LHRs in ramp in 3 axial positions

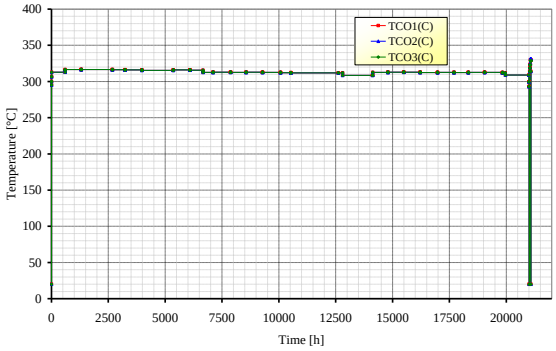

(c) Temperatures in total irradiation in 3 axial positions

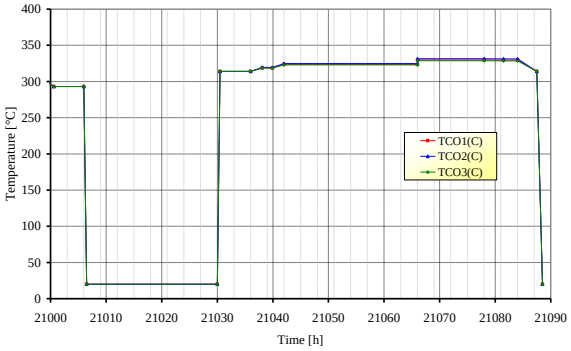

(d) Temperatures in ramp in 3 axial positions

Fig. A - 1 – Rod PK1/1 PWR Super-Ramp Project.

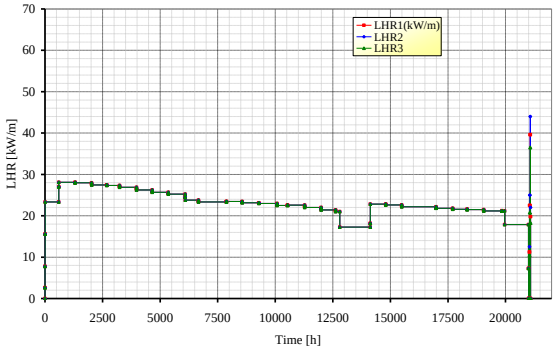

(a) LHRs in total irradiation in 3 axial positions

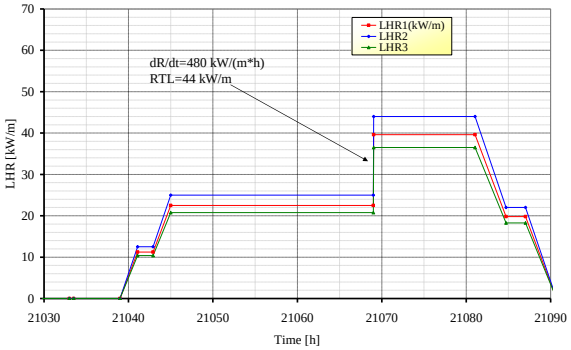

(b) LHRs in ramp in 3 axial positions

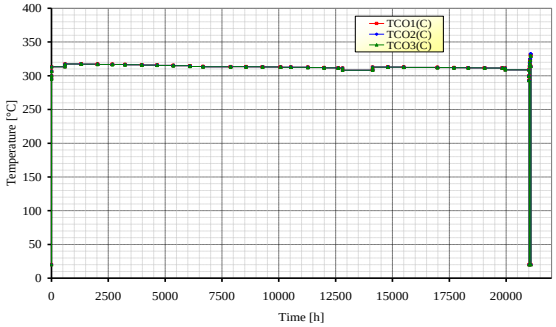

(c) Temperatures in total irradiation in 3 axial positions

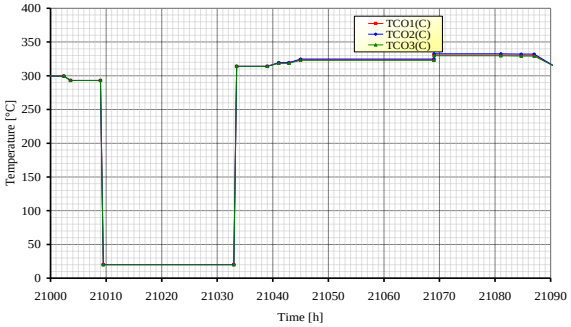

(d) Temperatures in ramp in 3 axial positions

Fig. A - 2 – Rod PK1/2 PWR Super-Ramp Project.

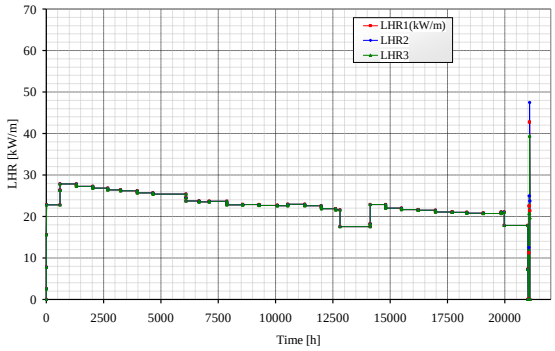

(a) LHRs in total irradiation in 3 axial positions

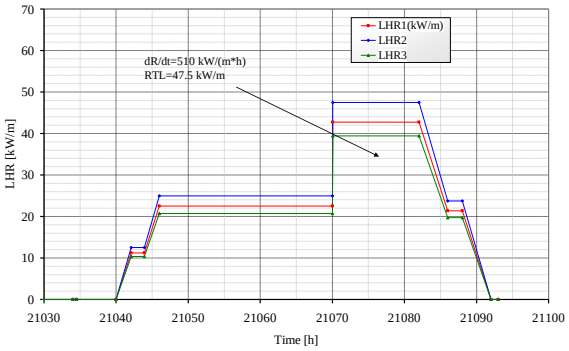

(b) LHRs in ramp in 3 axial positions

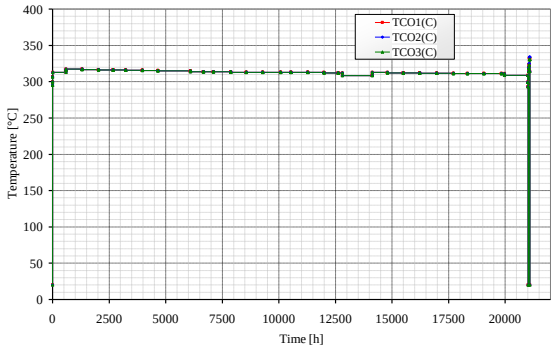

(c) Temperatures in total irradiation in 3 axial positions

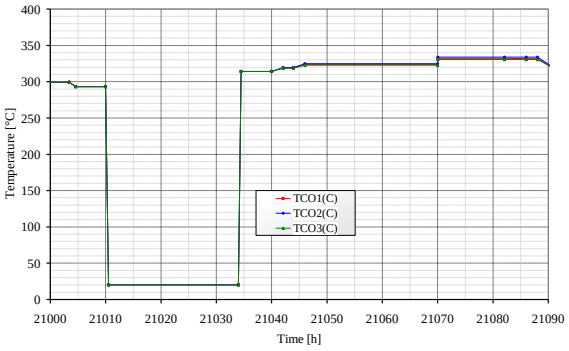

(d) Temperatures in ramp in 3 axial positions

Fig. A - 3 – Rod PK1/3 PWR Super-Ramp Project.

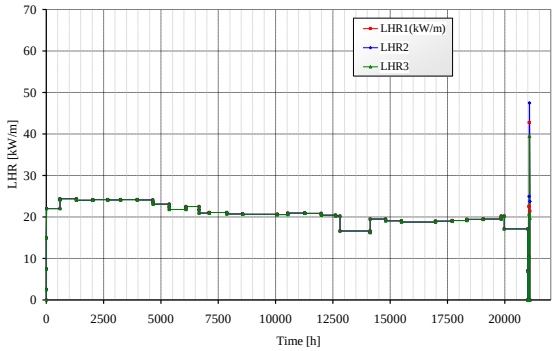

(a) LHRs in total irradiation in 3 axial positions

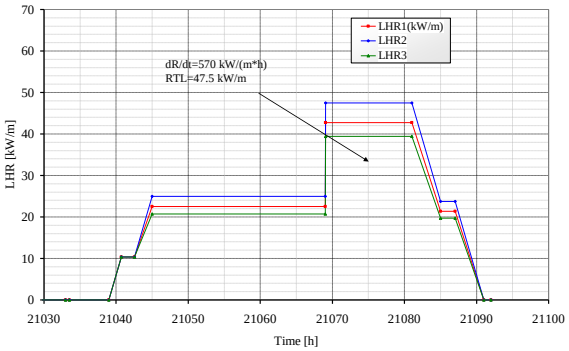

(b) LHRs in ramp in 3 axial positions

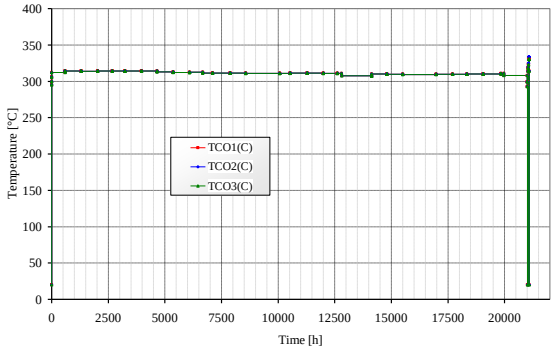

(c) Temperatures in total irradiation in 3 axial positions

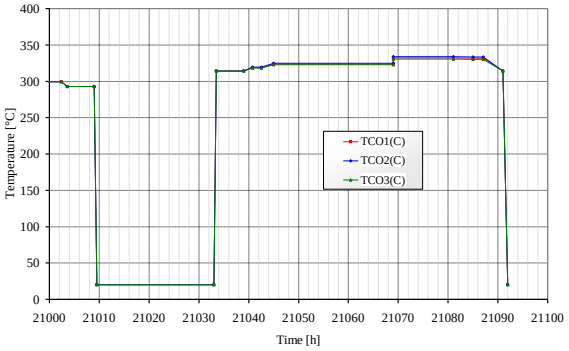

(d) Temperatures in ramp in 3 axial positions

Fig. A - 4 – Rod PK1/4 PWR Super-Ramp Project.

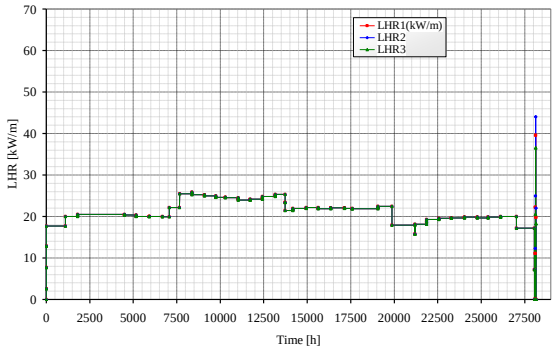

(a) LHRs in total irradiation in 3 axial positions

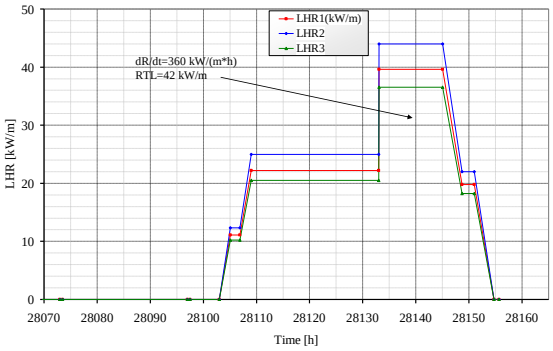

(b) LHRs in ramp in 3 axial positions

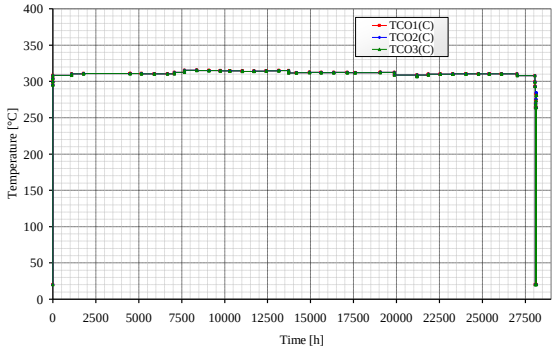

(c) Temperatures in total irradiation in 3 axial positions

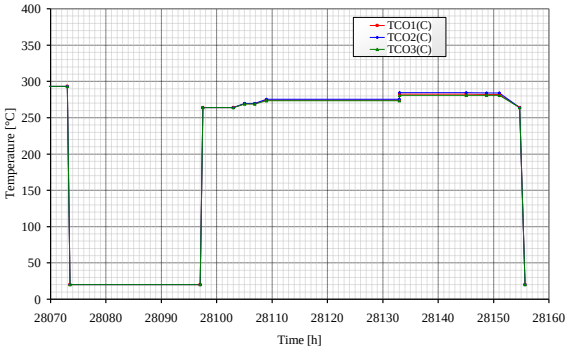

(d) Temperatures in ramp in 3 axial positions

Fig. A - 5 – Rod PK1/S PWR Super-Ramp Project.

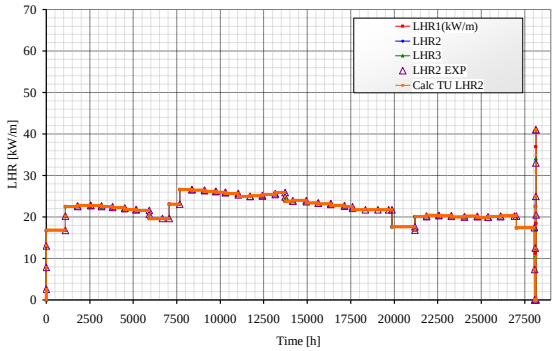

(a) LHRs in total irradiation in 3 axial positions

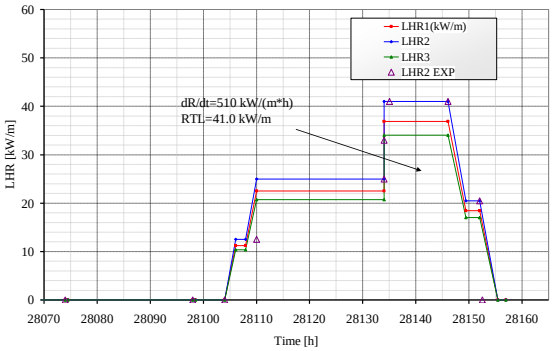

(b) LHRs in ramp in 3 axial positions

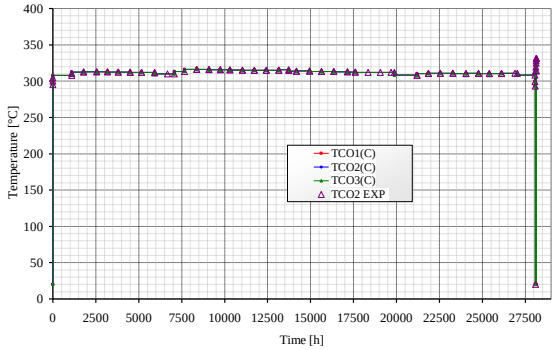

(c) Temperatures in total irradiation in 3 axial positions

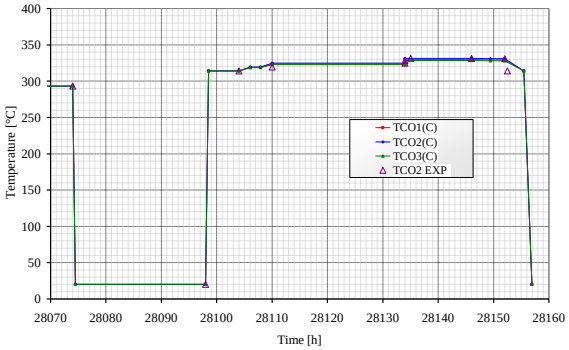

(d) Temperatures in ramp in 3 axial positions

Fig. A - 6 – Rod PK2/1 PWR Super-Ramp Project.

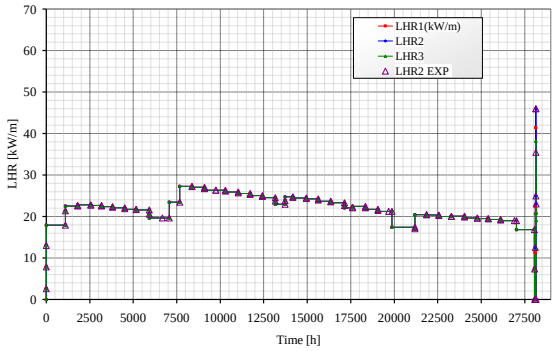

(a) LHRs in total irradiation in 3 axial positions

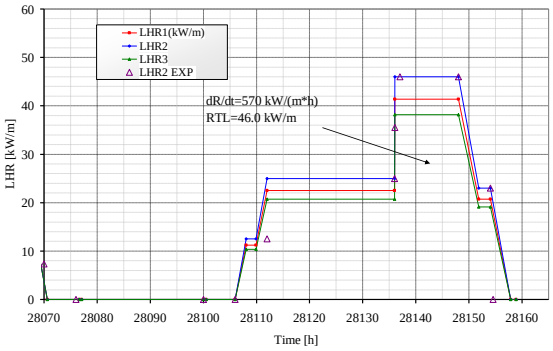

(b) LHRs in ramp in 3 axial positions

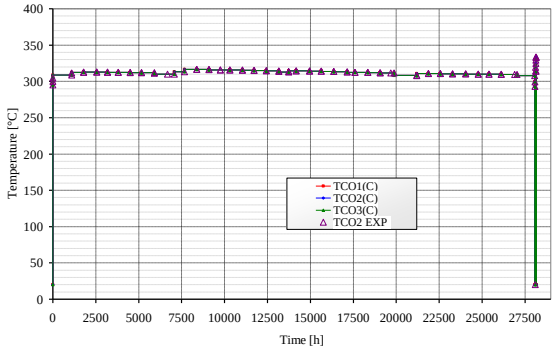

(c) Temperatures in total irradiation in 3 axial positions

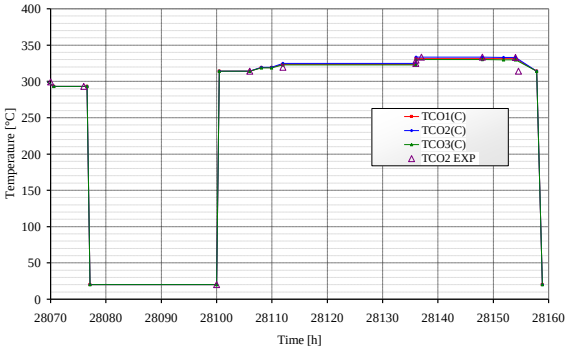

(d) Temperatures in ramp in 3 axial positions

Fig. A - 7 – Rod PK2/2 PWR Super-Ramp Project.

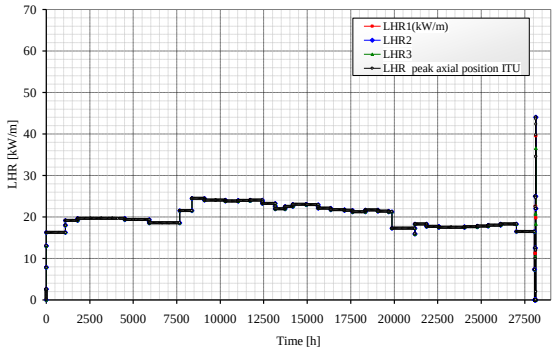

(a) LHRs in total irradiation in 3 axial positions

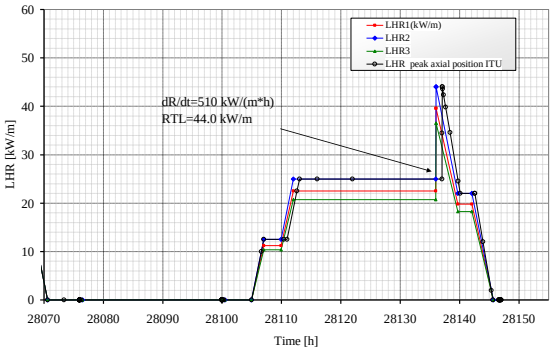

(b) LHRs in ramp in 3 axial positions

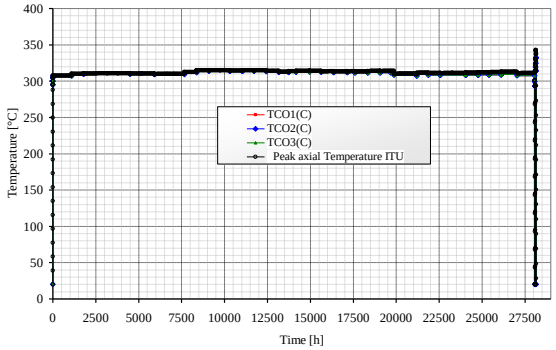

(c) Temperatures in total irradiation in 3 axial positions

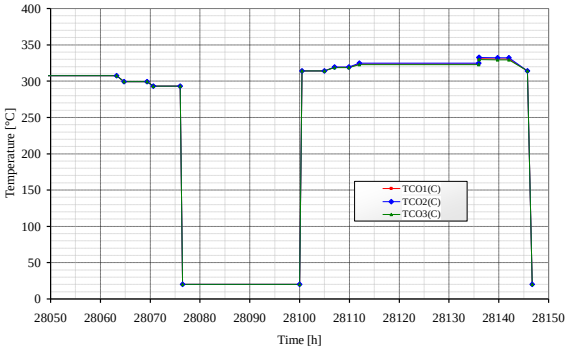

(d) Temperatures in ramp in 3 axial positions

Fig. A - 8 – Rod PK2/3 PWR Super-Ramp Project.

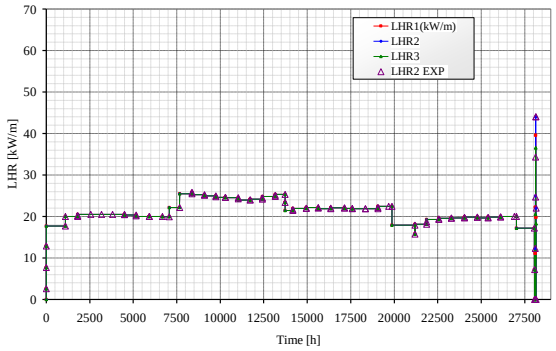

(a) LHRs in total irradiation in 3 axial positions

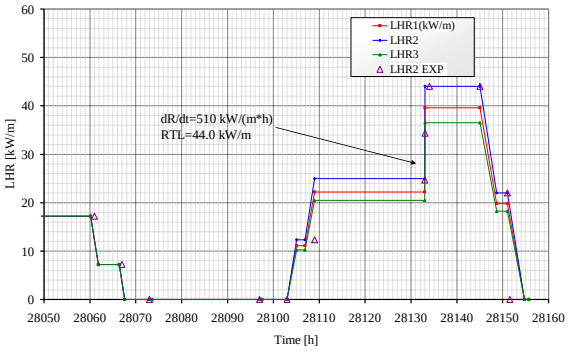

(b) LHRs in ramp in 3 axial positions

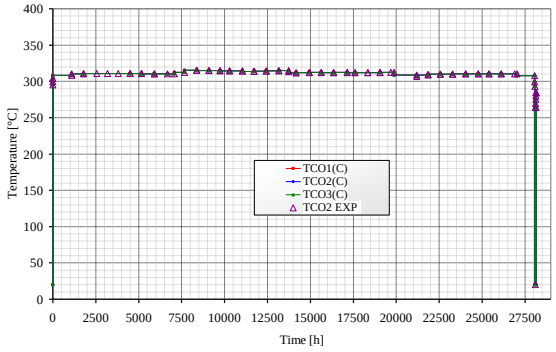

(c) Temperatures in total irradiation in 3 axial positions

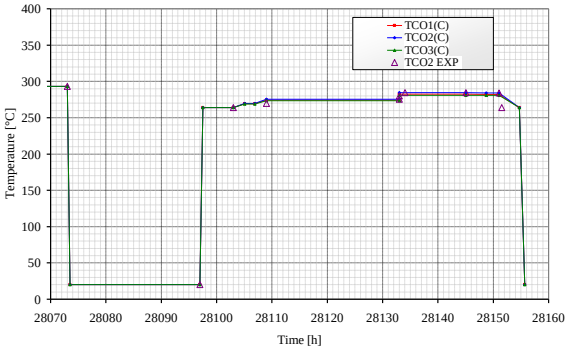

(d) Temperatures in ramp in 3 axial positions

Fig. A - 9 – Rod PK2/S PWR Super-Ramp Project.

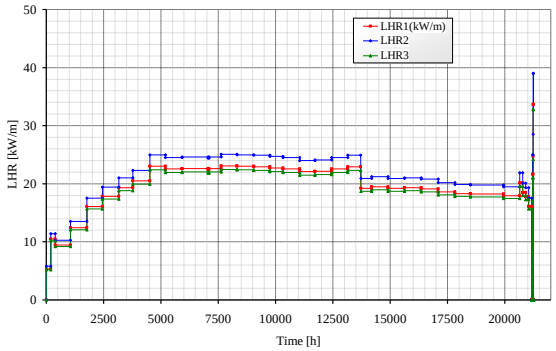

(a) LHRs in total irradiation in 3 axial positions

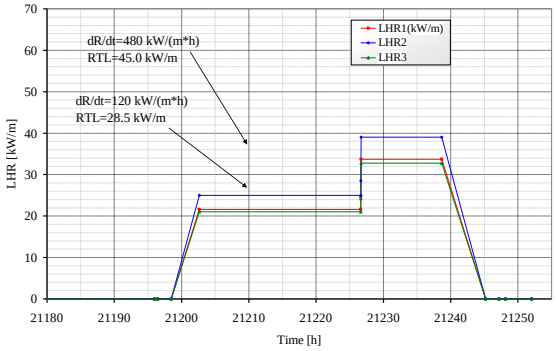

(b) LHRs in ramp in 3 axial positions

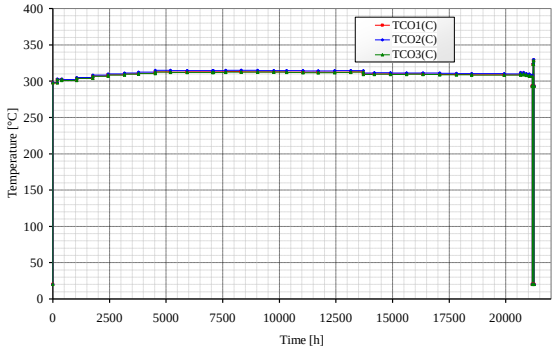

(c) Temperatures in total irradiation in 3 axial positions

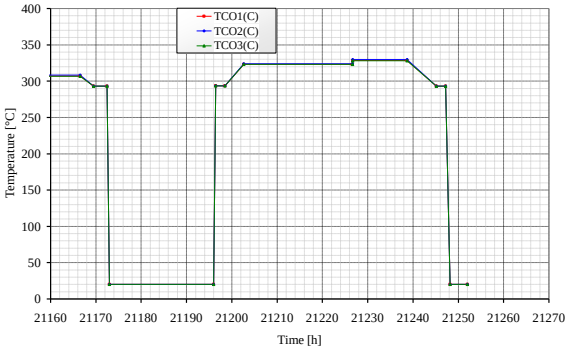

(d) Temperatures in ramp in 3 axial positions

Fig. A - 10 – Rod PK4/1 PWR Super-Ramp Project.

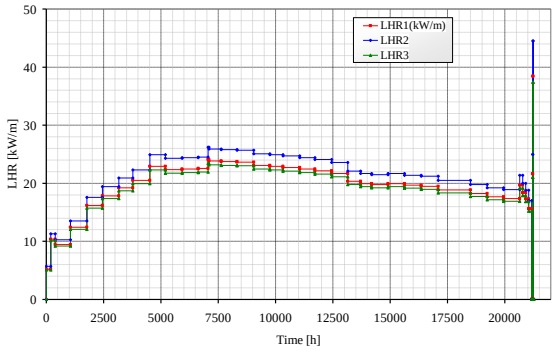

(a) LHRs in total irradiation in 3 axial positions

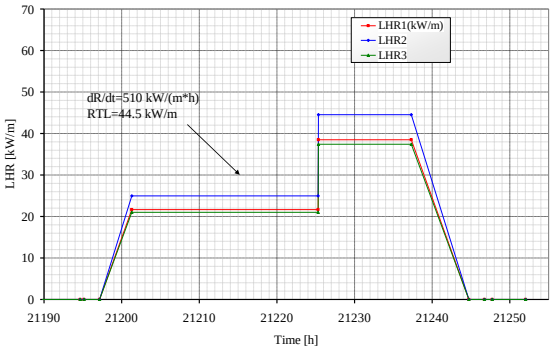

(b) LHRs in ramp in 3 axial positions

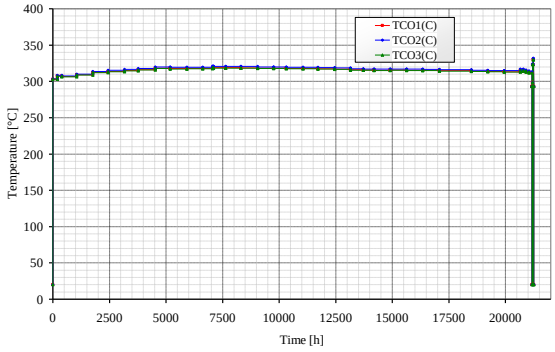

(c) Temperatures in total irradiation in 3 axial positions

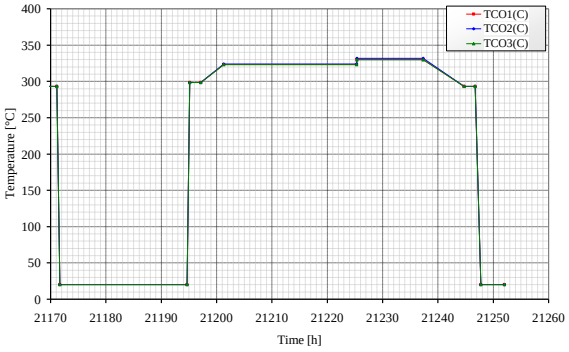

(d) Temperatures in ramp in 3 axial positions

Fig. A - 11 – Rod PK4/2 PWR Super-Ramp Project.

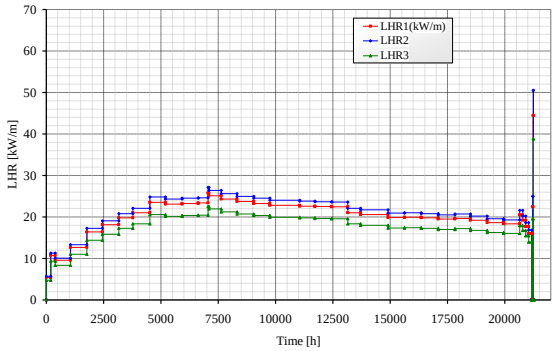

(a) LHRs in total irradiation in 3 axial positions

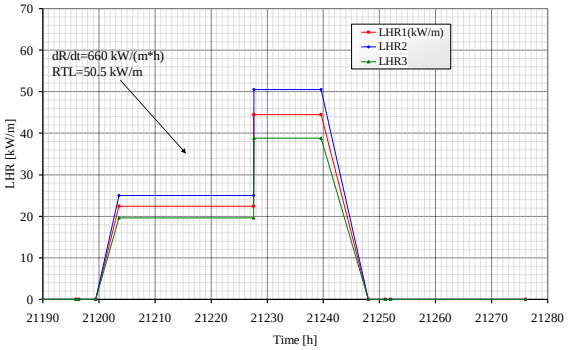

(b) LHRs in ramp in 3 axial positions

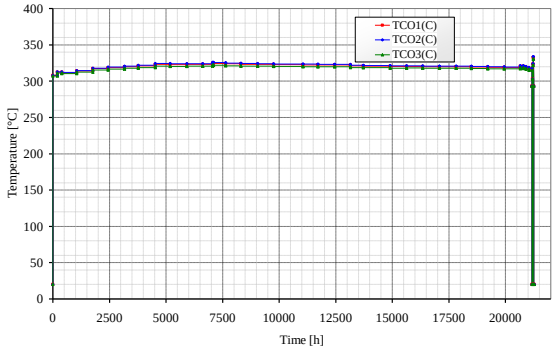

(c) Temperatures in total irradiation in 3 axial positions

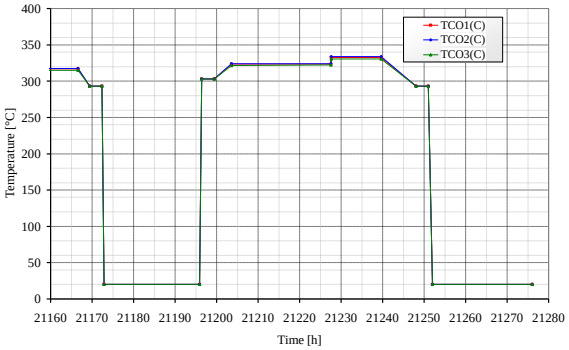

(d) Temperatures in ramp in 3 axial positions

Fig. A - 12 – Rod PK4/3 PWR Super-Ramp Project.

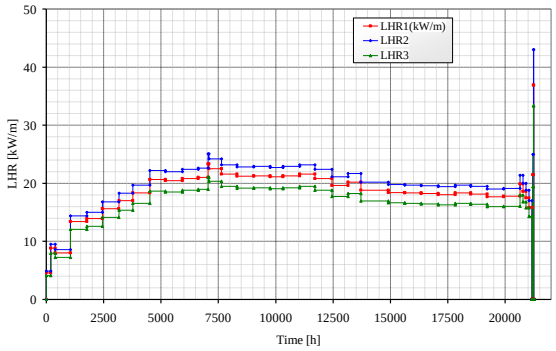

(a) LHRs in total irradiation in 3 axial positions

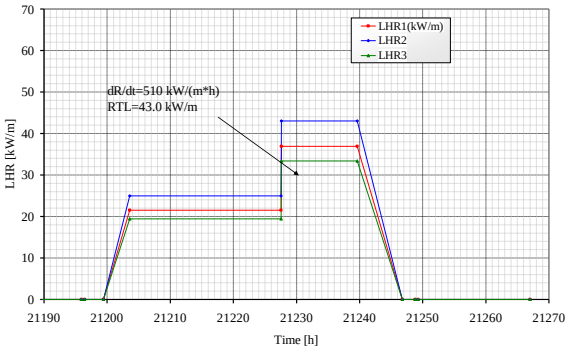

(b) LHRs in ramp in 3 axial positions

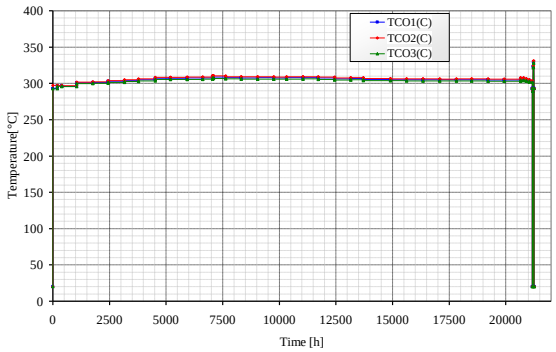

(c) Temperatures in total irradiation in 3 axial positions

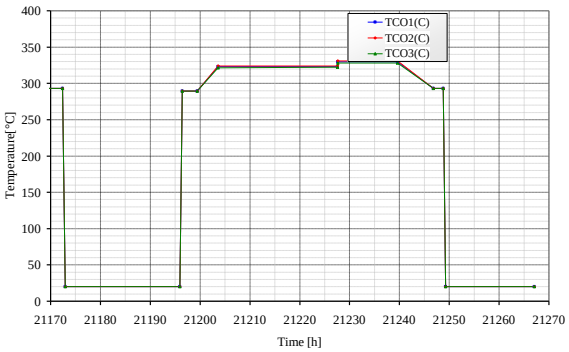

(d) Temperatures in ramp in 3 axial positions

Fig. A - 13 – Rod PK4/S PWR Super-Ramp Project.

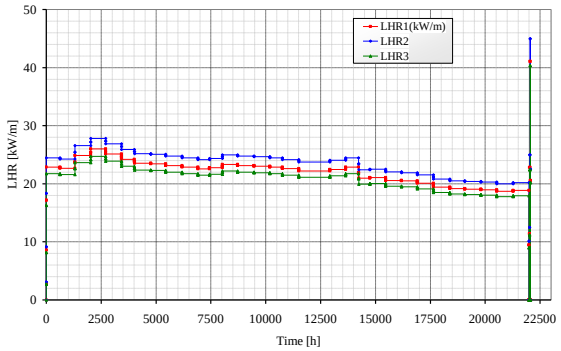

(a) LHRs in total irradiation in 3 axial positions

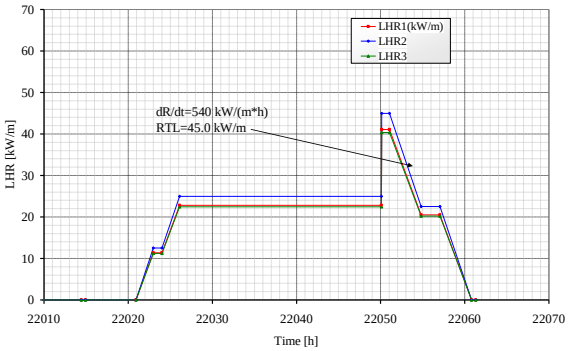

(b) LHRs in ramp in 3 axial positions

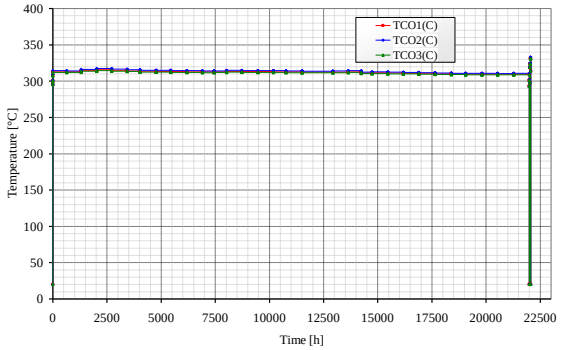

(c) Temperatures in total irradiation in 3 axial positions

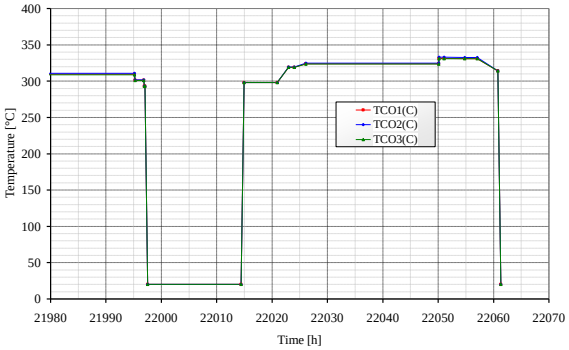

(d) Temperatures in ramp in 3 axial positions

Fig. A - 14 – Rod PK6/1 PWR Super-Ramp Project.

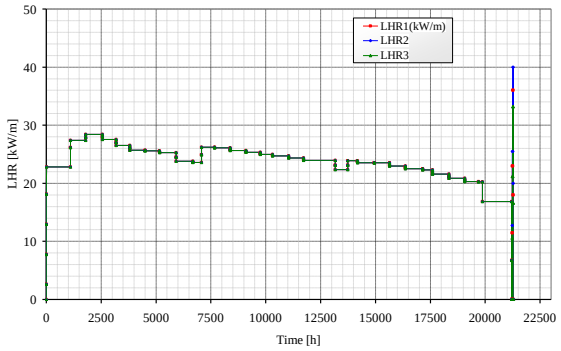

(a) LHRs in total irradiation in 3 axial positions

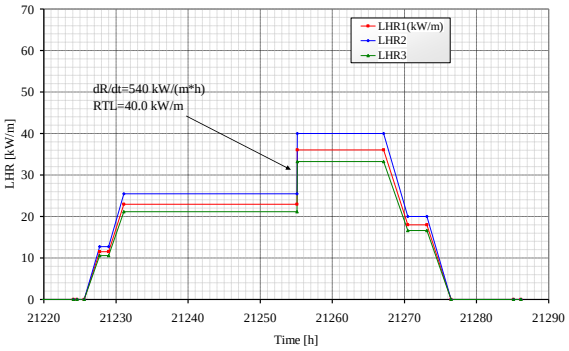

(b) LHRs in ramp in 3 axial positions

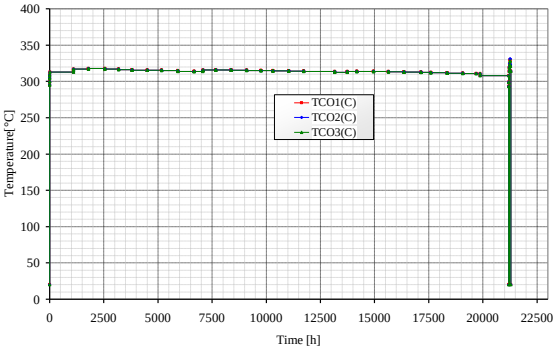

(c) Temperatures in total irradiation in 3 axial positions

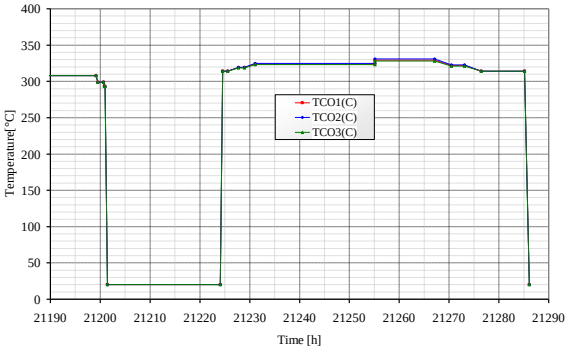

(d) Temperatures in ramp in 3 axial positions

Fig. A - 15 – Rod PK6/2 PWR Super-Ramp Project.

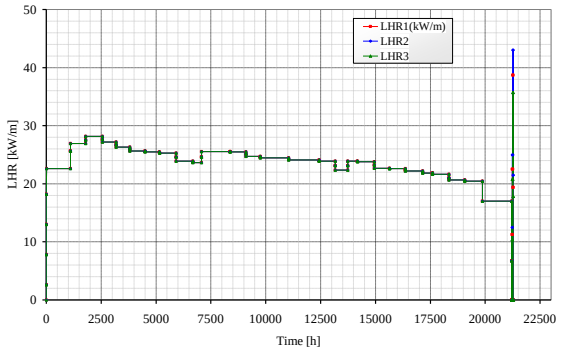

(a) LHRs in total irradiation in 3 axial positions

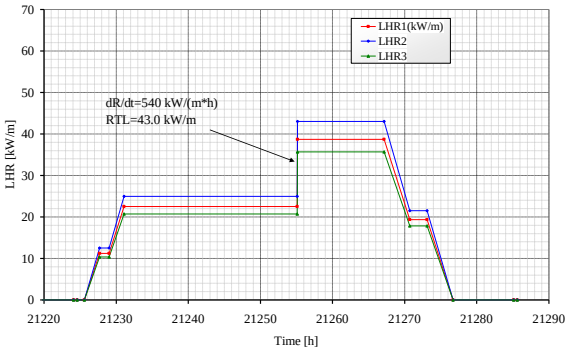

(b) LHRs in ramp in 3 axial positions

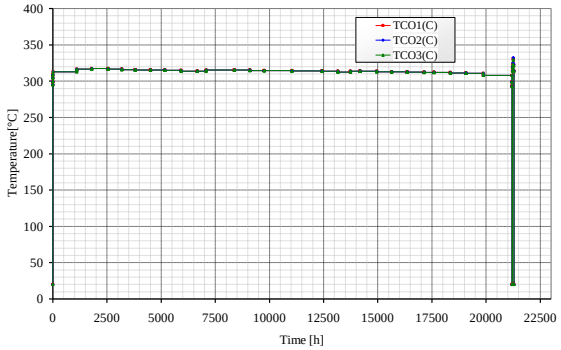

(c) Temperatures in total irradiation in 3 axial positions

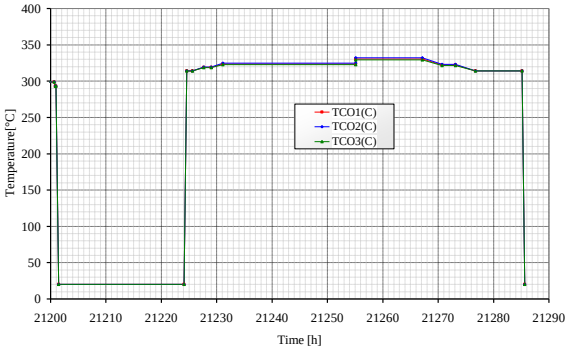

(d) Temperatures in ramp in 3 axial positions

Fig. A - 16 – Rod PK6/3 PWR Super-Ramp Project.

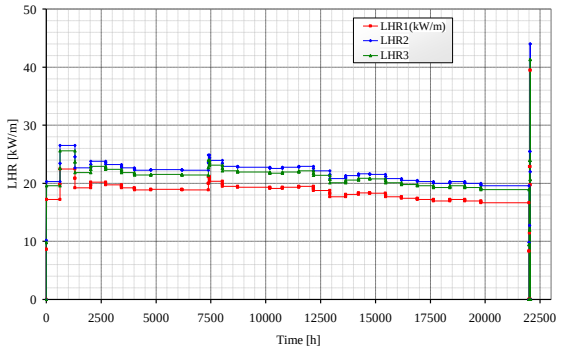

(a) LHRs in total irradiation in 3 axial positions

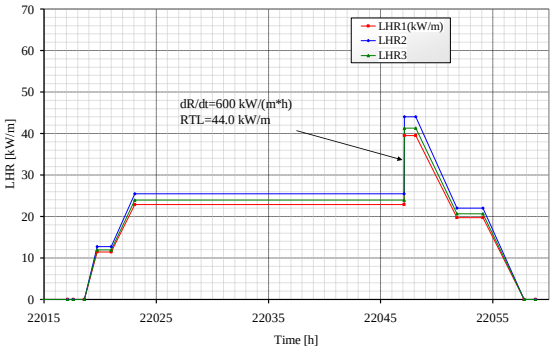

(b) LHRs in ramp in 3 axial positions

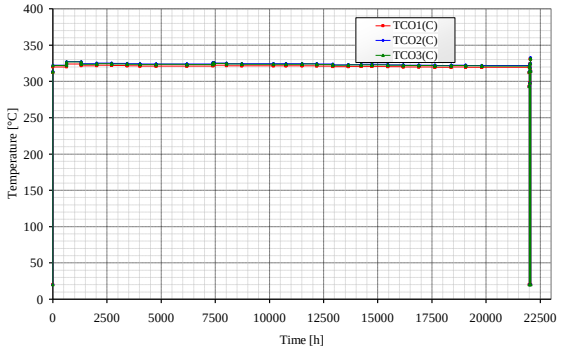

(c) Temperatures in total irradiation in 3 axial positions

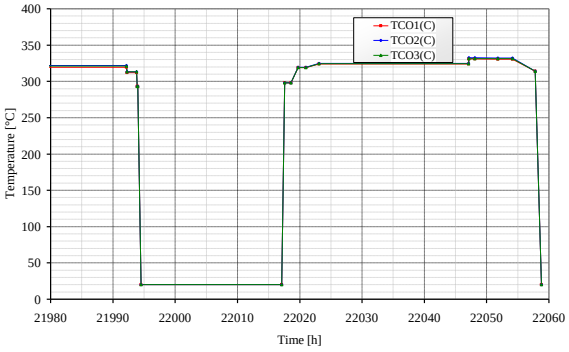

(d) Temperatures in ramp in 3 axial positions

Fig. A - 17 – Rod PK6/4 PWR Super-Ramp Project.

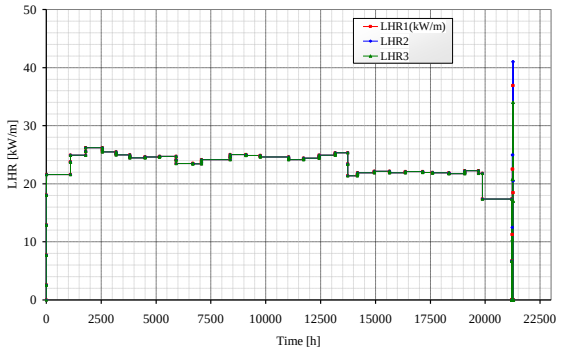

(a) LHRs in total irradiation in 3 axial positions

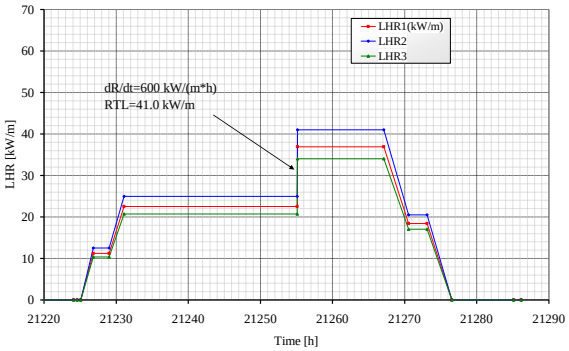

(b) LHRs in ramp in 3 axial positions

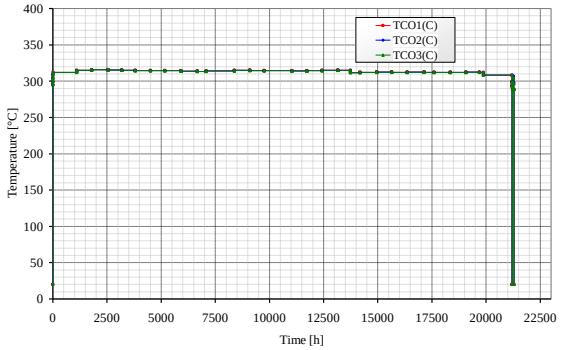

(c) Temperatures in total irradiation in 3 axial positions

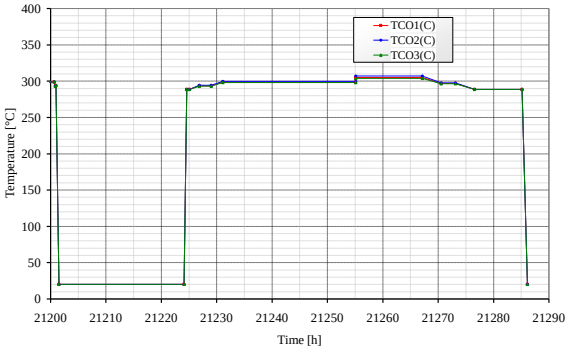

(d) Temperatures in ramp in 3 axial positions

Fig. A - 18 – Rod PK6/S PWR Super-Ramp Project.

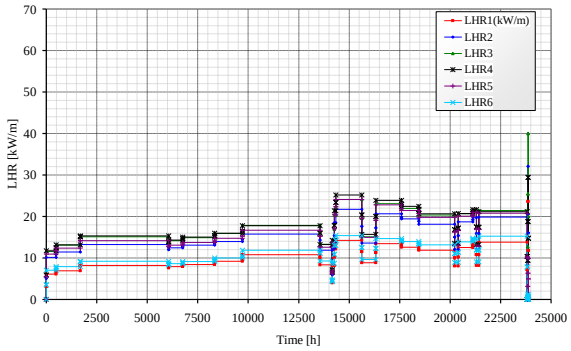

(a) LHRs in total irradiation in 6 axial positions

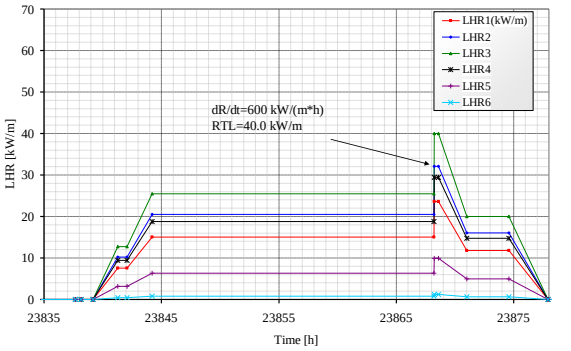

(b) LHRs in ramp in 6 axial positions

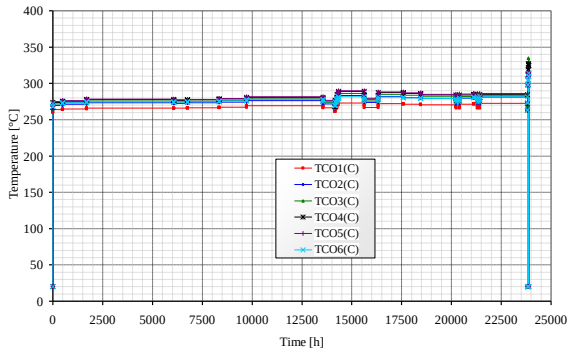

(c) Temperatures in total irradiation in 6 axial positions

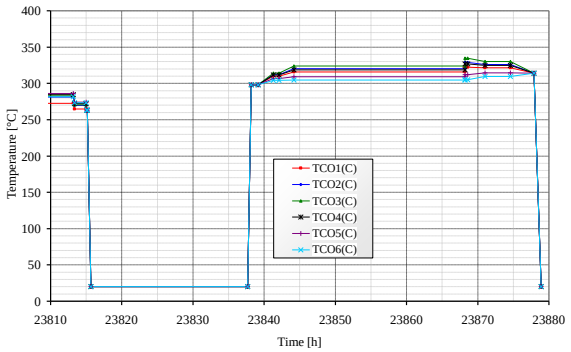

(d) Temperatures in ramp in 6 axial positions

Fig. A - 19 – Rod PW3/1 PWR Super-Ramp Project.

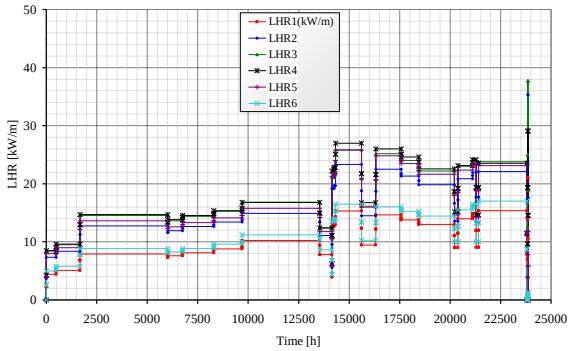

(a) LHRs in total irradiation in 6 axial positions

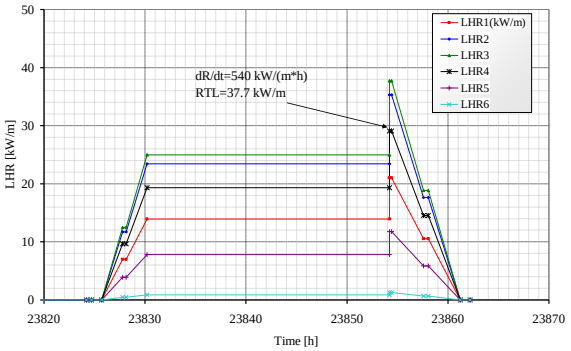

(b) LHRs in ramp in 6 axial positions

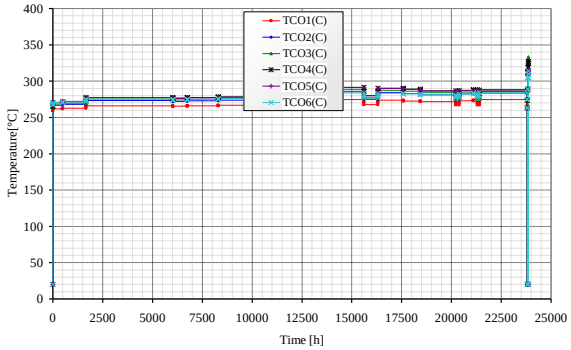

(c) Temperatures in total irradiation in 6 axial positions

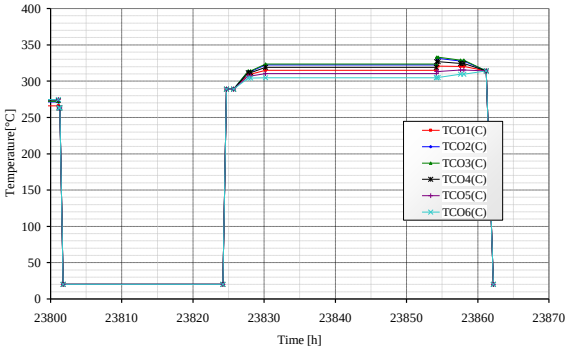

(d) Temperatures in ramp in 6 axial positions

Fig. A - 20 – Rod PW3/4 PWR Super-Ramp Project.

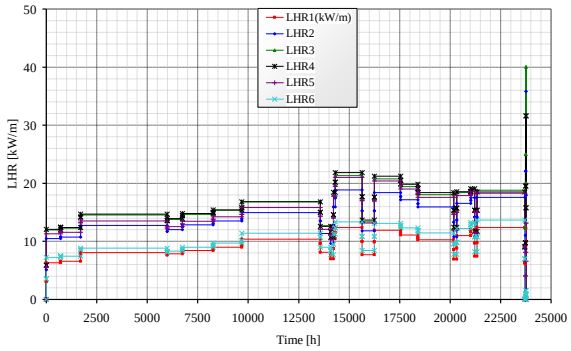

(a) LHRs in total irradiation in 6 axial positions

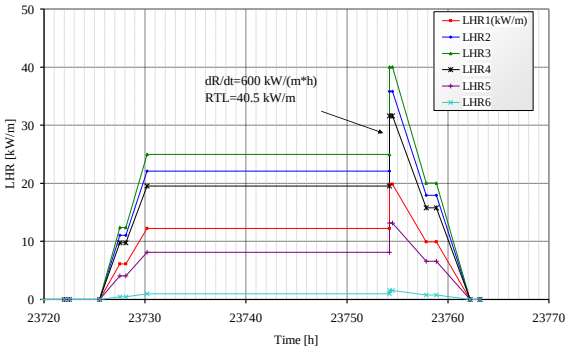

(b) LHRs in ramp in 6 axial positions

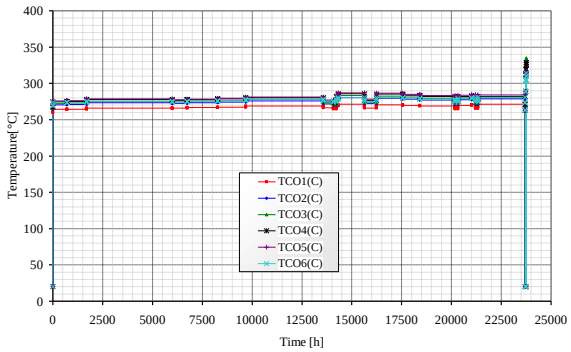

(c) Temperatures in total irradiation in 6 axial positions

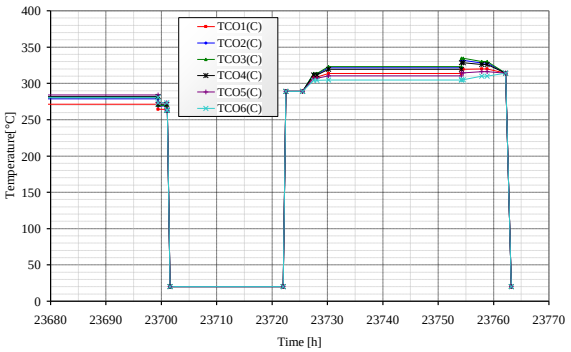

(d) Temperatures in ramp in 6 axial positions

Fig. A - 21 – Rod PW3/S PWR Super-Ramp Project.

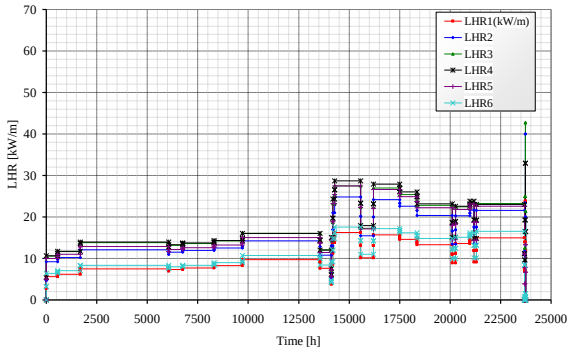

(a) LHRs in total irradiation in 6 axial positions

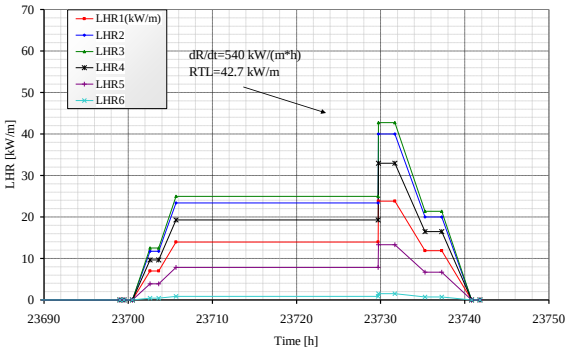

(b) LHRs in ramp in 6 axial positions

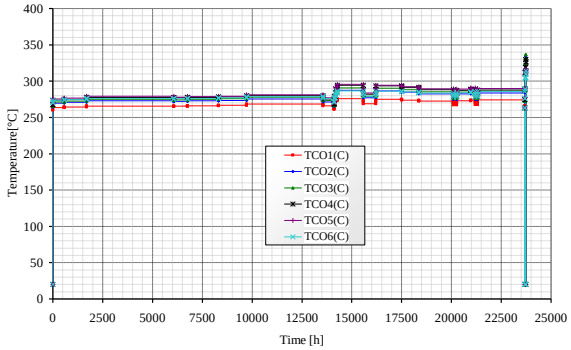

(c) Temperatures in total irradiation in 6 axial positions

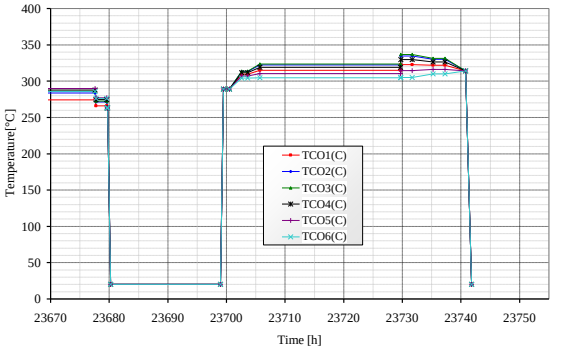

(d) Temperatures in ramp in 6 axial positions

Fig. A - 22 – Rod PW5/1 PWR Super-Ramp Project.

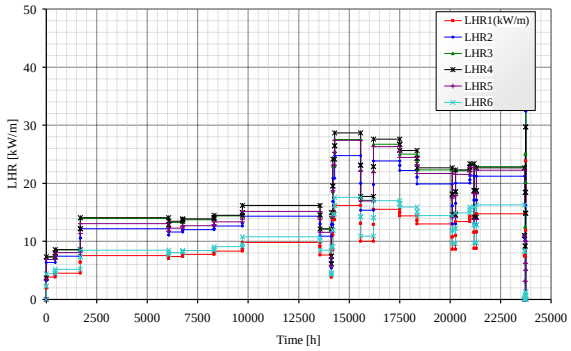

(a) LHRs in total irradiation in 6 axial positions

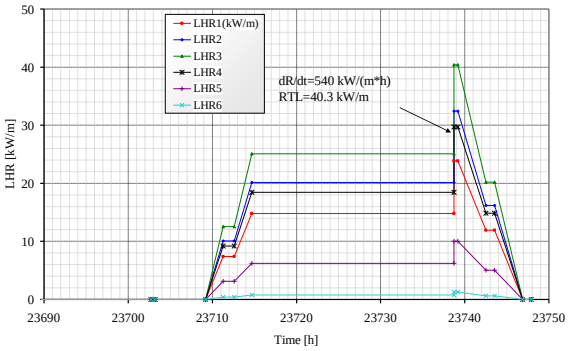

(b) LHRs in ramp in 6 axial positions

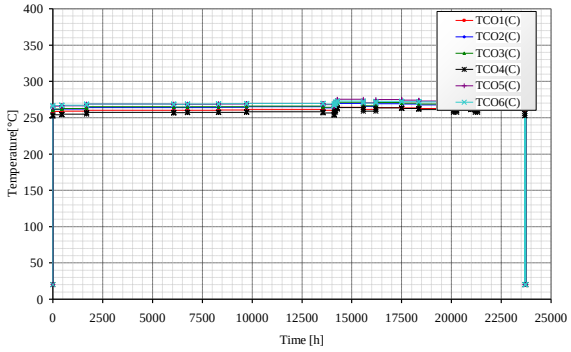

(c) Temperatures in total irradiation in 6 axial positions

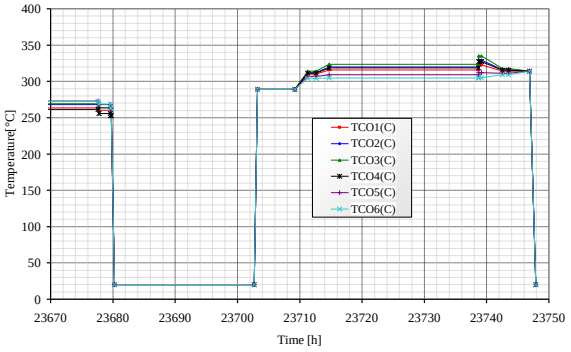

(d) Temperatures in ramp in 6 axial positions

Fig. A - 23 – Rod PW5/2 PWR Super-Ramp Project.

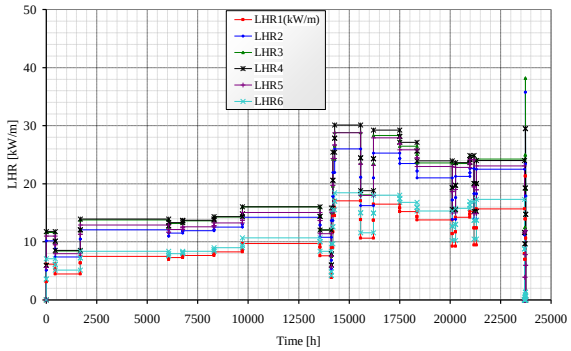

(a) LHRs in total irradiation in 6 axial positions

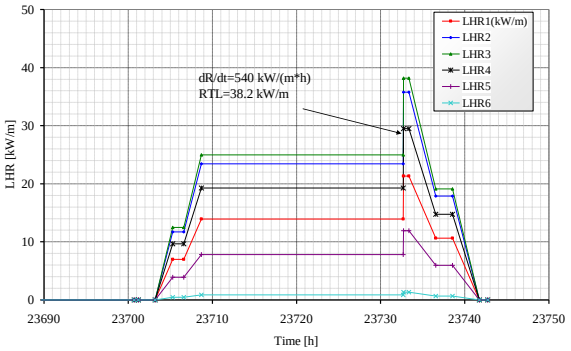

(b) LHRs in ramp in 6 axial positions

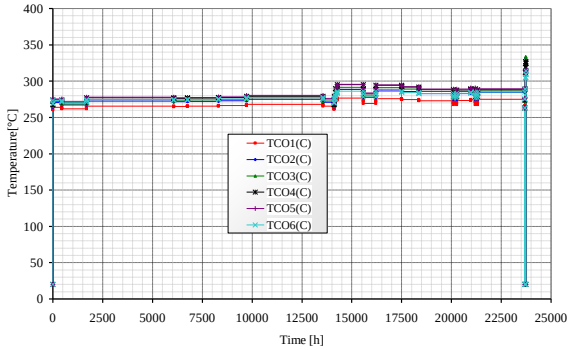

(c) Temperatures in total irradiation in 6 axial positions

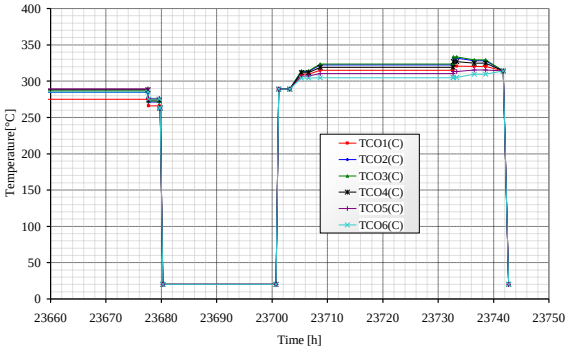

(d) Temperatures in ramp in 6 axial positions

Fig. A - 24 – Rod PW5/3 PWR Super-Ramp Project.

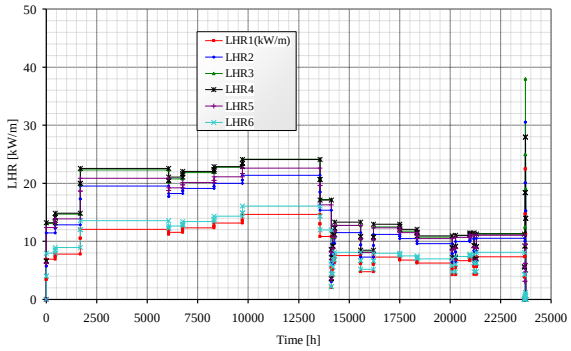

(a) LHRs in total irradiation in 6 axial positions

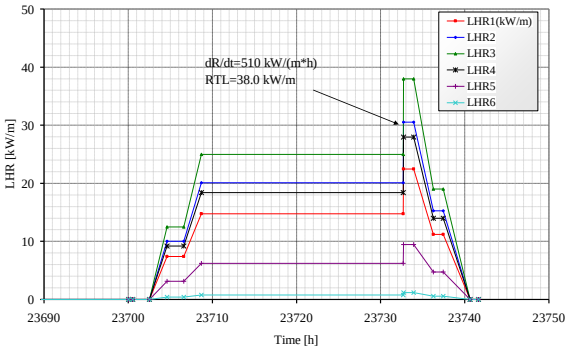

(b) LHRs in ramp in 6 axial positions

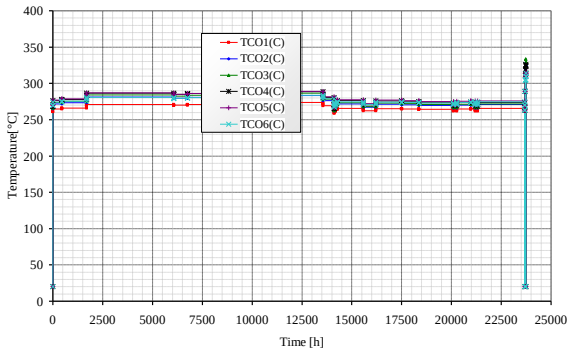

(c) Temperatures in total irradiation in 6 axial positions

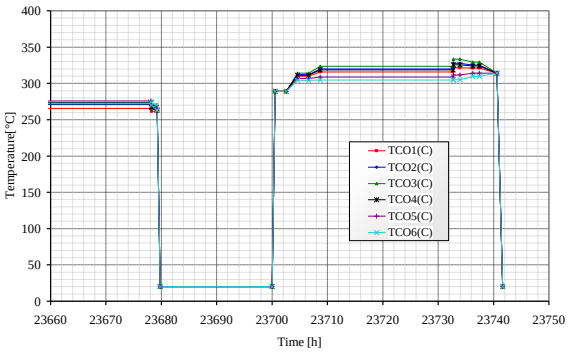

(d) Temperatures in ramp in 6 axial positions

Fig. A - 25 – Rod PW5/4 PWR Super-Ramp Project.